University of Alberta

An Investigation of Early Relapsing-Remitting Multiple Sclerosis Patients using Diffusion Tensor Imaging and Spectroscopy

by

Wan Hazlin Zaini

A thesis submitted to the Faculty of Graduate Studies and Research in partial fulfillment of the requirements for the degree of

Master of Science

Biomedical Engineering

Fall 2013
Edmonton, Alberta

ABSTRACT

Magnetic resonance imaging (MRI) of multiple sclerosis (MS) has shown evidence of both localized and widespread tissue damage in the brains of MS patients. Imaging at localized level may offer an insight into the mechanisms of fatigue in MS. Fatigue is reported to be the most common symptom in MS patients. Its cause, however, is still unknown. Whole brain imaging has shown evidence of widespread brain network disruption that may offer valuable markers of disease progression

The purpose of this dissertation is two fold:

1. To measure the brain metabolites in the pontine brainstem using MR spectroscopy in MS patients suffering from fatigue.
2. To investigate the network efficiency in brains of MS patients with low disability and various lesion loads using DTI tractography and graph theoretical analysis.

Potentially, results from these studies will assist physicians and researchers to better understand the underlying pathology of this multi-faceted disease.

ACKNOWLEDGEMENTS

These funding agencies, the Multiple Sclerosis Society of Canada (MSSOC), the End MS Research and Training Network (EndMS) and the Canadian Institutes of Health Research (CIHR) provided the funding necessary to operate and conduct the research study in which I was involved, and the stipend I was provided for this graduate degree.

I would like to thank my supervisor, Dr. Christian Beaulieu, and my supervising committee members, Dr. Chris Hanstock and Dr. Fabrizio Giuliani, for giving me a shot at pursuing this graduate degree. I appreciate the countless hours of writing assistance and extensive feedback on the manuscripts and presentations I passed through all of you. Thank you for overseeing the volunteer recruitments and scans, and for the endless encouragement given to me over the past couple of years.

I also cannot forget all the staff members and fellow students in the Department of Biomedical Engineering (especially Min, who has helped me in countless ways and all my friends who are together with me in this battlefield) for the endless outpouring of encouragement, and the emotional and psychological support!

I would like to thank my family members (parents, sisters, brothers, nieces and in-laws in Malaysia and England) who never

stopped loving, inspiring and supporting me throughout my life. Last but not least, I want to dedicate this work to my husband (Hun) and children (Alia and Aneeq) for always cheering on and never stopped listening to (or pretended to) my endless outpour about my research, the countless outbursts of cries, frustrations and the unnecessary tantrums. All were returned with love, encouragement and endless hugs and kisses.

TABLE OF CONTENTS

LIST OF TABLES

LIST OF FIGURES

LIST OF ABBREVIATIONS

AAL	Anatomical automatic labeling
AD	Axial diffusivity
ADC	Apparent diffusion coefficient
ANOVA	Analysis of variance
ARAS	Ascending reticular activating system
b_0	Non diffusion-weighted image, b = 0 s/mm2
bCC	body of the corpus callosum
B_0	External magnetic field
Cb	Cerebellum
CC	Clustering coefficient
Cho	Choline
CNS	Central nervous system
Cr	Creatine
CSF	Cerebrospinal fluid
CSI	Chemical shift imaging
CST	Corticospinal tract
DMN	Default-mode network
DTI	Diffusion tensor imaging
EAE	Experimental allergic encephalomyelitis
EDSS	Expanded disability status scale
E_{glob}	Global network efficiency
E_{loc}	Local network efficiency
E_{reg}	Regional efficiency
FA	Fractional anisotropy
FLAIR	Fluid-attenuated inversion recovery
FN	Fiber number
FOV	Field of view
FSS	Fatigue severity scale

gCC	Genu of the corpus callosum
GM	Gray matter
IFO	Inferior fronto-occipital fasciculus
ILF	Inferior longitudinal fasciculus
L_p	Average shortest path length
LL	Lesion load
MCP	Middle cerebellar peduncle
MD	Mean diffusivity
MPRAGE	Magnetization-prepared rapid acquisition gradient echo
MRI	Magnetic resonance imaging
MRS	Magnetic resonance spectroscopy
MS	Multiple sclerosis
NAA	N-acetylaspartate
NAWM	Normal-appearing white matter
OR	Optic radiation
PCr	Phosphocreatine
PET	Positron emission tomography
PP	Primary-progressive
ppm	parts-per-million
PPMS	Primary-progressive multiple sclerosis
PRESS	Point resolved spectroscopy
RD	Radial diffusivity
ROI	Region-of-interest
RR	Relapsing-remitting
RRMS	Relapse-remitting multiple sclerosis
RSN	Resting state network
sCC	Splenium of the corpus callosum
SCP	Superior cerebellar peduncle

SD	Standard deviation
SLF	Superior longitudinal fasciculus
SPMS	Secondary-progressive multiple sclerosis
tCr	Total creatine
T	Tesla (SI unit of magnetic flux density)
TBSS	Tract-based spatial statistic
TE	Echo time
TR	Repetition time
UNF	Uncinate fasciculus
v_1, v_2, v_3	Eigenvectors 1, 2, and 3
VBM	Voxel based morphometry
WM	White matter
λ_1, λ_2, λ_3	Eigenvalues 1, 2, and 3

CHAPTER 1 INTRODUCTION

Multiple sclerosis (MS) is one of the most common neurological diseases affecting young adults in Canada. It is known to affect twice as many women as men (Compston et al. 2008). It is thought that more than 2.1 million people worldwide suffer from MS (National Multiple Sclerosis Society). About 240 people per 100,000 Canadians have MS; which gives Canada one of the highest prevalence of MS cases in the world (Beck et al. 2005). The cause of MS is still puzzling to researchers, and no treatment has been discovered which can cure the disease. Early and accurate diagnosis allows for early intervention, and certain medications can be utilized to help control MS-related symptoms while physicians monitor disease progression. Aspects of MS, from its clinical manifestation to MS diagnosis, will be discussed in Chapter 2.

Magnetic resonance imaging (MRI) is the most useful tool in assisting in the diagnosis of MS. MRI provides images of the human brain non-invasively therefore allowing frequent monitoring of disease progression without the risk of exposure to ionizing radiation. Compared to other imaging methodologies such as computed tomography (CT) or positron emission tomography (PET) scans, MRI is the best method for “capturing” high contrast images of MS plaques or lesions. Advanced MR methods such as MR

spectroscopy and diffusion tensor imaging (DTI), have also been used to study MS. Basics of MR spectroscopy and DTI are reviewed in Chapter 3. Results from these studies have assisted the research community in better understanding the underlying mechanism of this disease. The focus of this dissertation is to use both MR techniques mentioned above to study the changes observed in brain metabolites, and to reveal structural differences in the brain, for relapsing-remitting MS (RRMS) patients (n = 19) when compared to a group of healthy controls (n = 18). All patients had low disability measures, but ten exhibited significant levels of fatigue. Fatigue is the most common and disabling symptom for up to 70% of MS patients (Beck et al. 2005). To date, the underlying origin and cause of fatigue in MS remains unknown.

In laying the groundwork for Chapter 5 and 6, which discuss our two studies in greater detail, Chapter 4 will describe the MS literature, which has made use of similar MR methodologies. This chapter will also discuss previous MS studies involving patients with fatigue.

The primary objective of our research study was to investigate the differences between the brains of MS patients with and without fatigue using MR spectroscopy. The MR spectroscopy study investigated metabolite differences in the pontine brainstem

of patients with fatigue compared to those of non-fatigue patients and controls. Results from this study will be discussed in Chapter 5.

Aside from focal disrupted lesions in MS, the resulting widespread inflammation alters the basic structures and functions of the brain. Some lesions show correlation with MS symptoms, while some do not, and even among early RRMS patients with low disability, the lesion load varies. Using graph theoretical analysis and DTI tractography, we examined the structural network alterations in our patient groups and assessed how lesion load is associated with such changes. This work is described in Chapter 6.

In Chapter 7, results from preliminary analysis using DTI tractography are presented and discussed here. This work involved the same group of patients described above. We tested the performance of deterministic tractography in tracing fiber bundles that may or may not be interrupted by lesion presence within the tract.

Limitations and future directions pertaining to the studies above are discussed in Chapter 8, and conclusion statement in Chapter 9.

CHAPTER 2 MULTIPLE SCLEROSIS

2.1 Clinical Manifestation of MS

In the late 1800s, multiple sclerosis (MS) was already known and defined as an inflammatory neurological disorder involving the central nervous system (CNS). Widespread areas of inflammation, demyelination and loss of axons are observed in the white matter of the brain and spinal cord.

According to the animal model of MS experimental allergic encephalomyelitis (EAE), the possible pathogenesis begins with the peripheral activation of T cells. This activation is triggered by unknown factors such as bacterial or viral agents that can have structural similarities to CNS self-antigens. After activation, T cells can cross the blood-brain barrier and attack the self-antigen in the CNS. The self-antigen could be represented by the lipid-insulating myelin sheath that surrounds and protects neuronal axons. Over time, infiltration of inflammatory cells cause damage and degradation of the myelin, and the axons are not spared from this inflammatory process. Damage to the WM results in focal demyelination and subsequent axonal dysfunction. At damaged tissue sites, loss of myelin-generating oligodendrocytes are replaced by inflammatory cells results in plaques or lesions. Lesions can accumulate in the brain and spinal cord, both can

contribute to the clinical progression of the disease (Capello et al. 2007).

2.2 Disability measures

The Kurtzke expanded disability status scale (EDSS) is a tool for quick assessment of a patient's neurological condition (Kurtzke 1983), which is used to quantify disability in MS. The EDSS was developed to measure the disability in eight functional systems of the human body, i.e. the pyramidal, cerebellar, brainstem, sensory, bowel and bladder, visual and cerebral functions. The EDSS score ranges from zero to ten, where 0 is "normal neurological exam" and 10 is "death caused by MS".

2.3 MS sub-types

According to the revised 2010 McDonald Criteria (Polman et al. 2011), an "attack" or relapse is defined as patient-reported symptoms or physical observation of an acute inflammatory event involving the CNS. The "attack" must last a minimum of 24 hours, and must be present without an accompanying fever or infection (Polman et al. 2011). During a relapse, symptoms manifest and reach a plateau stage which can last for several days or weeks. This is followed by a period of recovery from the presenting symptom, and while some patients recover fully, others only have a

partial recovery. When the disease is presented in this form, the patient is classified as having the relapsing-remitting (RR) form of MS which accounts for about 80-85% of all MS cases (Compston et al. 2008). Between “attacks”, most RRMS patients are in remission for months or even years, but some patients may be in remission for a much longer interval (greater than 20 years). This latter form of MS is known as benign MS (Filippi et al. 2011).

Unfortunately, the condition of most RRMS patients worsens over time, and the majority of RRMS patients enter the secondary progressive (SP) stage. At this stage, patients present with persistent MS-related symptoms, and often these symptoms do not resolve over time. SPMS patients are considered to be at an advanced clinical stage with an increased level of disability (higher EDSS score).

Only about 15% of MS patients are diagnosed with primary progressive (PP) MS (Filippi et al. 2011). The onset of the disease in PPMS patients is distinct from those of relapsing-remitting or secondary-progressive patients. Unlike the sudden attacks that occur in the relapsing-remitting form, symptoms in primary-progressive patients appear and progress slowly from disease onset (Filippi et al. 2011). An image representation of the disease course in all MS sub-types is shown in Figure 2.1.

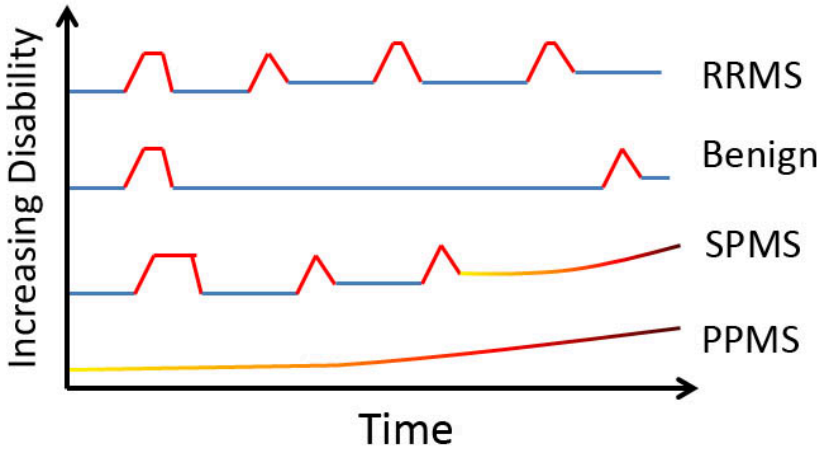

Figure 2.1: Classification of multiple sclerosis (MS) patients according to the disease course i.e. relapsing-remitting (RR), benign, secondary-progressive (SP) and primary-progressive (PP) MS patients. The red lines represent the "attacks" or relapses, while the blue lines represent the remission in RRMS, benign MS and in the early stage of SPMS patients before progression. The duration of a relapse varies within and between subjects and is represented by the various widths of the red lines. The plateau stage during an attack simply illustrates a longer duration before symptoms resolve. The disease onset of an SPMS patient usually starts off as a relapsing-remitting course. An RRMS patient converts to SPMS at the point of an incomplete resolution of MS-related symptoms and gradual accumulation of disability. This conversion is represented by the gradual colour change from yellow to red. Disease course in PPMS patients is represented by the curved line representing increased disability over time; the colour represents accumulation of disability that worsen over time. PPMS patients do not experience apparent "attacks" or relapses as in RRMS.

2.4 Symptoms in MS

Symptoms presented by MS patients are not unique to MS, however, certain symptoms are more frequently observed and

described in MS patients than in other neurological diseases (Rolak 2011). Symptoms can be categorized into motor, coordination, visual, cognitive and "other" categories. Examples of motor related symptoms in MS patients are numbness or tingling sensation in the arms or legs and stiffness of the leg or weakness in one leg that results in dragging of the foot while walking. MS patients also experience poor coordination or loss of balance. Eye pain precedes loss of vision, frequently occurring only in one eye. In cases where both eyes are affected, one eye is usually worse than the other. Other commonly reported visual symptoms include blurring, flashes of light and eye pain (Nordmann et al. 1987).

Cognitive impairment is estimated to affect between 40% and 65% of MS patients. Symptoms may appear in multiple forms, for example, short-term memory loss, trouble concentrating, difficulty in conveying thoughts, trouble recognizing familiar faces and an inability to navigate in familiar surroundings (LaRocca 2011). In addition, patients also report bowel and bladder incontinence and sexual dysfunction. The symptom that is most prevalent in MS patients is fatigue (Minden et al. 2006).

2.5 Fatigue in MS

Fatigue is the most common and disabling symptom for as many as 80% of MS patients (Minden et al. 2006; Induruwa et al.

2012). It is defined as “subjective lack of physical and/or mental energy to perform a desired task or activity” (Multiple Sclerosis Council for Clinical Practice 1998). Fatigue imposes limitations on patients’ lives, limiting their daily activities. Many patients limit their outdoor activities in order to “preserve” their daily energy level. Furthermore, heat exaggerates the feeling of fatigue. In some cases, fatigue cannot not be alleviated with rest (Shah 2009).

The unemployment rate is also higher among MS patients experiencing fatigue than among MS patients with a similar level of disability but without fatigue. Fatigue also impedes patients from performing daily tasks. Fatigue is found to be associated with depression in MS patients (Fisk et al. 1994), however, not all MS patients with fatigue necessarily suffer from depression (Chwastiak et al. 2005).

2.6 Fatigue assessment

To assess fatigue in MS patients, the most commonly used questionnaire is the Krupp fatigue severity scale (FSS) (Krupp et al. 1989). FSS is a nine-question self-administered questionnaire that allows patients to assess the implications of fatigue in their daily activities. FSS only assesses a patient’s condition over the past seven days. Its questions ask how fatigue relates to the physical functioning, work, exercise, family and social life of MS patients. A

patient indicates “1” to show strong disagreement, or “7” to show strong agreement, with each statement. A total score of 36 or more indicates that the patient may be suffering from fatigue. The score of any given patient on Day 1 does not imply that the patient experiences the same level of fatigue on Day 7. Similarly when patients have identical FSS scores, it does not mean that both individuals experience the same level of fatigue. Subjectivity or relativity is an issue, however, a successful method that measures fatigue objectively in MS patients has yet to be developed.

2.7 MS Diagnosis

MS symptoms vary widely between patients. The disease can mimic other autoimmune disorders and is non-specific. When attempting to diagnose a patient, a neurologist has to exclude all other possible neurological conditions before arriving at an MS diagnosis. A neurologist also has the assistance of several useful tools that may assist and confirm MS diagnosis. In older patients (50 years and up), the assessment of intrathecal inflammation in the cerebrospinal fluid (CSF) is useful. CSF is extracted from the spinal column in patients, where evidence of the oligoclonal band is present in more than 90% of MS patients. This allows for a laboratory-supported definite-MS diagnosis in patients who were previously classified as clinically probable MS (Compston et al.

2008). Evoked potential assessment is used to evaluate the involvement of the sensory and motor pathways by recording and measuring the response time of the electrical impulse when exposed to external stimulation. This response time is usually prolonged in MS patients (Compston et al. 2008). Perhaps one of the most useful diagnostic tools is magnetic resonance imaging (MRI). MRI has been adopted formally in MS diagnosis due to its sensitivity and ability to depict pathological features of MS (Polman et al. 2011). Through MRI, physicians now have the ability to image and assess MS lesions in vivo, and it plays an important role in monitoring disease progression.

According to the McDonald diagnostic criteria, in support of using MRI for MS diagnosis, lesion demonstration must be 'disseminated in time and space' (Polman et al. 2011).

Dissemination in time refers to lesions that are considered new if it is observed one month apart when compared to a baseline (first or previous) MRI scan. This criterion was simplified compared to the previous 2005 revision (Polman et al. 2005), whereby the 'dissemination in time' criterion is fulfilled when a Gadolinium-enhanced lesion is observed in T_1-weighted images and a T_2-hyperintensity lesion is observed in patients without a previous

baseline scan. This simplification allows for MS diagnosis to be done after examination of a single clinical relapse.

Dissemination in space refers to the presence of at least one lesion observed in 2 out of 4 locations (juxtacortical, periventricular, infratentorial, spinal cord) in a single MRI (Polman et al. 2011). Both conditions must be fulfilled during the diagnosis process, provided that other neurological disease has been ruled out.

CHAPTER 3 NON-CONVENTIONAL MR TECHNIQUES

3.1 Spectroscopy

Magnetic Resonance Spectroscopy (MRS) is one of many techniques in NMR that provides metabolic information using the same basic principles of MRI. MRI provides high contrast images of soft tissues by utilizing the strong proton signal from water and fat, however, MRS makes use of the MR signal to probe for biochemical information of hydrogen-containing metabolites in the tissue under study. The spectral lines allows us to identify the different metabolites according to their location on a frequency spectrum

3.1.1 Chemical shift

In the presence of an external magnetic field, B_0, the nuclei precess at the Larmor frequency.

$$\omega_0 = \gamma B_0 \qquad \text{(Equation 3.1)}$$

where ω_0 is the precessional frequency, B_0 is the static magnetic field strength and γ is the gyromagnetic ratio of the nuclei. But in truth, individual hydrogen nuclei experience a different frequency depending on the electron distribution in the chemical bond of that molecular structure. The difference in the Larmor frequency due to the molecular environment is called the chemical shift. When placed in a magnetic field, the electron cloud surrounding the

nucleus induces a magnetic field locally, B_L, that opposes the direction of B_0, where σ is the shielding constant.

$$B_L = \sigma B_0 \qquad \text{(Equation 3.2)}$$

The resultant net magnetic field, *B*, acting on the nucleus (difference between the external and locally induced opposing magnetic field) is altered.

$$B = B_0(1 - \sigma) \qquad \text{(Equation 3.3)}$$

This phenomenon alters the precessional frequency ($\omega_{precession}$) of the nucleus.

$$\omega_{precession} = \gamma B_0(1 - \sigma) \qquad \text{(Equation 3.4)}$$

The proton nuclei of each metabolite produce a peak on the measured spectrum according to the chemical shift of its unique molecular environment.

3.1.2 Spectrum

MRS produces a spectrum of the voxel or region under study. This spectrum shows the molecular distribution with area under the peak representing the metabolite concentration. According to Equation 3.4, the chemical shift of the nucleus depends on the magnitude of B_0, hence, frequency separations between peaks will differ with B_0. In spectroscopy, a spectrum is

typically displayed with a 'parts per million' (ppm) scale, which is a standardized unit independent of field strength.

3.1.3 Chemical Shift Imaging

Chemical Shift Imaging (CSI) is another term for multi-voxel spectroscopy where an extended region is studied beyond just a single voxel. CSI adds phase-encoding gradients after the RF pulse to allow for simultaneous acquisition of multiple voxels (Figure 3.1) through spatial-localization within a single sequence (Figure 3.2). Many sequences are available in MRS, but only one is used in our study that is point resolved spectroscopy (PRESS). PRESS (Ordidge et al. 1983; Bottomley 1984) utilizes long echo time (TE ~ 135 ms and longer) and is best for imaging metabolites with longer relaxation time such as N-acetylaspartate (NAA), total creatine (tCr) and choline (Cho). This sequence has approximately double the SNR and less susceptible to motion compared to another widely used MRS sequence i.e. stimulated echo acquisition method (STEAM).

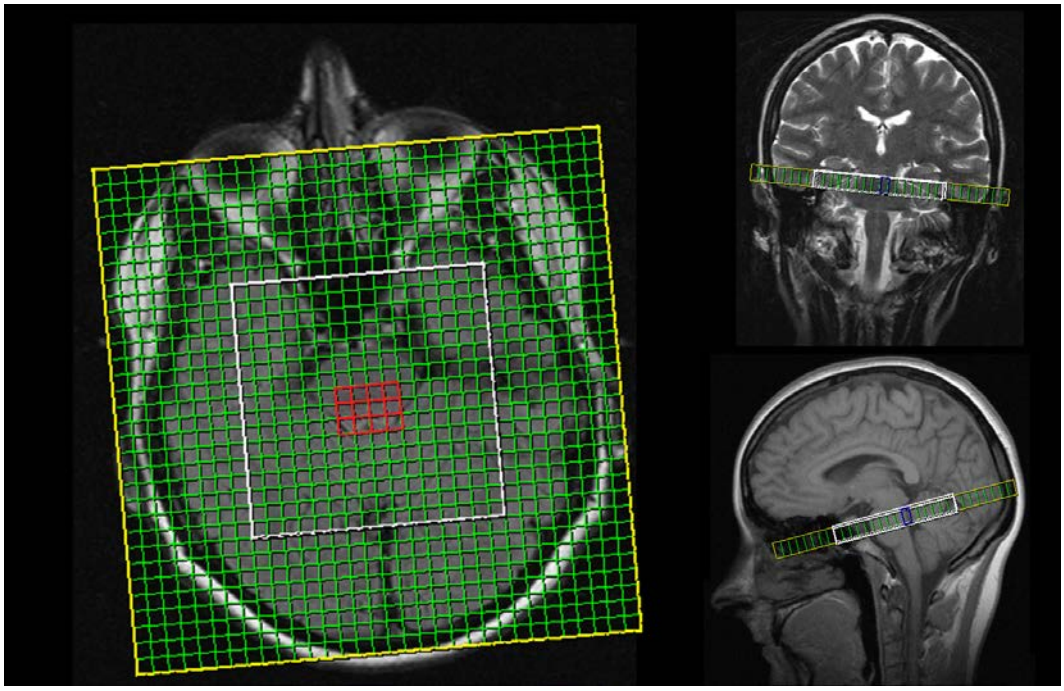

Figure 3.1: Two dimension chemical shift imaging (CSI) acquired using point resolved spectroscopy (PRESS) of 16x16 acquired matrix zero-filled to 32x32 total viewing elements.

3.1.4 Brain Metabolites

The human brain consists of many different chemicals or metabolites. Among the most abundant metabolites studied using spectroscopy are the N-acetylaspartate (NAA), total creatine (tCr) and choline (Cho), however, only NAA and tCr is studied and discussed in Chapter 5.

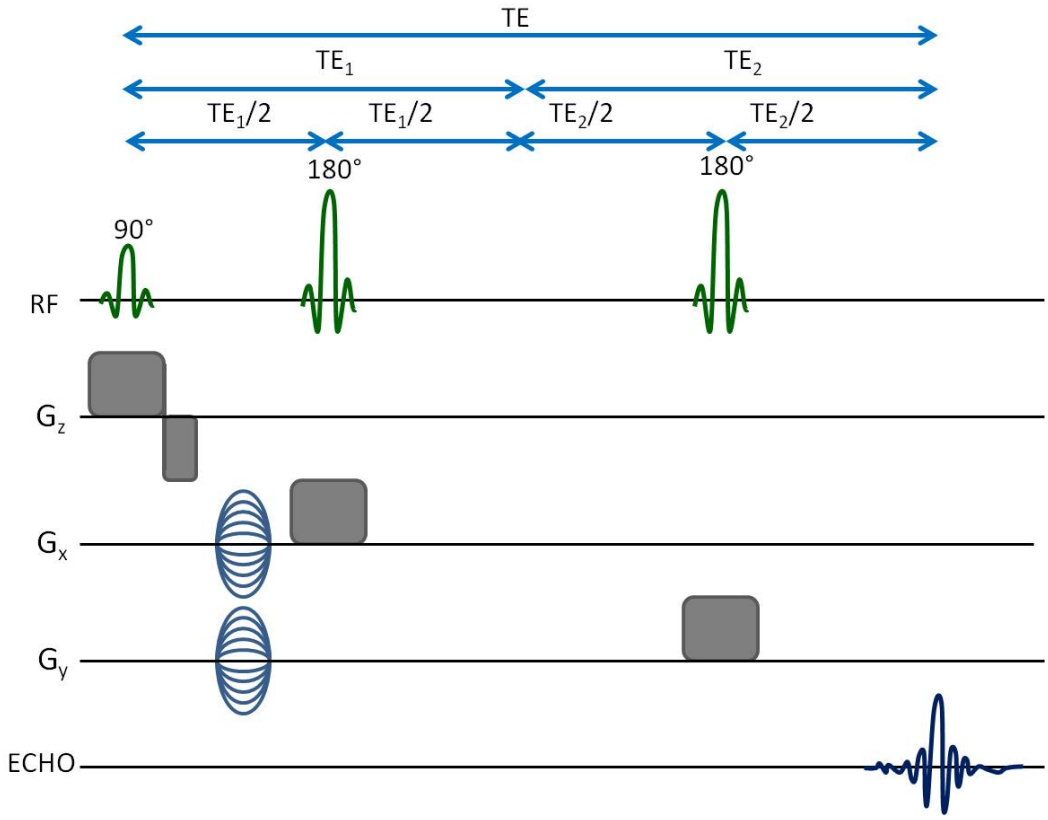

Figure 3.2: Pulse sequence diagram for 2D point resolved spectroscopy (PRESS) chemical shift imaging. This technique employs a 90° followed by two 180° radio frequency pulses at the interval shown where TE is the echo time. PRESS is generally used with longer echo time (TE = 135 - 270 ms) suitable for investigation of metabolites with longer relaxation time.

NAA is an amino acid found in high concentration in neurons and unique to the nervous system. It is the highest peak in the NMR frequency spectrum and the signal comes from the methyl-CH_3 group. Signal at 2.02ppm (Figure 3.3) comes from the metabolite NAA and N-acetylaspartateglutamate (a neuron-specific dipeptide, NAAG), but the NAAG is in much smaller amount (Caramanos et al. 2005). NAA is found only in neurons; it has been

used as a neuronal marker and reflects neuronal health. Reduced NAA levels suggest neuronal dysfunction or death of neurons

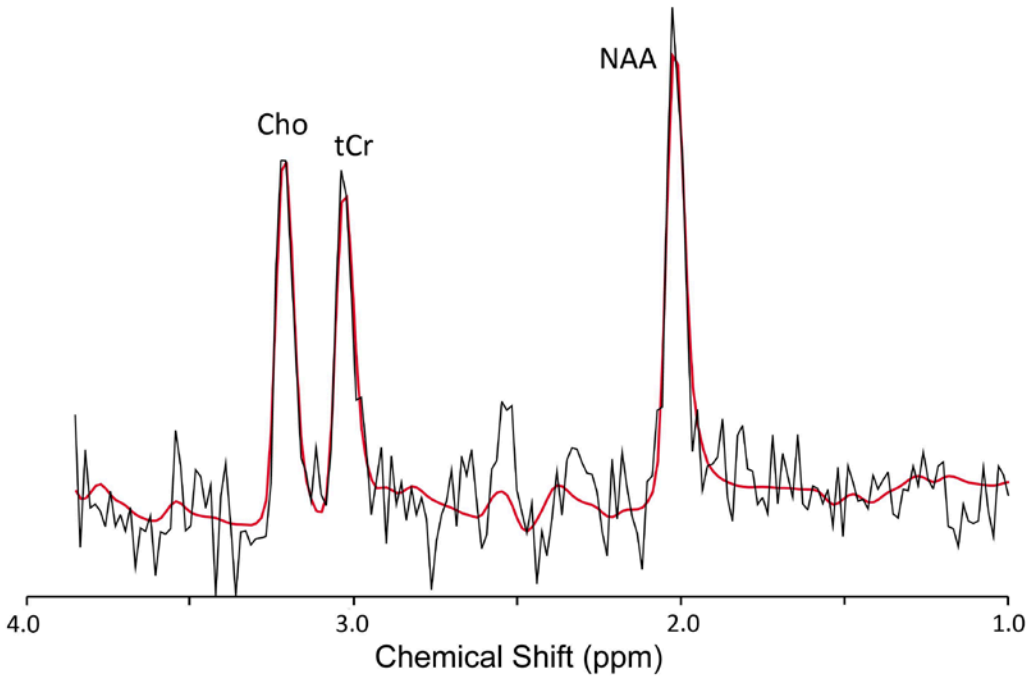

Figure 3.3: A water suppressed metabolite spectrum in an MS patient. The metabolite peaks shown here are the N-acetylaspartate (NAA), total creatine (tCr) and choline (Cho) at 2.0, 3.02 and 3.2 ppm respectively.

MRS measures tCr at 3.02ppm in the frequency spectrum and the signal is a contribution from both creatine (Cr) and phosphocreatine (PCr) (Figure 3.3) and is abundant in neurons and glial cells. The tCr concentration is thought to be generally stable in the human brain and often used as an internal reference for normalizing NAA and Cho measurements. However, the tCr has been shown to vary in some neurological conditions including multiple sclerosis (Sajja et al. 2009).

3.2 Diffusion

Diffusion refers to the random trajectory of a particle suspended in liquid or gas that is thermally governed by the Brownian motion. Its surrounding environment influences the diffusivity of water molecules in the human brain. The organization of the surroundings can be deduced by measuring the degree and direction of water diffusivity.

Diffusion can be described as a mathematical relationship (Equation 3.5) between time and distance in one dimension,

$$\langle r^2 \rangle = 2Dt \qquad \text{(Equation 3.5)}$$

where $\langle r^2 \rangle$ represents the mean squared displacement, D is the diffusion coefficient and t is the diffusion time. This equation can be extended to $\langle r^2 \rangle = 2Dtn$, for n dimensions. In 3-dimensions, the average squared displacement is $\langle r^2 \rangle = 6Dt$. From Equation 3.5, the distance travelled by water increases with time or diffusion coefficient, however, the average displacement of the particle remains constant at zero. This applies to 'free diffusion', where diffusion occurs in all directions. The diffusion coefficient, *D*, is a parameter that is indicative of the diffusion mobility. It can also vary within a substance depending on the temperature, pressure and viscosity. The diffusion coefficient of water is 2.4×10^{-3} $mm^2 s^{-1}$

at 25° C and about 3.04x10^{-3} mm^2s^{-1} at body temperature i.e. 37° C (Mills 1973).

3.2.1 Diffusion Weighting

Diffusion weighting can be added to a spin echo method by applying two consecutive diffusion-sensitizing gradients before and after the refocusing RF pulse. Both gradients are of strength G, duration δ and the leading edge of the diffusion-sensitizing gradients are separated by time Δ (Figure 3.4). The gradients can be applied in any direction. Its purpose is first to dephase the moment created by the spin particles and then to refocus them again in the second application. Spins that do not move in the direction of the pre-determined sensitizing gradient will be completely refocused by the second gradient. However, spins that moved between the two gradients will experience a slightly different magnetic field, thus, will not be able to completely refocus and results in signal loss. The diffusion time is the time allowed for spins to diffuse in the system and is calculated as Δ- δ/3.

The signal attenuation after the diffusion time can be measured in Equation 3.6,

$$\frac{S}{S_0} = e^{-bADC} \quad \text{(Equation 3.6)},$$

where, S is the signal acquired after the diffusion time, S_0 is the

signal acquired without the diffusion sensitizing gradients, *b* is the diffusion sensitivity and *ADC* is the *apparent diffusion coefficient*.

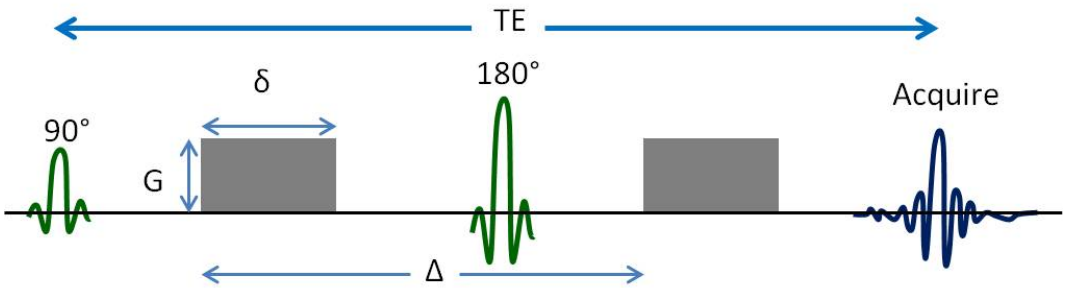

Figure 3.4: Pulse sequence diagram of the spin echo method with two consecutive diffusion-sensitizing gradients of strength, G, and of duration δ, before and after the 180° refocusing pulse, separated by time Δ. Note that imaging gradients are not shown.

The diffusion sensitivity, *b*, also known as the '*b* -value' reflects the degree of diffusion sensitization. A diffusion scan typically makes use of two *b*-values, b = 0 s/mm^2 (b_0) and a high b-value, ranging between 1000 and 2000 s/mm^2. The signal acquired from b_0 is the S_0 signal that produces the reference image without the sensitizing gradient.

The water diffusivity in the human brain is measured by solving for ADC in Equation 3.6 above. Diffusion does not occur freely in the human brain due to restrictions of the tissue microstructure, hence the term *apparent* diffusion coefficient.

3.2.2 Diffusion Tensor

Diffusivity is best described in two conditions; isotropic and anisotropic (Figure 3.5). An isotropic environment is when diffusion occurs equally in all directions due to absence of boundaries and best depicted as a sphere. Meanwhile, an anisotropic environment is when diffusion is restricted by the presence of oriented boundaries. It is best visualized as an ellipse.

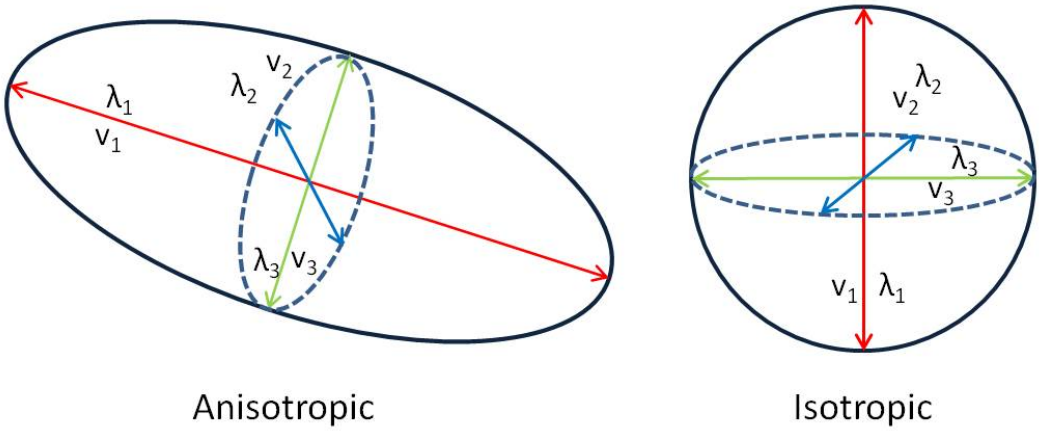

Figure 3.5: A representation of anisotropic and isotropic diffusion, along with its eigenvector components. In an anisotropic environment, the primary eigenvector direction (v_1) has an eigenvalue (λ_1) that is larger than the other eigenvalues, $\lambda_1 >> \lambda_2$ and λ_1. Whereas in an isotropic environment, diffusion occurs equally in all directions, $\lambda_1 = \lambda_2 = \lambda_3$. The eigenvectors v_1, v_2 and v_3 represent the direction of the eigenvalues λ_1, λ_2 and λ_3.

Diffusion measurement in tissue is often sensitive to the direction of the sensitizing gradient. If the gradient is applied along an axis, then the signal is sensitive only to diffusion along that direction. Diffusion tensor imaging (DTI) assumes that the

diffusivity in each voxel can be represented by magnitudes and directions that can be described by a tensor model. DTI (Basser et al. 1994) requires a minimum of 6 diffusion sensitized gradients that can estimate and calculate the tensor and is represented by a 3D ellipsoid for each voxel. The 6 diffusion-weighted gradients can be applied in any arbitrary direction; however, increasing number of in vivo studies are implementing higher number of directions. It can provide a more accurate interpretation of diffusivity in the human brain. In 3D, Equation 3.6 can be re-written as Equation 3.7 below.

$$\frac{S}{S_0} = e^{-\sum_{i=1}^{3}\sum_{j=1}^{3} b_{ij} ADC_{ij}} \qquad \text{(Equation 3.7)}$$

Equation 3.7 can be simplified and written in a 3x3 matrix,

$$ADC = \begin{bmatrix} ADC_{xx} & ADC_{xy} & ADC_{xz} \\ ADC_{yx} & ADC_{yy} & ADC_{yz} \\ ADC_{zx} & ADC_{zy} & ADC_{zz} \end{bmatrix} \qquad \text{(Equation 3.8)}$$

Then, a process called diagonalization relates the 3x3 matrix in Equation 3.8 to the eigenvalues and eigenvectors that best describes the magnitude of the longest (λ_1), middle (λ_2) and shortest (λ_3) axis of the ellipsoid, and the three eigenvectors (v_1, v_2, v_3) that describes the direction of the ellipsoid respectively (Figure 3.5). Diagonalization of the tensor is done by rotating the reference axis of the tensor to align with the ellipsoid in each voxel, where the resultant off-diagonal term is zero. The eigenvalues also

represent the scalar components of the eigenvectors and these parameters are calculated for each voxel in the image. After diagonalization, the term ADC can be written as in Equation 3.9 that includes the eigenvalue terms.

$$ADC = \begin{bmatrix} \lambda_1 & 0 & 0 \\ 0 & \lambda_2 & 0 \\ 0 & 0 & \lambda_3 \end{bmatrix} \quad \text{(Equation 3.9)}$$

The largest or the primary eigenvalue, λ_1, is also called the parallel or axial diffusivity (AD). It corresponds to the magnitude of the primary diffusion direction. The perpendicular or radial diffusivity (RD) is the average of the eigenvalues λ_2 and λ_3 and is orthogonal to the direction of the axial diffusivity.

3.2.3 Fractional Anisotropy and Mean Diffusivity

Two parameters reported in most diffusion studies are the mean diffusivity (MD) and fractional anisotropy (FA). The MD is calculated in Equation 3.10 and it is the average diffusivity measured in a voxel or region of interest, irrespective of the diffusion directions. The MD values are almost homogenous across the post-neonate brain; the highest values (appear brightest in MD image) are of the CSF (Figure 3.6).

$$MD = \frac{\lambda_1+\lambda_2+\lambda_3}{3} \quad \text{(Equation 3.10)}$$

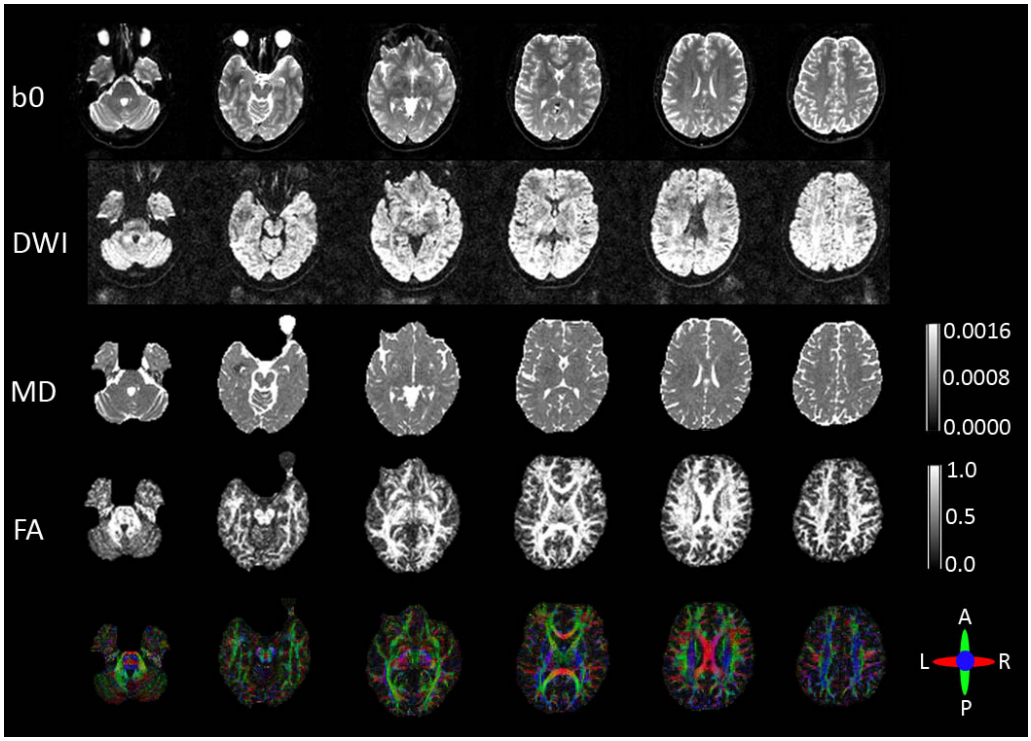

Figure 3.6: Top to bottom, axial slices of non-diffusion weighted (b_0), diffusion weighted images (DWI), mean diffusivity (MD), fractional anisotropy (FA) and colour map of the primary diffusion direction (red = right – left, green = anterior – posterior, blue = inferior – superior) in one healthy control.

The FA is calculated in Equation 3.11 and is a measure of the deviation of the three eigenvalues from their mean.

$$FA = \frac{\sqrt{3(\lambda_1 - MD)^2 + (\lambda_2 - MD)^2 + (\lambda_3 - MD)^2}}{\sqrt{2(\lambda_1{}^2 + \lambda_2{}^2 + \lambda_3{}^2)}} \qquad \text{(Equation 3.11)}$$

The FA value ranges from 0, represents a highly isotropic voxel, to 1 where the voxel is highly anisotropic. Higher FA suggests water diffusivity is anisotropic. On the other end, lower FA reflects the isotropic environment. In healthy young adults, FA varies greatly across the brain where cortical GM has low FA,

ranging about ~0.2 and slightly higher in the deep gray matter, between 0.2 and 0.39 (Bhagat et al. 2004). The FA in the subcortical WM and other major white matter structures are about 0.45 and higher. The CSF has the lowest FA in the brain (FA ~ 0.14), appearing almost black in FA images (Figure 3.6).

Coloured FA maps (Figure 3.6) provide additional information helpful to delineate particular tracts. The intensity of each voxel represents the magnitude of the anisotropy, while the colours represent the primary orientation. Red denotes that the primary orientation is left - right, blue is inferior - superior and green represents anterior - posterior direction.

There are a few methods to analyze diffusion tensor images; each method has its own advantages and disadvantages. In this dissertation, only tractography is used to delineate white matter tracts. Nonetheless, other methods such as voxel based morphometry (VBM) and tract-based spatial statistic (TBSS) have been demonstrated in the literature quite extensively (Ashburner et al. 2000; Smith et al. 2006).

3.2.4 Tractography

Tractography is a tool for researchers to visualize the white matter pathways in the human brain in vivo. The WM streamlines are reconstructed using the fractional anisotropy and the longest

eigenvector information from the tensor calculation. Tractography connects the primary direction of one voxel to another with certain restrictions to guide the connections. This method is simpler than drawing and delineating WM tracts manually. Tractography also allows for 3D visualization. Generally, there are two ways to perform fiber tracking i.e. deterministic or probabilistic tractography.

The deterministic method (Conturo et al. 1999; Jones et al. 1999; Mori et al. 1999; Basser et al. 2000) starts tracking by selecting a voxel or region as seed voxels. The direction of the connections is determined by connecting the direction of the longest eigenvector from one voxel to another. Additional constraints are placed to stop tracking. Tracking stops when a voxel has an FA of lower than user-defined threshold (e.g. 0.25) and the tracing angle (the angle between two primary eigenvectors of adjacent voxels) are larger than 60°. These restrictions allow for correct delineation of WM streamlines and excluding non-WM voxels with low anisotropy. However, drawbacks to this method rise due to the low anisotropy voxels from crossing or kissing fibers within one voxel. This occurrence is due to the poor imaging resolution and the relatively large sized voxels (1-2 mm) compared to the actual axon diameter (in the order of μm). A voxel that contains a population of several fibers (e.g. crossing of the superior

longitudinal fasciculus, corticospinal tract and the corpus callosum) that crosses one another appears to have low anisotropy with a tensor representation. Deterministic tractography is merely a reconstruction method. It does not provide a degree of confidence of the tracts reconstructed in vivo.

Probabilistic tractography (Behrens et al. 2003; Jones et al. 2005) takes into account some of the drawbacks of deterministic tractography. It is done by numerous reiteration (in the order of thousands) of the probable or likelihood direction of each voxel when connecting to adjacent voxels, hence the term probabilistic tractography. Probabilistic tractography is particularly useful to explore all possible WM connections between regions or for to study and identify new WM pathways.

CHAPTER 4 MAGNETIC RESONANCE IMAGING IN MS

The application of MRI in MS has advanced the basic understanding of MS pathology through various in vivo and ex vivo studies of the human brain and of the animal model of MS, EAE. But before iterating through previous findings from the use of MRS and DTI in MS, I will first discuss a feature of MS that is best imaged using MRI.

4.1 Lesions in MS

The most common feature in the central nervous system (CNS) of MS patients is the presence of plaques or lesions. MS lesions are focal damaged areas in the CNS with apparent inflammation, demyelination, gliosis and axonal loss. Demyelination occurs when the protective myelin sheath myelin is broken down. Remyelination of the axons may also occur in some lesions but this occurrence is limited (Filippi et al. 2011).

CNS lesions appear in many shapes and sizes (Figure 4.1). Lesions also occur in other neurological and demyelinating white matter diseases too. Hence, identifying the characteristics of lesions aids MS diagnosis, while excluding other types of possible diagnosis. Multiple ovoid shaped lesions extending from and perpendicular to the ventricles are typically seen in MS. Ovoid

shaped lesions are also called 'Dawson fingers'. These demyelinated lesions typically run along the small cerebral veins that extends from the ventricles. MS lesions can also be circular or oval in shape and are typically in the CNS, i.e. the periventricular WM, corpus callosum, cerebellum, spinal cord and the juxtacortical WM. Lesions in deep GM structures (e.g. thalamus, basal ganglia) have also been identified in MS patients (Ormerod et al. 1986). Presence of cortical GM lesions have been reported in studies using double-inversion recovery (DIR) sequence and at higher field strength (Mainero et al. 2009; Calabrese, Rocca, et al. 2010).

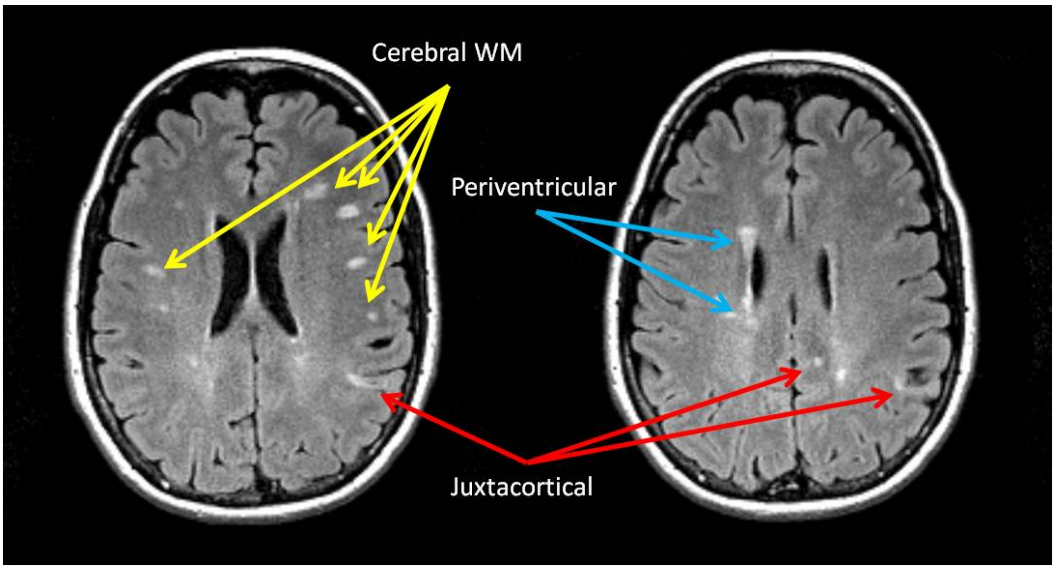

Figure 4.1: Distribution of T_2-hyperintensity lesions seen on fluid-attenuated inversion recovery (FLAIR) image. Various sized ovoid and circular shaped lesions seen in the cerebral, periventricular and juxtacortical white matter.

On clinical strength scanners (1.5T – 3.0T), lesions are easily identified using FLAIR and T_2-weighted images, where lesions appear bright or hyperintense on both images but isointense on T1-weighted images. However, black hole lesions appear hypointense (dark) on T1-weighted images and hyperintense on T2-weighted images (Figure 4.2). Black hole lesions suggest that these focal sites are associated with severe tissue damage i.e. demyelination and axonal loss (Filippi et al. 2011).

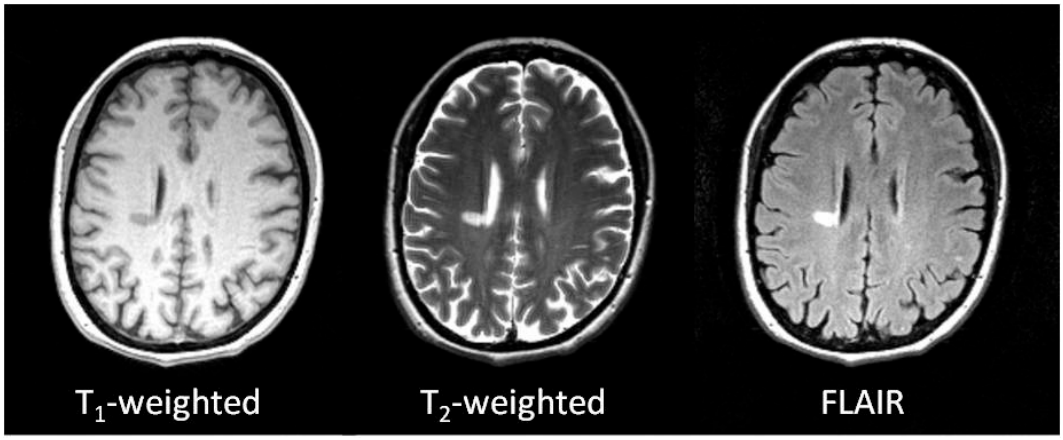

Figure 4.2: A T_1-hypointense lesion seen in the image above is also called a 'black hole'. However, black hole lesions appear hyperintense on both T_2-weighted and fluid attenuated inversion recovery (FLAIR) images.

New or active lesions can be detected on T_1-weighted images by injecting a Gadolinium (Gd) contrast agent into the patient's bloodstream before an MRI scan. Disruption of the blood-brain barrier (BBB) allows Gd to penetrate and shorten the water proton relaxation time. This effect produces a higher signal than surrounding tissue appearing like a bright ring. Enhanced lesions

may appear bright up to 6 weeks, and then slowly resolve to a smaller lesion that appears hyperintense on T_2-weighted images.

4.2 Spectroscopy in MS

MRS was used extensively to study metabolite changes in lesions, normal-appearing white matter (NAWM) and the whole brain in MS patients. Previous findings have greatly increased the understanding of MS pathology.

4.2.1 Lesions

It is widely accepted that the NAA decrease in MS lesions reflects neuronal and axonal loss. This observation was seen in lesions compared to WM in controls and is most pronounced in SPMS patients (Davie et al. 1997), though still observable in RRMS and PPMS patients. However, no noticeable differences were observed between benign patients and controls (Davie et al. 1997). Neuronal loss was particularly evident when black hole lesions were studied (He et al. 2005). A serial MRS study observed increased NAA levels in previous acute lesions. This observation could indicate two possible occurrences 1) reversible neuronal dysfunction (De Stefano et al. 1995) or, 2) previous decreased NAA was due to edema within the lesions that resolved in time (Sajja et al. 2009).

Other than NAA, alterations to other metabolite concentrations have been observed. Increased tCr and Cho levels in lesions represents glial abnormality that could possibly be a combination of inflammation, glial proliferation and axonal *de-* and *re-*myelination (Kirov et al. 2009). Gliosis was suggested as the reason for increased tCr, whereas Cho increase suggests cell membrane turnover and ongoing remyelination, especially in T1-isointense lesions (He et al. 2005).

When using shorter TE (typically ~ 35 ms) in spectroscopy, the spectrum may include signal from free lipids, lactate and myo-inositol (mI). Increased lipid and mI were observed in acute enhancing lesions (Davie et al. 1994). In about 4-8 months, the lipid signal gradually resolved to control levels, but the mI signal remained unchanged. In contrast, Narayana et al. reported that lipid was not always present in MS lesions (Narayana et al. 1998).

4.2.2 Normal-appearing White Matter

Non-lesion WM in MS patients is called 'normal-appearing white matter' (NAWM), due to its "normal" and isointense appearance on MRI images. However, NAWM is not as normal as its appearance, as one might think. Observations from spectroscopy (Rooney et al. 1997; Kapeller et al. 2001; He et al. 2005), magnetization transfer imaging and diffusion imaging

(Cercignani et al. 2001; Ciccarelli et al. 2001) studies, the microscopic tissues in NAWM is abnormal and incomparable to WM tissue in healthy individuals. Spectroscopy studies have shown that normalized NAA/tCr ratios are reduced in MS compared to controls (Kapeller et al. 2001; Chard, Griffin, Mclean, et al. 2002). Histopathology agrees with this notion and attributed it to a process secondary to axonal loss.

Increased mI (Chard, Griffin, Parker, et al. 2002; Fernando et al. 2004; Vrenken et al. 2005), Cho and tCr (Fernando et al. 2004; Vrenken et al. 2005) have also been described in NAWM across all MS phenotypes. Abnormality of these metabolites suggests similar ongoing activity as observed in lesions, i.e. increased glial cell numbers and inflammation of the tissue at microscopic level, however, not detectable at the current MRI resolution. Serial studies also found increased lipid (Narayana et al. 1998) and Cho (Narayana et al. 1998; Tartaglia et al. 2002) in NAWM that later developed into MR-visible lesion.

4.2.3 Whole-brain NAA

The diffuse pathology in MS is observed as an involvement of the NAWM. The ability of MRS to detect and measure this feature in MS argues that spectroscopy is a sensitive tool at monitoring disease progression in patients. Whole-brain NAA quantification in

MS patients has shown that axonal or neuronal loss occurs globally in the brain (Gonen et al. 2000). Whole-brain NAA was significantly decreased in PPMS (Rovaris et al. 2005), RRMS (Rigotti et al. 2012) and benign MS patients (Rigotti et al. 2011).

4.3 Diffusion in MS

Investigation of water diffusion in MS patients generally shows that FA decreases and MD increases in MS plaques and NAWM of this clinical population. A post mortem study found association between diffusivity changes in MS to demyelination and axonal loss. This is particularly true for anisotropy measures (Mottershead et al. 2003).

4.3.1 Lesions

In 1992, Larsson et al. first applied diffusion imaging to study diffusion in MS plaques. They found higher ADC in MS lesions compared to WM in healthy controls (Larsson et al. 1992) and their findings were extended to include lesions in benign and SPMS patients (Horsfield et al. 1996). The MD increment was in agreement with findings from an EAE study (Heide et al. 1993), that suggests diffusion changes reflects inflammatory demyelination in MS.

The MD was found to be higher in black hole lesions compared to enhancing and non-enhancing isointense lesions (Filippi et al. 2000). They also found no differences in MD measurements between enhancing and non-enhancing lesions. In contrast, Droogan et al. found higher ADC in enhancing lesions compared to non-enhancing lesions (Droogan et al. 1999). Discrepancy in previous findings can be attributed to the variability of 'true age' of the enhancing lesions in patients at the time of imaging. The extent of tissue damage in lesions also varies greatly between patients and within a patient. Over time, contrast enhancement in enhancing lesions disappears. Despite the inability of diffusion imaging to differentiate enhancing from non-enhancing lesions through MD measurements, Filippi et al. observed lower FA in enhancing lesions than non-enhancing lesions (Filippi et al. 2001). Hence, anisotropy could be a more sensitive measure of diffusivity changes in MS brains.

Increased MD and reduced FA in MS reflects a disorganization of the tissue structure with increased intracellular space and a disruption of the myelin and axons (Ge 2006).

4.3.3 Normal-appearing white matter

DTI has shown abnormal diffusion tensor in the peri-plaque regions, which is not observable on a conventional MRI image (Commowick et al. 2008). Guo et al. further described an abnormal outward FA pattern involving the NAWM. The outward pattern starts with low FA in lesions and increases as it spreads out to the surrounding tissue (Guo et al. 2002). Anisotropy of the infratentorial and supratentorial NAWM also differ significantly between patients and controls (Ciccarelli et al. 2001), but the MD was not different when all NAWM regions were analyzed together.

A combined study using diffusion and magnetization transfer ratio (MTR) found reduced FA in NAWM that suggests the microstructure barriers in the NAWM were disrupted (Cercignani et al. 2001). Longitudinal observation found that MD increases moderately in prelesional NAWM, then increases rapidly at time of lesion enhancement and slowly decreases after the cessation of enhancement (Werring et al. 2000).

Diffusion is altered in MS patients; increased MD and reduced FA in NAWM could reflect a few possible pathological processes in the tissue. Edema associated with inflammation, increased fluid quantity hence increasing extracellular diffusivity. Myelin degeneration of the axons removes the limiting physical

barrier of diffusivity in the perpendicular direction of the axons (Filippi et al. 2001).

4.3.4 Tractography in MS

Fiber tractography was reviewed as a potential tool that provides a measure of the degree of demyelination and axonal loss in MS lesions and NAWM (Ge et al. 2005). Tractography can be used to probe WM tracts in MS to measure the "integrity" of functional WM tracts especially in regions adjacent to lesions, which are often located in the cerebral WM.

Periventricular lesions surrounding the anterior and posterior part of the lateral ventricle often intersect fiber bundles of the corpus callosum. The corpus callosum is the largest WM structure and is formed of densely packed axons that connect the brain hemispheres. Analysis of the corpus callosum involves subdividing the entire corpus callosum into smaller sections. Most studies divide the corpus callosum into three main regions, the genu (most anterior), body (middle part) and the splenium (most posterior). In cognitively-impaired benign MS patients, Mesaros et al. found increased MD associated with the extent of increased lesion volume in corpus callosum (Mesaros et al. 2009). Increased MD and reduced FA in non-lesioned corpus callosum can partially explain the cognitive and upper-extremity dysfunction in early

RRMS (Rimkus et al. 2011) and across all MS phenotypes (Ozturk et al. 2010).

The corticospinal tract (CST) projects from the cortex through the brainstem, sending sensory and motor information down the spinal cord to the entire body. In MS patients, the CST was found to be asymmetrical in up to 50% of MS patients and increased mean, axial and perpendicular diffusivity in RRMS, PPMS and SPMS patients compared to controls (Reich et al. 2007; Ceccarelli et al. 2010; Preziosa et al. 2011). In contrast, FA was not different in any MS phenotypes compared to controls (Reich et al. 2007; Ceccarelli et al. 2010; Spanò et al. 2010). This observation could be attributed to the inability of tractography to resolve the directionality of the CST in voxels containing crossing fibers with low anisotropy. This results in a spherical shape of the tensor with low FA (Reich et al. 2007). Another possible reason is the presence of extensive demyelination as observed by increased diffusivity measures, but absence of axonal damage measured by FA (Spanò et al. 2010).

Other fiber tracts studied in MS patients include the inferior longitudinal fasciculus (ILF), uncinate fasciculus (UNF), optic radiation (OR), superior cerebellar peduncle (SCP) and the middle cerebellar peduncle (MCP) using either deterministic (Dasenbrock

et al. 2011) or probabilistic (Ceccarelli et al. 2010; Anderson et al. 2011) tractography. The MD was higher along the entire OR tract in all MS patients. The FA was found to be lower but did not reach significance in all phenotypes when compared to controls (Dasenbrock et al. 2011) except for PPMS patients (Ceccarelli et al. 2010).

Motor network dysfunction in PPMS patients measured by increased functional activation were correlated with increased MD and decreased FA of the ILF and OR tracts (Ceccarelli et al. 2010). In a group of PPMS patients, diffusivity of the MCP increased while the FA decreased in comparison to RRMS patients and controls. In the same group of PPMS patients, the FA and MD of the SCP were associated with the upper limb function and walking ability. However, no differences in the cerebellar tracts were observed between RRMS patient and control group (Anderson et al. 2011).

4.4 Imaging 'fatigue' in MS

With fatigue being the most commonly reported symptom in MS, numerous imaging studies have investigated possible causes of fatigue. An early positron emission tomography (PET) study investigated and found altered regional cerebral energy metabolism particularly in the frontal lobe and including the basal ganglia, internal capsule, the parietal, temporal and occipital lobe (Roelcke

et al. 1997). Follow-up MRI studies of the lesion load in the locations above found contradicting results in its association with fatigue (Bakshi et al. 1999; Tedeschi et al. 2007; Sepulcre et al. 2009; Morgante et al. 2011). This could be attributed to the low spatial resolution of MRI that is unable to image microscopic damages and the differences between patient selection in all studies.

One CSI study found widespread NAA/tCr decrease in the cerebral WM, which included parts of the corpus callosum (Tartaglia et al. 2004). They also found lower NAA levels that correlated with higher FSS scores in fatigue MS patients. Later, a spectroscopy study of the basal ganglia found reduced NAA/tCr in the lentiform nucleus in high fatigue patients, but not in the frontal white matter (Téllez et al. 2008).

Filippi et al. suggested that fatigue is related to a cortical-subcortical dysfunction (Filippi et al. 2002). Brain volume measurement studies revealed significant atrophy in MS patients with fatigue. Studies have shown frontal and temporal GM atrophy (Sepulcre et al. 2009), cortical atrophy in the parietal region (Pellicano et al. 2010) and atrophy of the primary sensorimotor region (Riccitelli et al. 2011). All these studies also found that GM atrophy was correlated with fatigue. Calabrese et al. also found

atrophy of the frontal-parietal white matter pathway in RRMS patients with fatigue (Calabrese, Rinaldi, et al. 2010).

Using voxelwise comparison, several regions with lower FA were found to be associated with higher fatigue score (Pardini et al. 2010). These regions include the frontal deep WM, the inferior fronto-occipital fasciculus (IFO), anterior limb of the internal capsule, anterior thalamic radiation, and the anterior cingulate bundle (Pardini et al. 2010).

All previous findings in MS patients with fatigue showed a widespread abnormality and the involvement and dysfunction of several brain regions. Nevertheless, the underlying mechanism of fatigue is still poorly understood. Patients suffering from fatigue also have sleep-related problems and reduced level of alert and wakefulness. The pontine brainstem contains a complex network composed of several groups of projecting neurons, which makes up the ascending reticular activating system (ARAS). These groups of neurons diffusely innervate the brain, including the neocortex, hippocampus, thalamus, hypothalamus and cerebellum (Chaudhuri et al. 2004). Damage to a group of nuclei in the pontine has been seen histologically in MS and EAE model (Polak et al. 2011) and in Parkinson's disease patients (Chan-Palay et al. 1989). Loder et al. also suggested that lesion formation in the brain

might cause local damage to the axons. Diffuse inflammation will inevitably cause damage to the axons that is part of the ARAS projections. This puts stress on the ARAS network causing hyperactivity that leads to failure of the system. Failure of the projection system in the brain may possibly be an effect seen by the various symptoms presented in MS patients (Loder et al. 2002).

We attempt to answer this question using spectroscopy to measure axonal or neuronal damage in the pontine brainstem. This work is presented in Chapter five of this dissertation.

4.5 Network Analysis in MS

The human brain is composed of a very complex network; at the microscale level, a brain network is composed of single neuronal elements that connects adjacent and distant cortical regions either structurally (i.e. cortico-cortical regions connected by physical axonal connections) or functionally (e.g. the language network, functionally connected distant cortical regions, but without physical direct connections). The brain network could be interpreted using advanced methodological analysis i.e. graph theoretical analysis in conjunction with structural and functional MRI data (e.g. diffusion tractography, functional MRI). This methodology has provided new measures of the human brain organization and the implications of brain diseases on the

functional and structural human brain network. The basic understanding of the graph theoretical analysis of structural and functional systems can be reviewed elsewhere (Bullmore et al. 2009; Guye et al. 2010). The main network parameters measured in our participants, are also described in the methods section of Chapter 6.

The notion that the MS phenotype is only expression of focal lesions, is no longer adequate. Network studies in MS patients have shown a whole-brain involvement through network measures of the cortical thickness and the cerebral WM. He et al. studied the correlation between lesion load and cortical thickness and they found topological reorganization of the cortical GM is associated with the WM lesion load in multiple sclerosis patients (He et al. 2009). A network analysis examining the connectivity between cerebral WM and cortical regions have observed reduced global and local network efficiencies of the cerebral WM network and were associated with clinical variables such as the EDSS, disease duration and lesion load in wide range relapsing-remitting MS patients (Shu et al. 2011). Another study assessed for direct and indirect connections between various gray and white matter regions that can be interrupted by lesion presence (Li et al. 2012). They found increased deep GM connectivity and decreased cerebral

WM connectivity particularly of the thalamus, the putamen, and in the frontal region in early RRMS patients (Li et al. 2012).

From the observations described above, lesion load and location seems to influence connectivity in MS patients even at the early stages of the disease. The widespread alterations in the brain network of MS patients were also suggested to be affected early during the disease course. My goal for my thesis was to investigate the brain network in our group of low disability RRMS patients. The lesion load in patients varies highly between subjects, even when comparing those with similar disability level. The patients were sub-grouped into low and high lesion load groups, and assessed the global and local network efficiencies between both patient groups and controls. The average shortest path length of the brain network was measured in each patient, where increased path length denotes a reorganization of the basic structural brain connectivity. This work is presented in Chapter 6.

CHAPTER 5 FATIGUE IN MULTIPLE SCLEROSIS: ASSESSING THE INVOLVEMENT OF THE PONTINE THROUGH PROTON MR SPECTROSCOPY

5.1 Introduction

Multiple sclerosis (MS) is an inflammatory disease of the central nervous system, which results in focal areas of demyelination. Multiple sclerosis is known to affect the white matter (WM) with axonal injury or loss as a common pathological feature occurring in the brain of MS patients (Filippi et al. 2010). This injury and resulting dysfunction has been observed to affect both normal appearing white matter (NAWM) and normal appearing grey matter (NAGM) even during the early course of the disease (Narayana 2005).

Fatigue has been shown to be the most common and disabling symptom, experienced by 50 to 80% of MS patients. Considering the significant impact of fatigue in MS patients, and despite the extensive research done to further our understanding of MS, the underlying pathophysiology of fatigue remains unknown (Induruwa et al. 2012).

In efforts to understand fatigue in MS, several brain regions and specific brain structures have been investigated using conventional magnetic resonance imaging (MRI), diffusion tensor

imaging (DTI), and positron emission tomography (PET) to determine whether they are associated with fatigue symptoms (Roelcke et al. 1997; Induruwa et al. 2012). One structure suggested to be involved with fatigue symptom in MS patients is the pontine brainstem, located at the base of the midbrain (Loder et al. 2002). Originating within the pontine is a complex network composed of several groups of projecting neurons, which makes up the ascending reticular activating system (ARAS). These groups of neurons diffusely innervates the brain, including the neocortex, hippocampus, thalamus, hypothalamus and cerebellum (Chaudhuri et al. 2004). The ARAS is responsible for arousal and sleep-wake cycle (Aston-jones et al. 1999) and plays an important role in responses to stress (Korf et al. 1973), attention and behaviour (Aston-jones et al. 1999). These functions are often impaired in MS patients with displays of related symptoms. It is thought that damage to structures of the ARAS in MS patients might impair its function in response to arousal and stimuli, thereby causing fatigue (Blomstrand et al. 1989; Loder et al. 2002).

Magnetic resonance spectroscopy (MRS) serves as a complimentary tool to MRI, and can be used to evaluate the neuronal integrity of the brain by examining the metabolite N-acetylaspartate (NAA). This metabolite marker is readily observed in proton MR spectra of the brain, and is found primarily in

neurons. Decreases in the concentration of NAA has been interpreted as resulting from neuronal damage or loss (Sajja et al. 2009). NAA measures are often normalized to total creatine (tCr) to yield an NAA/tCr ratio. The concentration of tCr in MS brain tissue (excluding lesion) has been debatable but is typically stable and has been considered to be unaffected by the disease process compared to controls (Narayana 2005).

Here we report proton MRS observations of metabolite concentration changes (NAA and tCr) in the pontine brainstem, which contains the ARAS nuclei for groups of relapsing-remitting MS patients with lower and higher levels of fatigue compared to a group of healthy controls. A decrease in levels of NAA in the pons would reflect metabolic dysfunction of the neurons that constitutes the ARAS impairing its regular function.

5.2 Methods

5.2.1 Participants

Nineteen women with relapsing remitting multiple sclerosis (RRMS) (ages 40±7 years, range 27-56 years) and 18 age-matched healthy women (ages 40±7 years, range 26-50 years) participated. Screening of the healthy controls ensured that none had suffered neurological conditions (e.g. epilepsy, seizures, chronic fatigue

syndrome) or psychological conditions (e.g. depression) in the past. The research study protocol was approved by the University of Alberta Health Research Ethics Board. Informed consent was obtained from all participants. In the MS group, participants with low-disability as measured by the expanded disability status scale (EDSS) scores (median: 1.5, range: 0 to 2.5) were selected, while fatigue in all participants were assessed using the fatigue severity scale. The FSS is a self-administered test with nine statements that rates the severity of fatigue symptoms from a patient's perspective; a value of 1 indicates strong disagreement and 7 indicates strong agreement with each statement. The FSS evaluates the severity of fatigue that affected one's self in the past week. MS Patients were split into low (n = 9, FSS = 22±10) or high (n = 10, FSS = 52±6) fatigue based on an FSS cutoff of 36. Fatigue and depression are highly associated in MS patients (Induruwa et al. 2012). To ensure confounding factors were removed, those suffering from depression were excluded from this study. Depression was evaluated using the Beck Depression Inventory (BDI I-II). Clinical assessments were done immediately prior to the MR scan.

5.2.2 Magnetic resonance image acquisition

All MRI data were acquired on a 1.5T Siemens. A set of MR imaging protocol was used to guide the placement of the multivoxel

proton spectroscopy (^{1}H-MRS) chemical shift imaging (CSI) matrix, such that consistent registration of the pons was achieved. Then, another set of high-resolution images was used for volume segmentation and lesion detection.

5.2.3 Chemical shift imaging

Three sets of images were used to guide the CSI volume placement. First, a T_1-weighted sagittal image was obtained to identify the brainstem, using the following parameters (slice thickness = 5 mm, TR = 199 ms, TE = 4.6 ms, flip angle = 90°, scan time = 0:50 min). Then an axial Fluid Attenuated Inversion Recovery (FLAIR) was placed perpendicular to the sagittal image and brainstem, to identify the fourth ventricle in the pons (slice thickness = 5 mm, TR = 9000 ms, TE = 106 ms, T1 = 2400 ms, scan time = 3:02 min). Finally, a coronal T_2 image was obtained by placing it perpendicular to previously described sagittal and axial images (slice thickness = 5 mm, TR = 7510, TE = 113 ms, scan time = 1:17 min)

The ^{1}H-MRS CSI data were acquired from a PRESS localized region as a 16x16 matrix (zero-filled to 32x32). The CSI parameters were: water saturated, volume thickness = 10 mm, FOV = 160x160 mm^2, acquired volume = 80x80 mm^2, voxel dimension = 5x5x10 mm^3, TR =1750 ms, TE = 135 ms, 2 averages, flip angle = 90°, scan

time = 15 min 10 sec. The CSI volume was placed in the brainstem guided by the series of images described above. First, using (Figure 5.1a) the brainstem was identified on the sagittal view and the volume was placed perpendicular to the brainstem. Next, level of the rostral pons was identified in the FLAIR image (Figure 5.1b); the volume was placed in a way so that the height of the volume was centered on the rostral pons level. On the coronal view, the volume was rotated so that the width edges were parallel to the axial slice (represented by the blue line) and volume was centered in both hemispheres (Figure 5.1c). Finally, using the axial FLAIR image, the CSI matrix was placed such that the pontine was centrally placed and the left and right floor of the fourth ventricle were each contained by one voxel at the pontine level (Figure 5.1d).

A whole brain 3D T_1-weighted image was acquired for brain segmentation, with parameters as follows: TR = 1890 ms, TE = 4.89 ms, slice thickness = 1 mm, flip angle = 15°, FOV = 256x256 mm^2, voxel dimension = 1x1x1 mm^3, number of slices = 144, scan time = 4 min 38 sec.

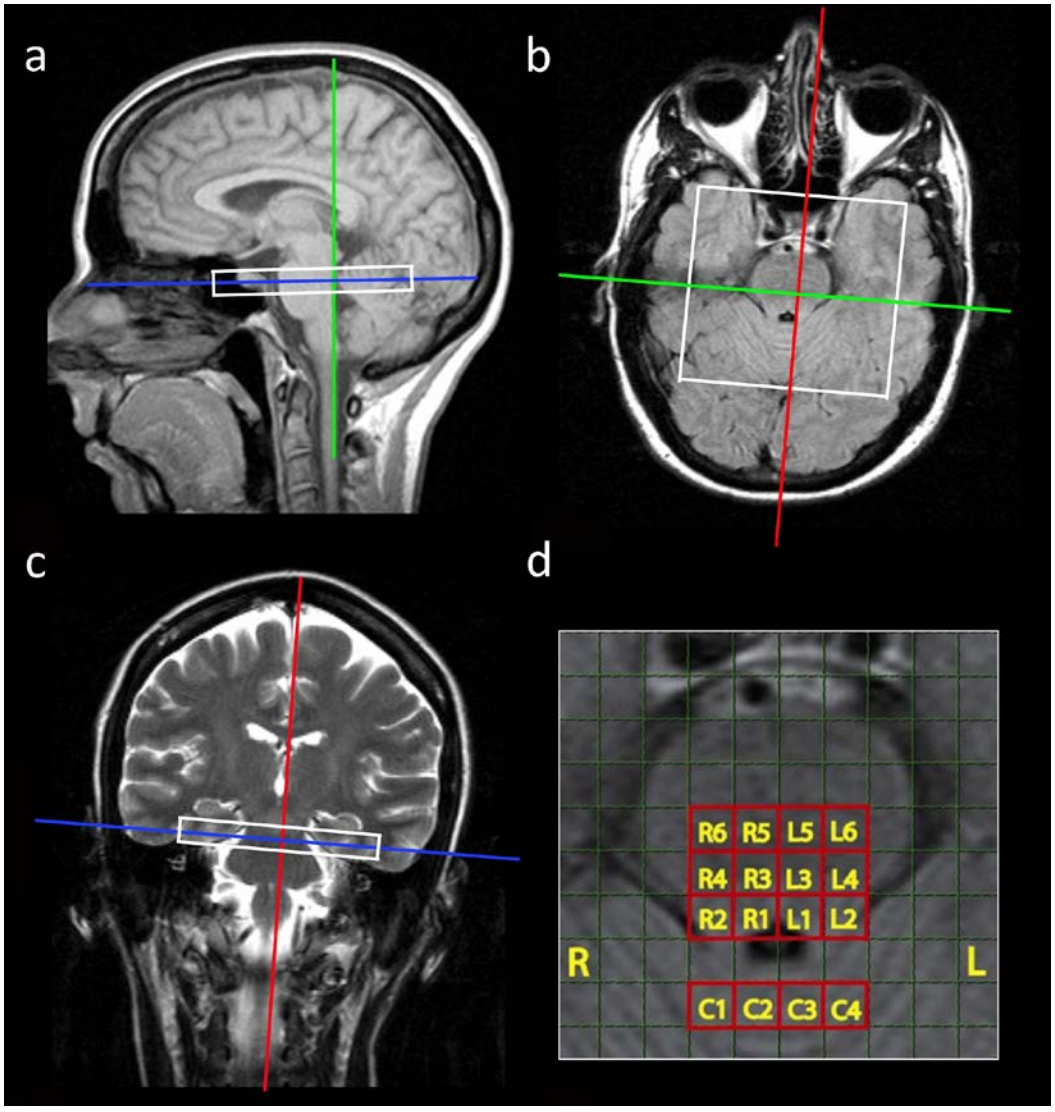

Figure 5.1: Field of view of the CSI volume (160x160x10 mm^3) placement in one subject in sagittal (a), axial (b), and coronal (c) view. Zoomed in axial view of the pons (d) in one subject, sixteen CSI target voxels in the right (R1-R6) and left (L1-L6) and 4 reference voxels in the cerebellum (C1-C4). Each voxel size is 5x5x10 mm^3

The high-resolution image was aligned to the CSI volume through systematic visual inspection in MATLAB 7.8.0 (The MathWorks, Inc Nattick, MA). To quantify the mixed composition of brain tissue in an individual CSI voxel, the high-resolution image

was also segmented into gray matter (GM), white matter (WM) and cerebrospinal fluid (CSF) using SPM8 (Wellcome Department of Cognitive Neurology, London, United Kingdom). The GM and CSF percentage in each voxel were calculated using the following equations:

$$\%GM = GM/((GM + WM)) * 100\% \quad \text{Equation 5.1}$$

$$\%\text{CSF} = CSF/((GM + WM + CSF)) * 100\% \quad \text{Equation 5.2}$$

Lesions are frequently observed in the brains of MS patients, hence we measured the lesion load (LL) in every patient. Whole-brain axial FLAIR and T_2-weighted images were used for detecting MS plaques and lesion volume calculation. Lesions were identified and drawn using an in-house semiautomated threshold intensity technique developed in MATLAB. Imaging parameters for both images were as follows: 50 slices with thickness = 2.5 mm, FOV = 256x256 mm^2, acquisition matrix = 256x256, voxel dimension = 1x1x2.5 mm^3. Additional parameters for the FLAIR image: TR = 9000 ms, TE = 97 ms, acquired in 4 min 5 sec; and the parameters for the T_2-weighted image: TR = 7200 ms, TE = 102 ms, acquired in 4 min 6 sec. Lesions were delineated on the FLAIR image and saved as a binary mask; 1 to denote lesion voxels and 0 elsewhere.

5.2.4 CSI data analysis

The CSI data from 37 subjects were analyzed using automated baseline fitting and metabolite peak quantification with LCModel (Provencher 2001). Objectively, voxels with standard deviations higher than a Cramér-Rao lower bound (Provencher 2001) of 20% were excluded from subsequent analysis. Probably due to excessive patient motion 5 entire datasets were rejected (3 controls and 2 patients), as well as several voxels from the remaining 33 subjects. The numbers of subjects, whose data are contributing to the final CSI matrix summary, as well as the mean % SD of the fit, are illustrated in Figure 5.2. The remaining numbers of subjects in each group were: 15 controls, 7 low fatigue and 10 high fatigue.

Sixteen voxels from the CSI matrix were selected for final analyses; six voxels were located in the right pons, six in the left pons and four in the cerebellum (Figure 5.1d). To correct for partial volume effect, we corrected each metabolite (NAA and tCr) concentration for CSF contents in all 16 voxels according to Equation 5.3 (Weber-Fahr et al. 2002) below.

$$S = S_0/(1 - \%CSF/100) \qquad \text{Equation 5.3}$$

where S_0 is the uncorrected metabolite concentration in one voxel, CSF is the percentage of CSF content measured using Equation 5.2, and S is the corrected metabolite concentration in that voxel.

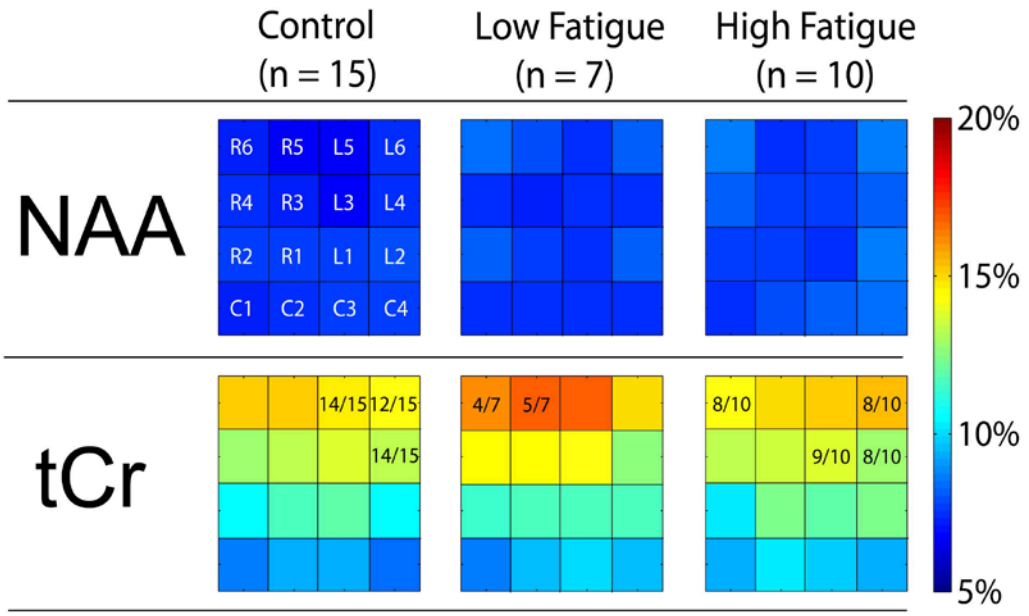

Figure 5.2: A color map of the mean standard deviation (SD) distribution produced from the LCModel fit for NAA and tCr; SD higher than the Cramer-Rao lower bound (i.e. > 20%) are excluded from further analysis. The fraction in tCr voxels shows the number of subjects included in the statistical analysis per total number of subjects in the group, if empty, the voxel included the concentration from all subjects in the group.

The NAA/tCr ratio was calculated in all 16 voxels. Additionally, NAA and tCr values from voxels 1-6 (left/right pons) were normalized to the average NAA or tCr that was measured for the 4 voxels in the cerebellum (Cb) (C1-C4) to yield an NAA/NAA_{Cb} or tCr/tCr_{Cb} ratio to examine whether changes in pons NAA or tCr were driving changes in the NAA/tCr ratio.

5.2.5 Statistical analysis

Analysis of variance (ANOVA) with %GM as covariate was used to compare NAA/tCr ratio between all groups (Van Au Duong et al. 2007). Only NAA/tCr ratio comparisons that reached statistical differences from ANOVA analysis above, was then the NAA/NAA_{Cb} and tCr/tCr_{Cb} were subsequently examined. Only comparisons that reached statistical significance at $p<0.05$ after FDR correction reported below.

Mann-Whitney test was used to compare lesion load, EDSS and age between high fatigue and low fatigue group. Pearson's correlation analysis was used to correlate fatigue scores (FSS) with disability measures (EDSS) and white matter LL in both patient groups.

5.3 Results

There was no significant difference between MS patients in low and high fatigue groups with respect to age and EDSS (Table 5.1). Fatigue score was significantly different between MS patients in low and high fatigue group ($p<0.0001$) (Table 5.1); additionally fatigue score was not different between low fatigue group and controls (22±10 and 18±5 respectively). Lesion load was highly variable between patients and was not significantly different between low and high fatigue groups (Figure 5.3). Correlation

analysis in both patient groups did not reveal any significant association between EDSS, FSS and LL.

Table 5.1: Characteristics of controls, low fatigue and high fatigue patient groups, and P-values from Mann-Whitney test between both patient groups.

Characteristics	Controls (n=15)	Low Fatigue (n=7)	High Fatigue (n=10)	P-value
Mean Age (years)	38 ± 7 (26 - 49)	38 ± 5 (29 - 43)	42 ± 8 (29 - 56)	> 0.4
Median EDSS	-	1.5 (1 .0– 1.5)	1.8 (1 .0– 2.5)	> 0.2
Range Lesion Load (cm^3)	-	0.15 - 16.25	0.44 - 37.17	> 0.8
Fatigue Severity Scale	18 ± 4 (13 – 26)	22 ± 9 (11 – 34)	52 ± 6 (42 - 59)	< 0.0001

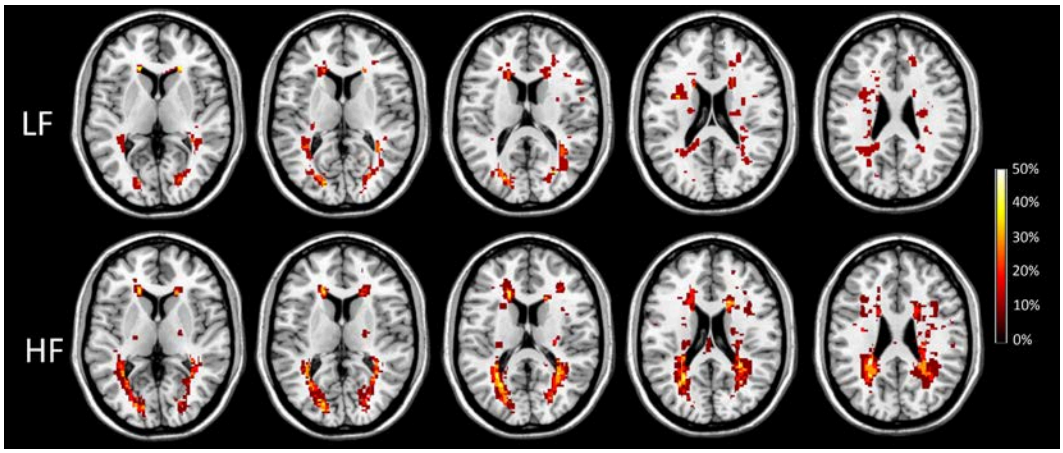

Figure 5.3: A lesion distribution map of RRMS patients in the low (top) and high fatigue (bottom) group. The percentage of subjects contributing to the lesion is shown on the color bar.

Color maps of the NAA/tCr ratio in all 16 voxels in low and high fatigue patient groups and controls are shown below in Figure 5.4.

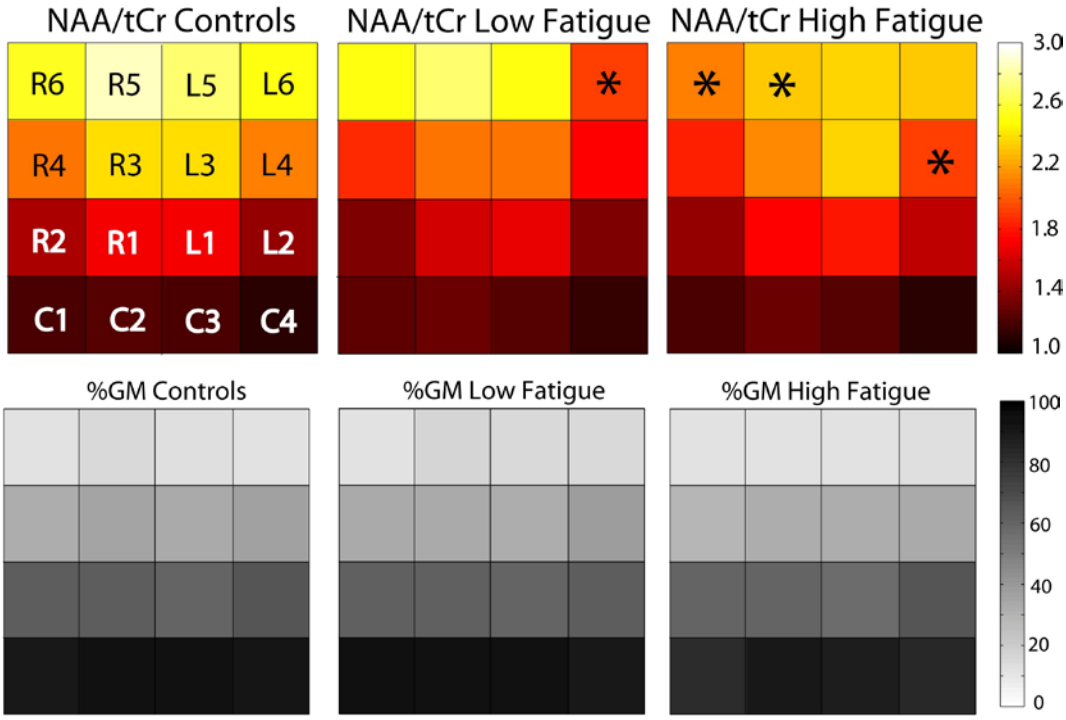

Figure 5.4: Color map showing the NAA/tCr ratio and the GM composition in the selected voxels in both patient groups and controls. Voxels in patient groups with significant comparisons to control group are marked with an asterisk (*).

In the pons, NAA/tCr was significantly lower in L4 and R5-R6 in high fatigue when compared to controls. In addition, L6 was significantly lower in low fatigue patients compared to controls (Figure 5.5).

Voxels with statistically different NAA/tCr ratio were subsequently examined for changes in NAA/NAA_{Cb} and tCr/tCr_{Cb}

ratio. A 12% increase in tCr/tCr_{Cb} ratio was observed in both L4 and R6 in high fatigue (0.75 ± 0.19, 0.67 ± 0.20) compared to controls (0.60 ± 0.13, 0.53 ± 0.10). Additionally, a 21% increase in tCr/tCr_{Cb} ratio was observed in L6 in low fatigue (0.63 ± 0.16) compared to controls (0.50 ± 0.09). There were no differences in NAA/NAA_{Cb} ratio in all voxels between patient groups and controls. The analyses for tCr/tCr_{Cb} ratio were repeated by including subjects' age as an additional covariate, however a similar level of significant difference remained.

5.4 Discussion

Our observations suggest an involvement of the tegmental pontine in MS patients with higher levels of fatigue. We observed lower NAA/tCr levels in MS patients suffering from fatigue compared to controls. Further investigation suggested that lower levels of NAA/tCr were driven by increases in tCr rather than lower levels of NAA. The analysis was also repeated with age as added covariate, as tCr levels increases with age (Chang et al. 1996). These findings remained significant even after removing the effects of age.

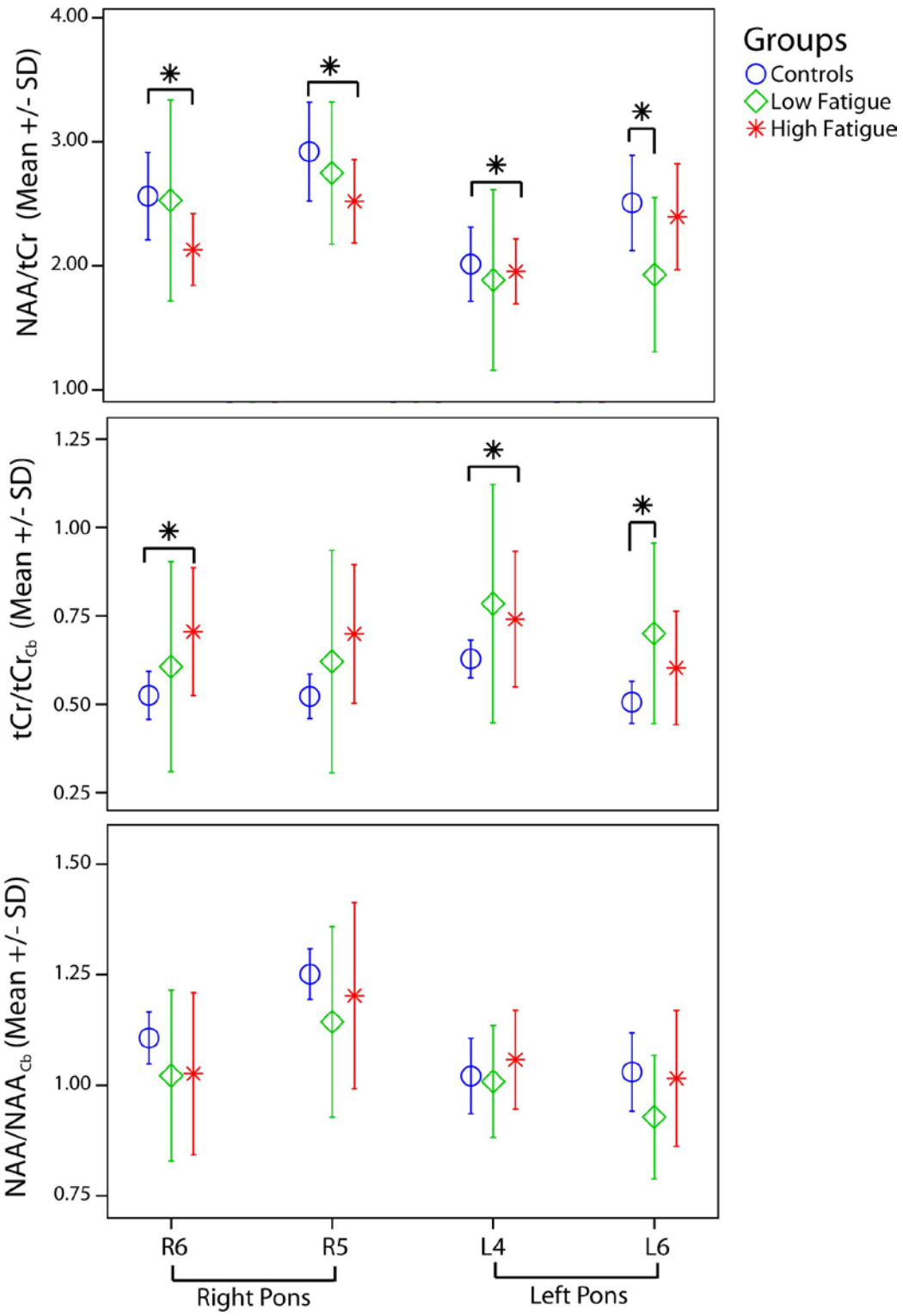

Figure 5.5: Mean plots showing the NAA/tCr, NAA/NAA_{Cb} and tCr/tCr_{Cb} in voxels with significant difference group comparisons i.e. R6, R5, L4 and L6. Significant comparisons are marked with an asterisk (*).

We investigated which metabolite was driving the change in NAA/tCr ratio, NAA or tCr. To do so, we normalized metabolite levels in the pontine to metabolite levels in the cerebellum, i.e NAA to NAA_{Cb} and tCr to tCr_{Cb}. We chose the voxels in the cerebellum given that this structure was in the CSI-PRESS box, easily identified and consistent between participants. Additionally, the NAA/tCr ratio in these voxels (C1-C4) was stable and was not significantly different between any groups (Figure 5.4).

Our results showed increased levels of tCr, which in MS patients could indicate abnormality of the glial cells (Suhy et al. 2000; Kirov et al. 2009). The tCr signal measured, which resonates at ~ 3.0 ppm, contains contributions from both creatine (Cr) and phosphocreatine (PCr). Cr and PCr is found in all cell types with higher concentration found in glial cells compared to neurons, especially in astrocytes and oligodendrocytes (Urenjak et al. 1993). Ke et al. found that the MRS measured tCr signal decay is biexponential since Cr and PCr have different transverse relaxation times (T_2 for PCr is significantly shorter than Cr). Therefore under high metabolic demand, where the PCr, Cr equilibrium is disturbed in favour of Cr, the effect on the 3.0 ppm signal results in TE dependant signal increase (Ke et al. 2002). A ^{31}P spectroscopy study observed increased PCr in MS patients suggested to

represent metabolic dysfunction in the NAWM (Husted et al. 1994; Steen et al. 2010).

However, another possible explanation to increased tCr levels could be attributed to gliosis as previously observed in cerebral NAWM and lesions using MRS (Suhy et al. 2000; Vrenken et al. 2005; Kirov et al. 2009; Hattingen et al. 2011), within patients early in the disease course, regardless of immunomodulatory treatment (Fernando et al. 2004; Kirov et al. 2009). Absolute quantification of Cr and PCr using concurrent ^{1}H and ^{31}P spectroscopy in NAWM at the level of centrum semiovale (including parts of the corpus callosum) observed increased tCr in MS patients and also suggested glial proliferation (Hattingen et al. 2011). They observed unchanged PCr to tCr ratio and indifferent NAA concentration in non-lesion voxels in patients compared to controls (Hattingen et al. 2011). Glial proliferation in cerebral NAWM has been observed ex-vivo (Moll et al. 2011) and in agreement with observations from histological studies (Winterfeld et al. 1977; Newcombe et al. 1980; Newcombe et al. 1986).

Many theories and hypotheses have been formulated to understand the underlying pathophysiology of fatigue. Damage to the ARAS has been proposed to play a role in fatigue (Blomstrand et al. 1989; Staub et al. 2001). The ARAS originates in the

brainstem and is connected to the neocortex (projecting frontally), thalamus and hypothalamus (Posner et al. 1990). It was suggested that dysfunction from within the originating region of the ARAS will influence functions of the diffused sites (Loder et al. 2002). In our study, tCr increase was observed in the tegmental pontine in high fatigue MS patients. A previous spectroscopy study suggested axonal damage in the right rostral dorsal pons in MS patients with selective attention deficit and low disability (Gadea et al. 2004); fatigue and attention is also known to be highly associated in MS patients (Induruwa et al. 2012).

It has been suggested that the underlying cause of fatigue is the functional and structural dysfunction between the frontal cortex with deep gray structures including basal ganglia and thalamus (Pardini et al. 2010). An MRS study attributed dysfunction of the basal ganglia, specifically of the lentiform nucleus, to the development of fatigue in MS patients (Téllez et al. 2008). A significant correlation was found between altered white matter integrity, by diffusion imaging, of the frontal cortex with its projections to the occipital, striatal, frontal and limbic network with fatigue perception in their MS patients (Pardini et al. 2010). A functional MRI study observed increased activations in the frontal, thalamus and caudate (Rocca et al. 2007). Together, all these observations suggest that the underlying mechanism of fatigue in

MS is not focal and involves many brain regions diffusedly inter-connected. Results from previous studies together with ours suggest that there may be a relationship between the structural and functional dysfunction of the ARAS and all the structures and brain regions to which the ARAS diffusely projects.

5.5 Conclusion

In conclusion, we used proton MRS to study brain metabolites in the pontine brainstem in relapsing-remitting MS patients with low disability and suffering from a range of levels of fatigue. We found a lower NAA/tCr ratio in several regions of the pons, and the change in this ratio was driven by elevation of the tCr levels in high fatigue patients compared to controls. Increased tCr levels possibly reflect increased glial cell numbers in those regions and may suggest an energy metabolic dysfunction of the pontine region in patients with fatigue.

CHAPTER 6 ALTERED WHITE MATTER CONNECTIVITY IN LOW DISABILITY RRMS PATIENTS WITH HIGH LESION[1]

6.1 Introduction

Brain network analysis have revealed structural connectivity patterns and topological organization of the cortical gray matter (GM) in healthy individuals (He et al. 2007; Gong et al. 2009). Structural network analysis combines diffusion tractography and graph theoretical analysis to study the cerebral WM and cortical regions and to probe the cerebral WM connectivity (Hagmann et al. 2007; Iturria-Medina et al. 2007; Gong et al. 2009). Simulated lesions located in hubs of healthy controls were shown to impair the global and local network efficiency (Gong et al. 2009) Previous network analysis of the cerebral white matter in RRMS patients group with wide-range disability have shown reduced global and

---

[1] A version of this work has been published. Hazlin Zaini, Zhang Chen, Min Liu, Fabrizio Giuliani, Chris Hanstock, Christian Beaulieu. Altered white matter connectivity between early Relapsing-Remitting Multiple Sclerosis patients, Abstract # 3610. Proceedings of the International Society for Magnetic Resonance in Medicine, 21st Annual Meeting, Salt Lake City, UT

local network efficiency that correlated with clinical variables such as expanded disability status scale (EDSS), disease duration and lesion load (Shu et al. 2011). Another study found increased deep gray matter connectivity and decreased regional cerebral white matter connectivity in early RRMS patients with increased lesion load in a group of RRMS patients (Li et al. 2012).

Lesion load (LL) varies greatly between MS patients, even in early-diagnosed patients. Understanding the degree that LL affects the structural network efficiency of this 'early' group of patients may provide insightful information on disease progression. Using graph theoretical analysis and diffusion tractography to investigate the cerebral WM structural network in early RRMS patients, we hypothesized that patients with low disability and high LL would have reduced local and global network efficiency and increased average path length when compared with either low LL or controls.

6.2 Methods

6.2.1 Participants

Our study included 19 women with RRMS (median EDSS = 1.5; 40±8 years) and 18 healthy women (39 ± 7 years). MS patients were recruited through the MS clinic at the University of Alberta Hospital. The Expanded Disability Status Scale (EDSS) was

assessed immediately prior to the MR scan. Only patients with mild functional disability (EDSS scores up to and including 2.5) were included in our study. Depression was evaluated using the Beck Depression Inventory (BDI I-II) and those suffering from depression were excluded from this study. Clinical assessments were done immediately prior to the MR scan. Control subjects were recruited through on-campus advertising and word of mouth. Screening of the healthy controls ensured that none had history of neurological and/or psychological diseases (e.g.: epilepsy, amyotrophic lateral sclerosis, depression). Written informed consent was obtained from every individual. The research protocol was approved by the University of Alberta Health Research Ethics Board.

6.2.2 Data Acquisition

All MRI images were acquired on a 1.5T Siemens Sonata. Total scan time was approximately 19 minutes that included whole brain coverage of diffusion tensor imaging (DTI), fluid-attenuated inversion recovery (FLAIR), T_2-weighted and high resolution T_1-weighted images. The imaging parameters for the axial images above are as follows: DTI - 50 slices, voxel dimension = 2x2x2.5 mm^3, TR = 7100 ms, TE = 95 ms, 12 diffusion directions with b = 1000 s/mm^2, one un-weighted diffusion image, 4 averages, scan

time = 6:32 min; FLAIR - 50 slices, voxel dimension = 1x1x2.5 mm^3, TR = 9000 ms, TE = 97 ms; T_2-weighted - 50 slices, voxel dimension = 1x1x2.5 mm^3, TR = 7200 ms, TE = 102 ms, 2 averages, scan time = 4:05 min; High resolution T_1-weighted - voxel dimension = 1x1x1 mm^3, TR = 1890 ms, TE = 4.38 ms, scan time = 4:38 min.

6.2.3 T_2 White Matter Lesion

Both FLAIR and T_2-weighted images were used for detecting hyperintense MS plaques and calculating LL. Lesions were delineated using an in-house semiautomated region-growing tool developed in. MATLAB 7.8.0 (The MathWorks, Inc Nattick, MA). Then, a binary lesion mask was obtained for each patient with a value of 1 to mark lesion voxels and 0 otherwise. To account for head size variation and orientation between subjects, the T_1-weighted images from every individual were normalized to the ICBM152 T_1 template (Montreal Neurological Institute) using SPM8 nonlinear transformation (Wellcome Department of Cognitive Neurology, London, United Kingdom). Then, we applied the inverse transformation matrix to the lesion mask. We visually inspect the normalization results to ensure the transformation process was valid. Normalized lesion location was obtained for each patient after the transformation. Patients were grouped into low (n = 9) or

high LL (n = 10) group, based on LL cutoff of 2 cm^3. Note that there is no definitive way to characterize a patient as 'low' or 'high' LL. Our approach allowed us to divide the patients into two groups with similar number of patients in low and high LL group (Table 6.1).

Table 6.1: Demographics and clinical characteristics of the participants.

Characteristics	Controls	Low-LL (n=9)	High-LL
Mean age (years)	39 ± 7 (26-50)	40 ± 6 (27-46)	40 ± 9 (29-56)
Range EDSS (median)	-	0 - 2.0 (1.5)	1.5 - 2.5 (1.5)
Range WMLL (cm^3)	-	0.06 – 2.0	3.7 - 37.2

6.2.4 Network Construction

Before we can construct the brain network, several preprocessing steps were carried out on the DTI images. First, non-brain tissue was removed from the baseline image (*b*-value = 0) for each individual. Then, the resultant brain mask was applied to all diffusion-weighted images. Subsequently, we applied eddy-current and motion correction to the diffusion images to account for distortions and any head movements using FMRIB's Diffusion Toolbox (FSL, www.fmrib.ox.ac.uk/fsl). For each voxel, the diffusion tensor ellipsoid was calculated and the diffusion coefficients and direction was obtained by solving the Stejskal and Tanner equation (Basser et al. 1994). Fractional anisotropy (FA) was calculated for every voxel. Then, we applied a deterministic

fiber tracking algorithm (FACT) to obtain streamlines of the whole brain (Mori et al. 1999). During this step, all WM voxels were selected as seed voxels to start fiber tracking, and tracking stopped if any one of the following occurred; the trace reached a voxel with a FA value less than 0.25, a voxel was classified as 'non white-matter' or if the trace angle was larger than 45°.

The fundamental components of a brain network analysis are the nodes and edges. The definition and construction of these nodes and edges made use of the following procedures. Using SPM8, the baseline image was co-registered to respective T_1-weighted image. The T_1-weighted image was non-linearly warped into the Anatomical Automatic Labeling (AAL) template (Tzourio-Mazoyer et al. 2002). Inverse transformation was applied to warp the AAL template back to subject space and 78 anatomical brain regions (Table 6.2) were extracted according to the AAL template (Gong et al. 2009). This image was subsequently used to define the nodes in the brain network for individual subjects. To define the network edges, we extracted the fiber bundles from tractography data that connects the 78 anatomical regions defined above. To characterize two nodes as connected, both regions must be connected by a minimum number (FN) of 3 fibers (Shu et al. 2009). A region-to-region connecting weight function was applied, defined by FA x FN normalized by the volume of the cortical region in each

subject defined by the AAL template after transformation. A symmetrical 78 x 78 association matrix that included all nodes and edges with a weighted function represents the resultant graph (Figure 6.1).

Table 6.2: Seventy-eight (78) cortical regions defined as nodes in the study. Note that all odd index numbers refer to regions in the left hemisphere, and even index numbers to the right hemisphere.

Index	**Cortical Region**	**Abbreviation**
1,2	Precentral gyrus	PreCG
3,4	Superior frontal gyrus, dorsolateral	SFGdor
5,6	Supeiror frontal gyrus, orbital part	ORBsup
7,8	Middle frontal gyrus	MFG
9,10	Middle frontal gyrus orbital part	ROBmid
11,12	Inferior frontal gyrus, opercular part	IFGoperc
13,14	Inferior frontal gyrus, triangular part	IFGtriang
15,16	Inferior frontal gyrus, orbital part	ORBinf
17,18	Rolandic operculum	ROL
19,20	Supplementary motor area	SMA
21,22	Olfactory Cortex	OLF
23,24	Superior frontal gyrus, medial	SFGmed
25,26	Superior frontal gyrus, medial orbital	ORBsupmed
27,28	Gyrus Rectus	REC
29,30	Insula	INS
31,32	Anterior cingulate and paracingulate gyri	ACG
33,34	Median cingulate and paracingulate gyri	DCG
35,36	Posterior cingulate gyrus	PCG
37,38	Parahippocampal gyrus	PHG
39,40	Calcarine fissure and surrounding cortex	CAL
41,42	Cuneus	CUN
43,44	Lingual gyrus	LING
45,46	Superior occipital gyrus	SOG
47,48	Middle occipital gyrus	MOG
49,50	Inferior occipital gyrus	IOG
51,52	Fusiform gyrus	FFG
53,54	Postcentral gyrus	PoCG
55,56	Superior parietal gyrus	SPG
57,58	Inferior parietal, but angular gyri angular gyri	IPL
59,60	Supramarginal gyrus	SMG

Index	Cortical Region	Abbreviation
61,62	Angular gyrus	ANG
63,64	Precuneus	PCUN
65,66	Paracentral lobule	PCL
67,68	Heschl gyrus	HES
69,70	Superior temporal gyrus	STG
71,72	Temporal pole: superior temporal gyrus	TPOsup
73,74	Middle temporal gyrus	MTG
75,76	Temporal pole: middle temporal gyrus	TPOmid
77,78	Inferior temporal gyrus	ITG

6.2.5 Network Measures

For an individual network, different characteristics were defined and calculated as the following. Connectivity is defined by the shortest distance traveled (means of edges) along a path to get from one node to another. An increased path length indicates increased effort to preserve structural function. To measure the network connectivity with N number of nodes, the average shortest path length, L_p, (Watts et al. 1998) is computed,

$$L_p = \frac{1}{N(N-1)} \sum_{ij} d(i,j), i \neq j \qquad \text{Equation 6.1}$$

Clustering coefficient (*CC*) measures the local connectivity of a node with its surrounding neighbourhood. Network *CC* is the average *CC* at all nodes,

$$CC = \frac{\sum \Gamma_i}{\sum deg_i (deg_i - 1)} \qquad \text{Equation 6.2}$$

where, deg_i is the number of neighbours at node i and $\mathbf{\Gamma}_i$ is the number of edges connected to that node.

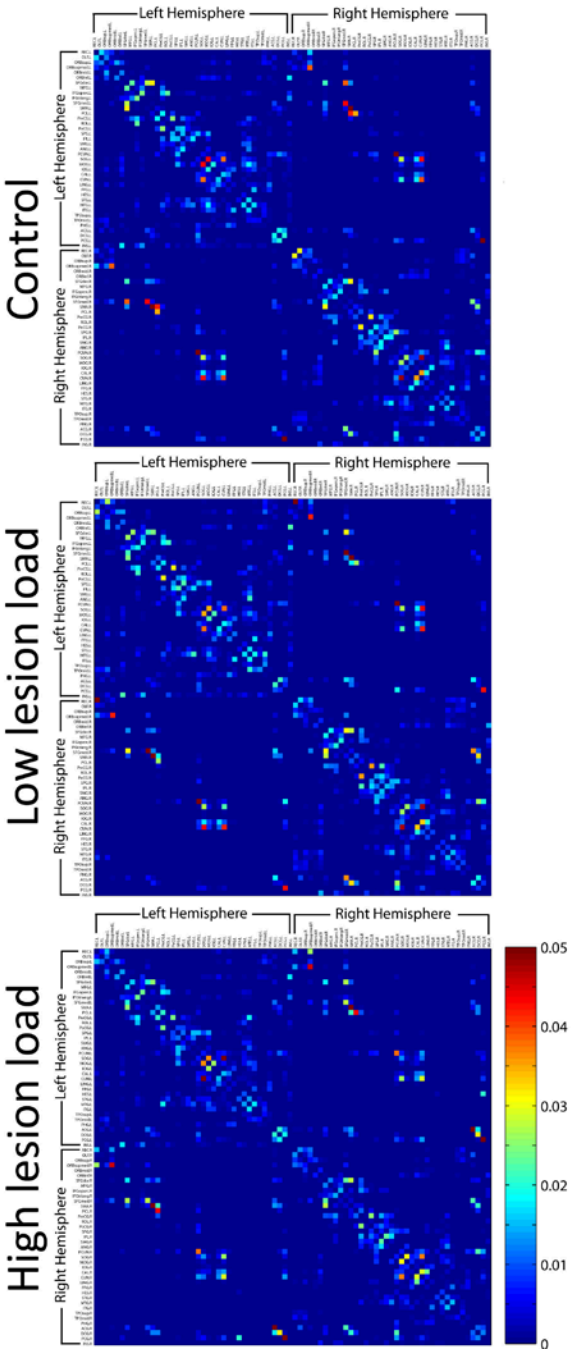

Figure 6.1: The average network matrix that represents 78 anatomical cortical regions (symmetrical 78x78 matrix) in controls, low and high lesion load groups. The matrix for each group was constructed by averaging matrices from all individuals in that group. The colorbar represents the average strength connectivity between any pair of nodes in the group average matrix.

Measures from CC and L_p are normalized to the metrics from 1000 random network metrics of equal degree as the brain network under study,

$$Gamma\ (\gamma) = CC/CC_{rand} \quad \text{Equation 6.3}$$

$$Lambda\ (\lambda) = L_p/L_{rand} \quad \text{Equation 6.4}$$

These small-world network parameters provide a measure of validity to the white matter connectivity network. The global network efficiency, E_{glob}, (Latora et al. 2001) measures the connectivity efficiency of the entire network within an individual. It makes use of the shortest path length information while taking into account inexistence pathways in the network. Calculation from a pair of nodes without a connection would result in an infinite connectivity, however, E_{glob} uses the reciprocal from the path length calculation of two nodes. Inexistence pathways would result in 0,

$$E_{glob} = \frac{1}{N(N-1)} \sum_{i \neq j} \frac{1}{L_{i,j}} \quad \text{Equation 6.5}$$

In addition, we calculate the average local network efficiency (Latora et al. 2001),

$$E_{loc} = \frac{1}{N} \sum_{i \in G} E_{glob}(G_i) \quad \text{Equation 6.6}$$

where G_i measures the average connectivity efficiency of each node i with its nearest neighbouring nodes. Another network

characteristic measured in our participants is the regional efficiency, E_{reg} (Achard et al. 2006), which computes the connectivity efficiency of each node i with all nodes in the network.

$$E_{reg} = \frac{1}{N-1}\sum_{i \neq j \in G} \frac{1}{L_{i,j}} \quad \text{Equation 6.7}$$

6.2.6 Statistical analysis

To determine if there were significant differences in the structural network between our patient groups and controls, we used univariate analysis to compare the network parameters (E_{glob}, E_{loc}, E_{reg}, L_p, CC) with age effects removed. We used Pearson's correlation test to investigate for possible associations between the network parameters (E_{glob}, E_{loc}, E_{reg}, L_p, CC) with clinical parameters (LL, EDSS) in the patients group. We applied the false discovery rate (FDR) correction to correct for multiple comparisons (Hochberg et al. 1990; Benjamini et al. 2000). Only significant results with $p < 0.05$ after correction were reported below.

6.3 Results

Mean age and median EDSS were similar between low (40 ± 6 years, EDSS: 1.5) and high (40 ± 9 years, EDSS = 1.5) LL groups. Normalized lesion volume ranged between 0.06 – 2.0 cm^3 in the low and 3.7 – 37.2 mm^3 in the high load group (Figure 6.2).

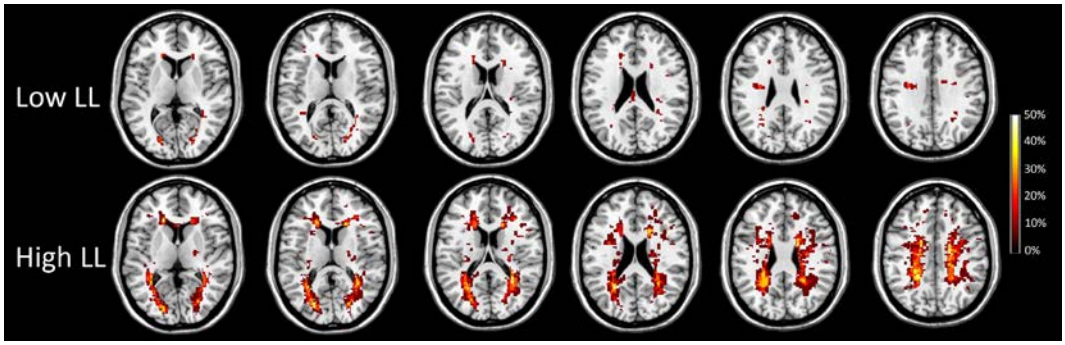

Figure 6.2: The mean normalized WM lesion distribution map of RRMS patients in the low lesion load (top) and the high lesion load (bottom) group, overlaid on the ICBM 152 T1 template. The colorbar shows the percentage of patients within patient group having lesion-marked voxels.

The WM structural network in both control and patient groups exhibited small-world properties. Gamma (CC/CC_{rand}, Controls = 3.09 ± 0.28, low LL = 3.59 ± 1.06, high LL= 3.31 ± 0.52) displayed a higher clustering coefficient, while lambda (L_p/L_{rand}, Controls = 1.17 ± 0.04, low LL = 1.17 ± 0.03, high LL = 1.17 ± 0.06) displayed similar path length compared to 1000 randomized networks. In general, a small-world network would demonstrate gamma (CC/CC_{rand}) > 1, while lambda (L_p/L_{rand}) ≈ 1.

In agreement with our hypothesis, the high LL group showed significantly decreased global (controls = 0.79 ± 0.06, high LL= 0.69 ± 0.14, p = 0.019) and local (controls= 1.15 ± 0.07, high LL = 1.06 ± 0.13, p = 0.028) network efficiency, with increased shortest path length (controls = 1.27 ± 0.09, high LL = 1.51 ± 0.36, p = 0.015) when compared to controls. There were no regional

efficiency differences between any of the group comparisons. There were also no differences between the low LL group and controls or high LL group (Figure 6.3).

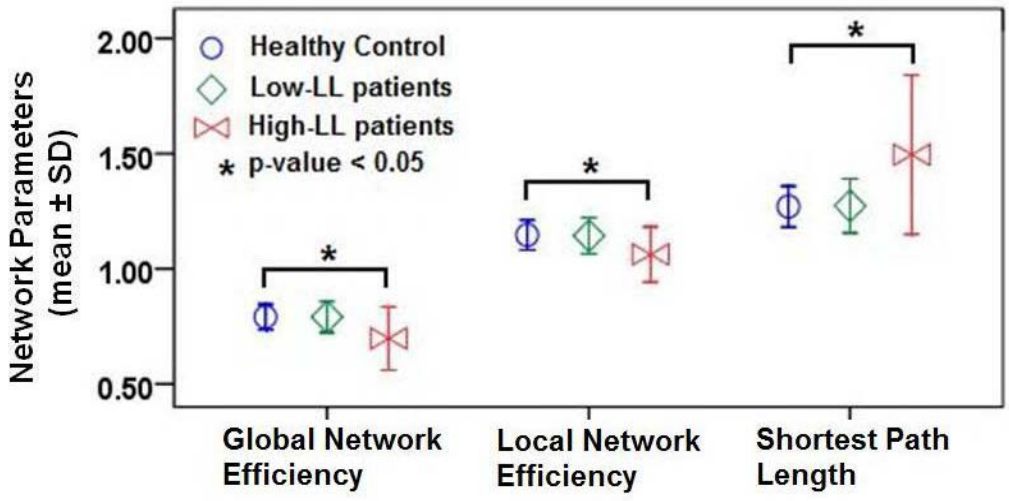

Figure 6.3: Mean plots of global and local network efficiency and shortest path length in controls and both MS patient groups. Only pair comparisons showing a significant difference ($p < 0.05$, FDR) between two groups are marked '*'.

MS patients were analyzed together in a Pearson's correlation analysis revealing significant correlations between lesion load and global network efficiency ($\rho = -0.601$, $p = 0.007$), local network efficiency ($\rho = -0.534$, $p = 0.018$) and shortest path length ($\rho = 0.557$, $p = 0.013$). In addition, significant inverse correlations were identified between lesion load and regional efficiency of nineteen nodes: left ORBmid, bilateral ORBinf, right ORBsupmed, bilateral PCUN, right SOG, bilateral CUN, bilateral MOG, bilateral LING, bilateral FFG, left ITG, left PHG, right MTG

and right STG (Figure 6.4). No correlation was found between EDSS with any network parameters in the patient groups. Additionally, lesion load was not correlated to EDSS scores when patients were analyzed at subgroup (low and high LL) or group level ($p > 0.05$).

6.4 Discussion

Employing the graph theoretical analysis, we demonstrated the robustness of this methodology to study the cerebral WM structural network in RRMS patients with low disability and varying lesion load. In support of our hypothesis, our findings indicate a more profound disruption of the WM structural connectivity in our group of RRMS patients with high LL, while the brain connectivity in our low LL patients group remained intact or preserved. Our results include disrupted global white matter network, reduced local white matter connectivity and increased average path length in high LL MS patients. Correlation analysis in our patients group revealed significant associations between lesion load and the global network efficiency, local network efficiency, average path length and regional efficiency in nineteen regions in the white matter network.

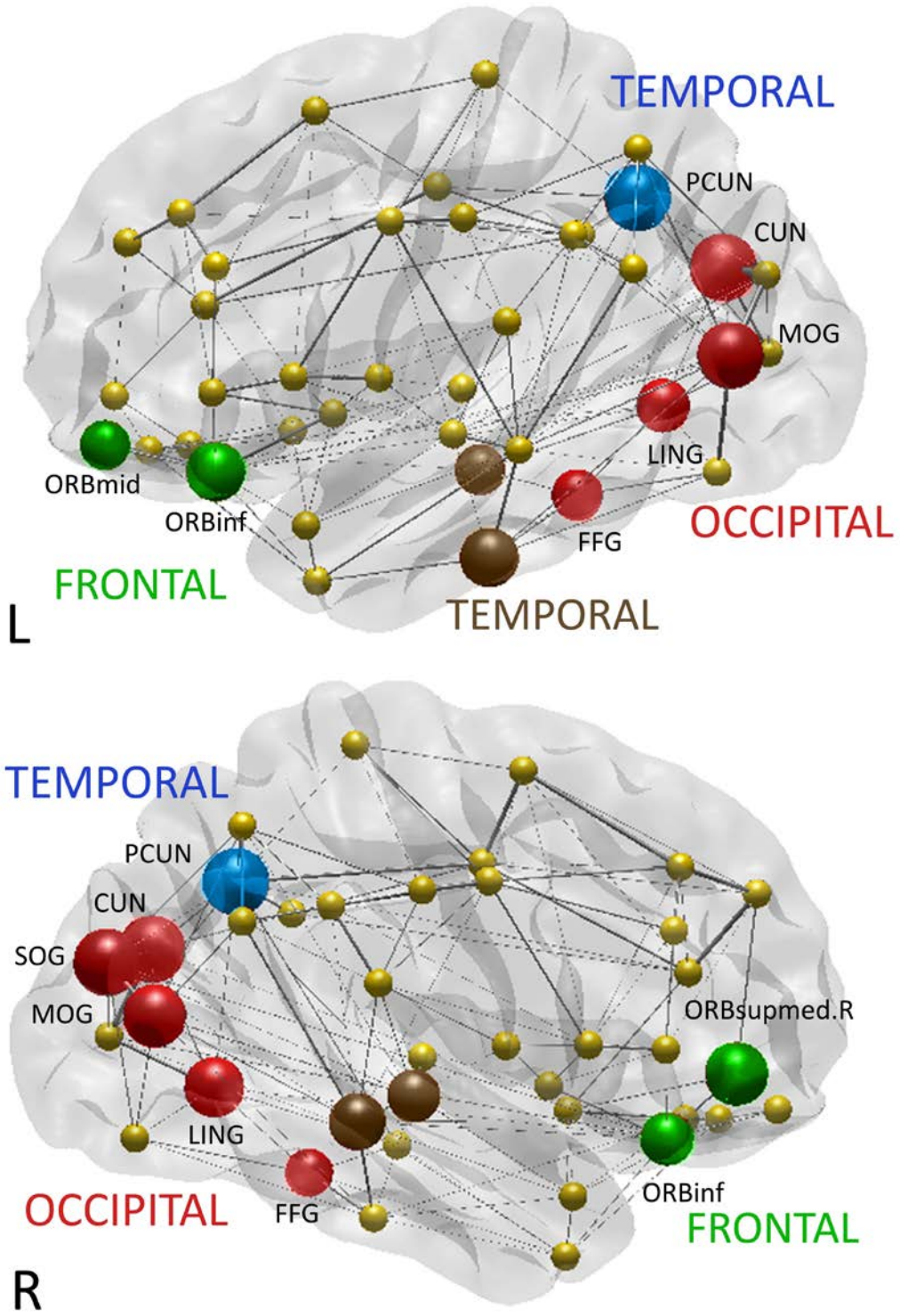

Figure 6.4: The cortical network distribution of nodes with significant inverse correlation between regional efficiency and lesion load in MS patients.

6.4.1 Global and Local Network Efficiency

Small world-properties exist in both groups of MS patients; however, there is an apparent disruption to the WM structural network in MS patients with high lesion load. Reduced efficiency of the global network in MS patients with high LL reflects overall ability of the brain to transfer information between distant cortical brain regions connected by long-range white matter fibers. We also observed reduced local network efficiency in high LL patients compared to controls that is attributed to the reduced communication efficiency between local (adjacent) nodes, i.e. short-range connections. Our patients group with low disability and low LL displays intact WM structural connectivity through measures of global and local network efficiency comparable to our controls. Structural connectivity is interrupted by increased lesion presence resulting in declining efficiency.

When analyzed all patients as a group, lower global and local network efficiency were strongly correlated with increased lesion volume. Our findings indicate that the disruption in the topological organization of the white matter structure in MS patients can be explained by lesion presence. In patients, MS plaques are located mainly in the periventricular white matter, surrounding the anterior and posterior horn of the lateral ventricle. High

concentrations of lesions also lie in the pathways of major white matter fibers (Figure 6.2). Our observations can be supported by a previous postmortem study of the NAWM in MS patients, which showed a reduced axonal density and volume that reflects axonal loss in patients (Evangelou et al. 2000). Axonal loss affects the brain connectivity and its ability to transfer information efficiently in MS patients. Disruption of these white matter fiber pathways would inevitably influence distant and local cortico-cortical connectivity. However hyperintense lesions on T_2-weighted images lack specificity, indicating possible edema, inflammation, demyelination, remyelination, gliosis and axonal loss. Nevertheless, lesion presence influences the efficiency of information transfer within the network. A previous network study of the cortical structure in MS patients found altered global and local network efficiency, which indicates a disruption in the topological organization of cortical thickness in MS patients. Their results also showed decreasing global mean cortical thickness correlation with increasing lesion load (He et al. 2009). Moreover, functional connectivity studies in early RRMS patients revealed increased global activation of the resting-state network (RSN), which can be attributed to increasing WM lesions (Faivre et al. 2012; Richiardi et al. 2012). A tract-based spatial statistics (TBSS) diffusion study in MS patients observed widespread reduced FA and increased axial,

radial and mean diffusivity that correlated with higher lesion volume. This alteration was not confined to within lesion locations and its surroundings, but extends across the whole-brain WM suggesting myelin and axonal damage with compromised WM integrity in MS patients (Liu et al. 2011). Based on observations from this along with previous MRI studies, we suggest that the white matter structural network connectivity in MS patients is disrupted both globally and locally, and is highly influenced by lesion volume. Our findings further extend a previous study of the white matter networks in RRMS that included patients with wider range of disability (Shu et al. 2011).

6.4.2 Average Path Length

We observed an increase in the average shortest path length in high LL patients compared to controls. This increase was also correlated with increasing lesion load in patients group. With increasing amount of lesion transecting the WM structure, edges are non-travelable or considered 'deleted' from the network measures. This suggests brain plasticity where the brain employs a 'new route' around the lesions in order to re-connect two associated brain regions in order for it to regain its function (Bullmore et al. 2009). Our findings are supported by a previous study that measured regional connectivity within RRMS patients

and found increased path length involving mainly the orbitofrontal cortex to other cortico-cortical region (Liu et al. 2012). A study of the functional connectivity within the RSN for early RRMS patients demonstrated this feature with increased functional connectivity being observed only during the early stage of the disease. It was suggested that this represented a compensatory mechanism to dealing with the initial inflammation. This compensation mechanism was shown to fail later during disease progression (Roosendaal et al. 2010; Faivre et al. 2012). Together, results from functional and structural connectivity studies shows signs of compensatory mechanism to cope with structural and functional alterations in the network in order for the brain to regain its function. A further investigation that combines structural and functional connectivity in early RRMS patients would assist in the evaluation of brain plasticity in RRMS patients.

6.4.3 Clustering Coefficient

The *CC* remains unchanged in both patient groups when compared to controls. The *CC* measures the number of existing connections between nodes in a local neighborhood. Our observations show that the connections between nodes remained present, but local network efficiency measures shows a decreased value in high LL compared to controls. In this case, our data

suggests that connections are intact, but the ability of the local edges involved in transferring information between adjacent nodes is decreased. A typical brain network has a high clustering coefficient and short path length (Bullmore et al. 2009), but our results indicated differently in our high LL patients. In high LL the average path length increased but the clustering coefficient remained comparable to controls. While high *CC* reflects the robustness of the network if individual nodes were deleted from the network, low *CC* reflects the network losing its organization and is comparable to a random network (Bullmore et al. 2009). Our results indicate that the organization of the brain network in low disability MS patients with high LL remained robust and is not affected by the lesion presence in the network.

6.4.4 Lesion Load Association with Regional Efficiency

Correlation analysis reveals significant negative association between white matter LL with regional efficiency of several regions in patients. As shown in Figure 6.4, these nodes are parts of the prefrontal cortex (left ORBmid, bilateral ORBinf, right ORBsupmed), parietal cortex (bilateral PCUN), occipital cortex (right SOG, bilateral CUN, bilateral MOG, bilateral LING, bilateral FFG) and temporal cortex (left ITG, left PHG, right MTG and right STG).

Shu et al. reported several correlations between regional efficiency and lesion load in their group of RRMS patients (Shu et al. 2011). Among the regions that coincide with our results are left MOG, bilateral PCUN, right SOG and right CUN. MOG, CUN and SOG are part of the visual system and additional regions (LING, FFG) were also observed in our results thus, strongly indicating a reduced connectivity of the visual system in MS patients that is highly associated to the lesion volume. Implication of the visual system have been previously shown using network analysis (Shu et al. 2011; Li et al. 2012) and supported with evidence from diffusion studies of the optic radiation in patients after optic neuritis (Ciccarelli et al. 2005; Roosendaal et al. 2009; Dasenbrock et al. 2011). A previous functional connectivity study in mild MS patients with and without history of optic neuritis found increased activation in right MOG and reduced activation in right LING (Gallo et al. 2012). It was found that RRMS without optic neuritis has a significant impairment of the visual resting-state network (RSN) compared to controls. Concurrently, a RSN study in clinically early RRMS patients found increased connectivity in the left LING, bilateral MOG, left CUN and right MOG (Faivre et al. 2012). However, their study did not observe a correlation between any regional activation and lesion load. We identified 3 low fatigue and 5 high fatigue patients with lesions identified in the white matter of

the occipital lobe. These lesions transect the white matter tracts that connect the occipital lobe to other parts of the brain, hence influencing the efficiency of the nodes in this region.

PCUN is part of the default-mode network (DMN) and this region was found to be one of the brain hubs in a normal brain network (Gong et al. 2009). A brain hub is a central node with high importance, where deletion of this node may impact the efficiency of the entire network (Bullmore et al. 2009). Structural network study revealed reduced efficiency of the PCUN in RRMS patients (Shu et al. 2011; Li et al. 2012), while functional network study shows increased activation in the PCUN in RRMS (Forn et al. 2012; Richiardi et al. 2012). Our results showed significant reduced regional efficiency with increased LL in patients. Lesion presence appears to interrupt the connectivity of hub regions.

Associations between the regional efficiency of orbitofrontal cortex (ORBmid, ORBinf, ORPsupmed) and lesion load in our study is in agreement with a previous connectivity study in RRMS patients (Li et al. 2012). They found reduced communication efficiency of the orbitofrontal region with other regions in the network. A more recent study using the Iowa Gambling Task suggested that impaired decision-making processes in MS patients

were explained by a functional dysfunction of the orbitofrontal cortex with other cortico-subcortical regions (Molina et al. 2008).

The white matter consists of major association fibers i.e. inferior longitudinal fasciculus (ILF), superior longitudinal fasciculus (SLF), uncinate fasciculus (UNF) and inferior fronto-occipital (IFO). The ILF, SLF and IFO are long association fibers that run anterior-posterior frontal-occipital, while the UNC connects the frontal and temporal lobes with c-shaped fibers. By observing the lesion distribution in our patients, bulk of the lesions are located in the periventricular white matter transecting parts of the ILF, SLF, UNF and IFO. A previous study reported the UNF had the greatest yearly atrophy in MS patients while observing high association between atrophy of the association fibers with lesion load in RRMS patients (Kezele et al. 2008), while another study found high probability of lesions to be present in these white matter bundles in MS patients (Bodini et al. 2011). Previous cortical volume analyses studies have shown greatest cortical volume loss and cortical thinning in both frontal and temporal lobes in MS patients and were associated with higher lesion volume (Sailer et al. 2003; Chen et al. 2004; Charil et al. 2007). Additionally, a network analysis of the cortical thickness in MS patients also found significant correlation between increasing lesion load with reduced regional efficiency in the prefrontal and

temporal cortex (He et al. 2009). Brain lesion analysis found significant frontal-parietal functional dysfunction, which suggests impairment is influenced by lesion presence (Sperling et al. 2001).

Combinations of different methodologies have proven high association of these brain regions to the extent of the lesion load involvement. MS lesions or plaques reflects MS pathology which are essentially inflammation, demyelination, and axonal loss in the CNS, which may be caused by localized and diffused inflammatory activity (Filippi et al. 2007). Over time, the myelinated fibers surrounding these lesions are compromised by the ongoing inflammatory activity that results in demyelination and subsequently axonal dysfunction and loss. As a result, the structural network connectivity is fundamentally altered inevitably impairing important brain functions.

6.4.5 Lack of EDSS association to network parameters

A previous structural network study found significant reduced nodal efficiency of the sensorimotor system (Shu et al. 2011), which was not observed within our group of MS patients with low EDSS measures. Within our cohort of patients with maximum EDSS score of 2.5, these patients have minimal disability. From the EDSS assessment, it suggests that the movement-associated functions in our patients remained intact.

Additionally, EDSS failed to show association with any network parameters in the patients group. Previous functional network study also failed to associate EDSS with the network measures in their MS patients (Faivre et al. 2012). In our study, when analyzed either as a group or subgroups of patients, the lesion load failed to correlate with EDSS scores. Our study focused on differences between MS patients with low disability measures.

6.5 Conclusion

In summary, we have combined diffusion tensor tractography and graph theoretical analysis to investigate cerebral connectivity in early RRMS patients and found significant changes in low disability MS patients with higher LL compared to controls. These changes included reduced global and local network efficiency with increased average path length in high LL patient group. We also observed an association between regional efficiency of several regions with lesion load in both patient groups. Brain connectivity in patients with low LL remained intact and comparable to controls. Measures from the network analysis provide a unique insight into the alterations of cerebral white matter connectivity in low disability RRMS patients with high lesion load.

CHAPTER 7 WHITE MATTER TRACTS AND LESION ASSESSMENT USING DETERMINISTIC TRACTOGRAPHY IN RRMS PATIENTS

7.1 Introduction

The use of tractography in imaging the white matter tracts of patients with multiple sclerosis (MS) is restricted by the presence of brain lesions in this clinical group. Previously, tractography has been implemented in MS studies using either deterministic (Simon et al. 2006; Audoin et al. 2007; Fink et al. 2010; Reich et al. 2010; Dasenbrock et al. 2011; Laganà et al. 2011) or probabilistic (Gorgoraptis et al. 2010; Spanò et al. 2010; Anderson et al. 2011; Kern et al. 2011) tractography. A comparative study of the use of the two tractography methods in MS patients has shown that both methods are feasible and are able to visualize the disruptions and reductions of WM streamlines in MS patients (Hu et al. 2011).

In two tractography studies of healthy brain development (Lebel et al. 2008; Lebel et al. 2010), the fractional anisotropy (FA) threshold was set to 0.25. This parameter threshold served two purposes; first, to start and continue fiber tracking, and second, to avoid inclusion of non white matter (WM) voxels generally lower than 0.2. This level of threshold (or even higher) has also been implemented in clinical populations, including those with epilepsy

(Liu et al. 2011) and Parkinson's disease (Wiltshire et al. 2010). However, previous MS studies implementing deterministic tractography have used a lower FA threshold (0.1 – 0.2) while ignoring inclusion of WM lesions during comparisons (Audoin et al. 2007; Fink et al. 2010; Reich et al. 2010; Spano et al. 2010; Harrison et al. 2013). It was argued that a low FA threshold was necessary to ensure inclusion of fiber tracts that contained transecting lesions with low FA values. Low FA values (below FA threshold) can cause early termination of fiber tracking. However, a low FA threshold during fiber tracking inevitably caused bias to the reported diffusion parameters that were either driven by low FA and high MD values from lesions, or by the inclusion of gray matter voxels (FA ~ 0.2).

The purpose of this study was to investigate the performance of deterministic tractography at a higher FA threshold (0.25) in MS patients. We compared the differences of the diffusion parameters, i.e. fractional anisotropy (FA), mean diffusivity (MD), radial diffusivity (RD) and axial diffusivity (AD), in eleven WM tracts between MS patients and healthy controls. We also investigated the diffusion parameters and frequency of WM lesions in the WM tracts delineated based on the results of tractography.

7.2 Methods

7.2.1 Participants

Our study included nineteen women with RRMS (median EDSS = 1.5, range 0 - 2.5; 40 ± 8 years) and 18 age-matched healthy women (39 ± 7 years). MS patients were recruited through the MS clinic at the University of Alberta Hospital. The Expanded Disability Status Scale (EDSS) was assessed immediately prior to the MR scan. Only patients with mild functional disability (EDSS scores up to and including 2.5) were included in our study. Control subjects were screened to ensure that none had a history of neurological and/or psychological diseases (e.g.: epilepsy, amyotrophic lateral sclerosis, depression).

7.2.2 Data Acquisition

All MRI images were acquired on a 1.5T Siemens Sonata. Total scan time was approximately 14 minutes, which included diffusion tensor imaging (DTI), fluid-attenuated inversion recovery (FLAIR) and T_2-weighted images that covered the whole brain. The imaging parameters for the images above are as follows: DTI - 50 slices, voxel dimension = 2x2x2.5 mm^3, TR = 7100 ms, TE = 95 ms, 12 diffusion directions with b = 1000 s/mm^2, 4 averages, scan time

= 6:32 min; FLAIR - 50 slices, voxel dimension = 1x1x2.5 mm^3, TR = 9000 ms, TE = 97 ms, scan time = 4:05 min; T_2-weighted - 50 slices, voxel dimension = 1x1x2.5 mm^3, TR = 7200 ms, TE = 102 ms, 2 averages, scan time = 4:06 min.

7.2.3 Fiber Tracking

Eleven white matter pathways (Figure 7.1) — i.e. the uncinate fasciculus (UNF), corticospinal tract (CST), cingulum (Cg), superior longitudinal fasciculus (SLF), inferior longitudinal fasciculus (ILF), inferior fronto-occipital fasciculus (IFO), middle cerebellar peduncle (MCP), superior cerebellar peduncle (SCP) and the genu, body and splenium of the corpus callosum (gCC, bCC, sCC) — were extracted from every individual using a semi-automated tractography method previously described by Lebel et al. (2008).

7.2.4 Tract Asymmetry

For bilateral tracts (i.e. CST, UNF, IFO, ILF, SLF, SCP and Cg), tract asymmetry was tested using a paired t-test. No asymmetry was observed in any of the 11 tracts delineated. Subsequent statistical analyses made use of averaged values from the right and left tract diffusion parameters; they are reported below.

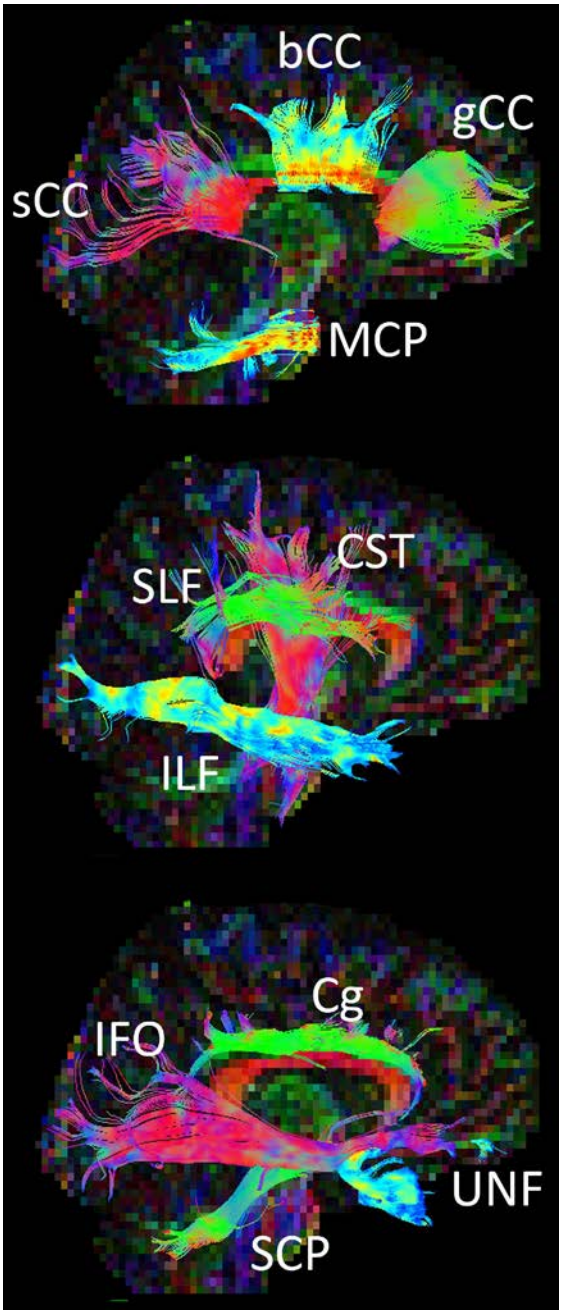

Figure 7.1: Example of white matter tracts delineated using deterministic tractography in a control subject. Shown above are the genu, body and splenium of the corpus callosum (gCC, bCC, sCC), middle cerebellar peduncle (MCP), superior longitudinal fasciculus (SLF), inferior longitudinal fasciculus (ILF), corticospinal tract (CST), cingulum (Cg), inferior fronto-occipital (IFO), superior cerebellar peduncle (SCP) and the uncinate fasciculus (UNF).

7.2.5 Lesion voxels

Hyperintense lesions were delineated on FLAIR and T2-weighted images. Then, each lesion mask was warped into the subject's diffusion space using SPM8 (Wellcome Department of Cognitive Neurology, London, United Kingdom). During WM tracing, lesion voxels with an FA larger than threshold values were included, creating a dilution effect on the calculated diffusion parameters. A MATLAB (The MathWorks, Inc Nattick, MA) algorithm was used to read the FA map, lesion and tract masks simultaneously. It checked for lesion voxels included in any of the WM tract masks. To distinguish lesion voxels included in delineated WM tracts from global T2-hyperintense lesions, the former are called "in-tract lesions". The diffusion parameters of the in-tract lesions were calculated and are reported below. After the in-tract lesions are removed, the remaining portion of the WM tract is called the NAWM tract. The diffusion parameters of the NAWM tracts are reported below.

7.2.6 Statistical analysis

An Independent t-test was used to compare the FA, MD, AD and RD of 1) the whole WM tract and 2) the NAWM tract between the patient and control groups for each of the eleven tracts. The diffusion parameters FA and MD for in-tract lesions were compared

to the NAWM tract using a paired t-test on the patient group. Since this is an exploratory study, none of the comparisons were corrected for multiple testing.

7.3 Results

7.3.1 Whole WM tract comparisons

For whole WM tract comparisons between the control and patient groups, the FA and MD of the IFO, UNF and the CST were significantly different between both groups (Figure 7.2). The patient group also showed increased MD in the ILF and had decreased FA in the SLF compared to controls (Figure 7.2). A further investigation of the FA and MD changes showed elevated RD in all the tracts reported above, and an additional AD increase in the ILF (Figure 7.2).

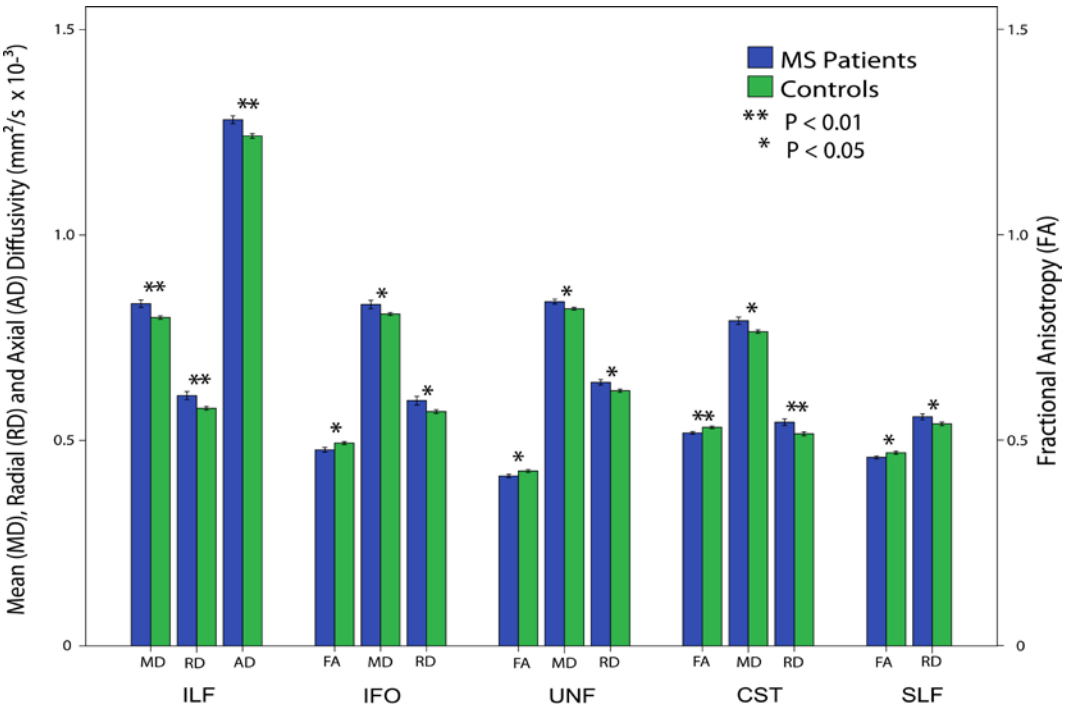

Figure 7.2: Significant differences ($p < 0.05$) of whole tract comparisons for the fractional anisotropy (FA), mean diffusivity (MD), radial diffusivity (RD) and axial diffusivity (AD) between the patient and control groups using one-way ANOVA testing. Tracts in the patient group with significant alterations compared to controls are the inferior longitudinal fasciculus (ILF), inferior fronto-occipital fasciculus (IFO), uncinate fasciculus (UNF), corticospinal tract (CST) and the superior longitudinal fasciculus (SLF). Comparisons that reached $p < 0.01$ are marked (*).

7.3.2 NAWM tract comparisons

After removing in-tract lesions from the delineated WM tracts in patients, the remaining NAWM tract was compared again to controls. A significant FA decrease was found in the UNF and IFO (Figure 7.3). The MD increased significantly in the UNF and ILF; in contrast, an MD decrease was found in the bCC (Figure 7.3).

Examination of the AD and RD revealed significant RD and AD increases in the UNF and ILF, while the RD and AD decreased significantly in the bCC (Figure 7.3). While the SCP did not show changes in its MD and FA measures, significant AD and RD decreases were found in comparison to controls (Figure 7.3).

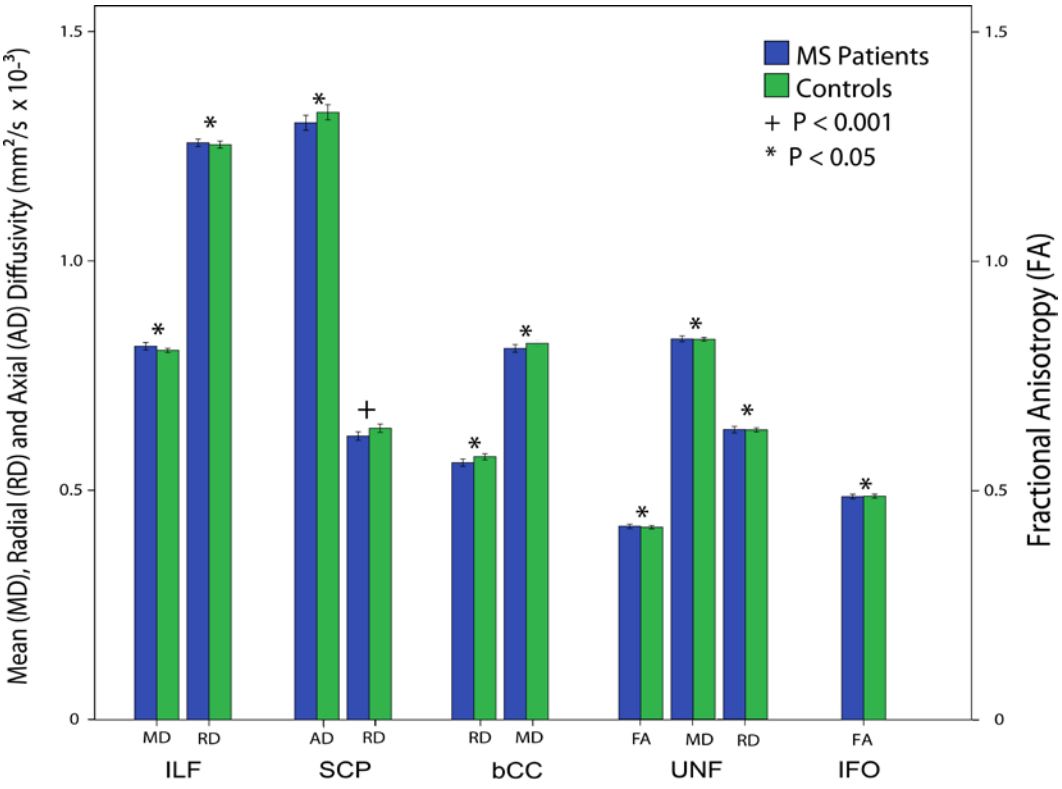

Figure 7.3: After removing lesion voxels, the remaining NAWM tracts of the patients were compared to the control group. Significant alterations ($p < 0.05$) of the fractional anisotropy (FA), mean diffusivity (MD), radial diffusivity (RD) and axial diffusivity (AD) were found between the patient and control groups using one-way ANOVA testing. WM streamlines with significant differences in its diffusion parameters are the inferior longitudinal fasciculus (ILF), superior cerebellar peduncle (SCP), body of the corpus callosum (bCC), uncinate fasciculus (UNF) and the inferior

fronto-occipital fasciculus (IFO). One comparison reached $p < 0.001$ and is marked (**).

7.3.3 In-tract Lesions

In-tract lesions were observed in all eleven tracts studied (Table 7.1 and Table 7.2). Only one patient had a small lesion (volume ~ 0.09cm^3) present in her MCP tract, while 17 patients had various sized lesions (volume, min ~ 0.03 cm^3, max ~ 1.52 cm^3) present in their ILF tracts. Most in-tract lesions had lower FA and higher MD compared to their corresponding NAWM tracts, except for the MCP and SCP, where the FA was higher in in-tract lesions than in the remaining NAWM tract(s).

Table 7.1: The fractional anisotropy (FA) of the white matter lesions in eleven WM tracts included during the delineation of WM tracts using the semi-automated tractography algorithm at threshold of FA > 0.25. Paired t-test found decreased in-tract lesion FA compared to controls (* $p<0.01$, ** $p< 0.001$).

WM Tract	**In-tract lesions in *n* subjects**	**FA in-tract lesion**	**FA NAWM tract**	**FA tract in controls**
MCP	1	0.52	0.50 ± 0.02	0.51 ± 0.01
SCP	2	0.55 ± 0.14	0.47 ± 0.04	0.46 ± 0.02
UNF	6	0.33 ± 0.05*	0.41 ± 0.02	0.43 ± 0.02
Cing	8	0.40 ± 0.04*	0.44 ± 0.01	0.45 ± 0.01
SLF	12	0.33 ± 0.06**	0.46 ± 0.01	0.47 ± 0.02
CST	13	0.41 ± 0.04**	0.53 ± 0.01	0.53 ± 0.01

WM Tract	In-tract lesions in *n*	FA in-tract lesion	FA NAWM tract	FA tract in controls
IFO	14	0.28 ± 0.18**	0.48 ± 0.02	0.49 ± 0.01
gCC	14	0.37 ± 0.04**	0.50 ± 0.02	0.51 ± 0.02
bCC	14	0.37 ± 0.06**	0.52 ± 0.02	0.51 ± 0.02
sCC	16	0.36 ± 0.07**	0.55 ± 0.02	0.54 ± 0.01
ILF	17	0.31 ± 0.08**	0.47 ± 0.03	0.47 ± 0.01

Table 7.2: The mean diffusivity (MD) of the white matter lesions in eleven WM tracts included during the delineation of WM tracts using the semi-automated tractography algorithm at threshold of FA > 0.25. Paired t-test found increased in-tract lesion MD compared to controls (* $p<0.01$, ** $p< 0.001$).

WM Tract	In-tract lesions in *n* subjects	MD in-tract lesion (10^{-3} mm^2/s)	MD NAWM tract (10^{-3} mm^2/s)	MD tract in controls (10^{-3} mm^2/s)
MCP	1	0.90	0.74 ± 0.02	0.74 ± 0.01
SCP	2	0.83 ± 0.07	0.81 ± 0.02	0.88 ± 0.04
UNF	6	1.18 ± 0.17*	0.84 ± 0.03	0.82 ± 0.01
Cing	8	1.10 ± 0.13**	0.78 ± 0.02	0.77 ± 0.02
SLF	12	1.06 ± 0.07**	0.75 ± 0.03	0.74 ± 0.02
CST	13	1.01 ± 0.11**	0.77 ± 0.03	0.76 ± 0.02
IFO	14	1.11 ± 0.11**	0.82 ± 0.03	0.81 ± 0.02
gCC	14	1.06 ± 0.12**	0.81 ± 0.03	0.81 ± 0.02
bCC	14	0.99 ± 0.09**	0.80 ± 0.04	0.83 ± 0.02
sCC	16	1.10 ± 0.09**	0.81 ± 0.04	0.83 ± 0.03
ILF	17	1.11 ± 0.09**	0.82 ± 0.03	0.80 ± 0.02

7.4 Discussion

In this study, we assessed the performance of fiber tracking in low disability MS patients with brain lesions. Eleven WM tracts were successfully delineated using deterministic tractography at an FA threshold of 0.25, which is higher than that of most previous tractography studies in the MS literature (Simon et al. 2006; Audoin et al. 2007; Fink et al. 2010; Reich et al. 2010; Dasenbrock et al. 2011; Laganà et al. 2011)In general, a lower FA and higher MD of the reconstructed WM tracts were observed in MS patients than in those of controls, specifically in the ILF, IFO, UNF, CST and SLF. A further investigation of the five tracts above, we observed significant increases of the AD and RD of these tracts in patients. After removal of in-tract lesions, some NAWM tract comparisons (CST and SLF) were no longer significant. The MD of the ILF and UNF, and the FA of the UNF remained significant. These changes were mainly driven by increased AD and RD in the tract. Interestingly, only the FA of the IFO is lower in patients than in controls, without other parameters (MD, AD and RD) being different.

The RD reflects the water diffusion perpendicular to the main fiber direction, whereas the AD is a reflection of water diffusion along the main fiber direction. Based on previous

observations in animal models of MS, it was suggested that changes in AD and RD reflects axonal and myelin dysfunction (Song et al. 2005; DeBoy et al. 2007; Zhang et al. 2009). In a post-mortem study of MS brains, the low FA and high MD in the NAWM was shown to correlate with axonal loss and myelin damage (Evangelou et al. 2000; Mottershead et al. 2003). The previous findings were observed mainly in acute inflammatory animal models or in the brains of patients with progressive MS where severe tissue damage occurs more often in this group of patients compared to relapsing-remitting patients. It was also suggested that other possible underlying pathology contribute to the AD and RD changes in human studies. Firstly, tissue inflammation and edema should not be ruled out; secondly increased AD could suggest compensation of axonal trauma (Fink et al. 2010). Altered diffusivities of the NAWM tracts may also reflect other changes known to occur in the NAWM, including edema, gliosis, myelin thinning and axonal loss (Trapp et al. 1998; Cercignani et al. 1999).

The AD and RD of the NAWM SCP was also found to be lower in the patient group than in controls. We know of only one other study that has assessed cerebellar tract differences in RRMS and PPMS patients (Anderson et al. 2011). However, the authors found no differences between the SCP tract of their RRMS and control

groups. However, they found significant correlations of the FA, MD and RD of the SCP with upper limb function and speed of walking in their PPMS group. In our study, all patients have low levels of disability as measured using the EDSS. This scale is used to assess a patient's current clinical condition, but it does not provide comprehensive and specific representation of the limb/physical performance in a patient. Hence, we are unable to either replicate or disagree with the previous findings.

A previous study reported that WM lesions only contributed 1-2% of the total diffusivity profiles in their study of the optic radiation, corticospinal tract and corpus callosum (Harrison et al. 2013). Exclusion of the WM lesions in their study was deemed unnecessary. However, after removal of in-tract lesions in our group of patients, the NAWM tract comparisons altered the statistical analysis of previous WM tract comparisons, especially those of the CST and SLF between the patient and control groups. In-tract lesions have lower FA and higher MD values than the NAWM tract. Our observations suggest that in-tract lesions do contribute to the alterations of the tractography-derived parameters in the patient group. Lesion inclusion could have contributed to the significant findings of tract comparisons in previous literature (Audoin et al. 2007; Fink et al. 2010; Reich et al. 2010; Spano et al. 2010; Harrison et al. 2013).

In-tract lesions were observed in all white matter tracts. One lesion was observed in the MCP of one patient, while the highest incident of in-tract lesions is in the ILF of 17 MS patients. Two patients had very low whole brain lesion loads, at 0.058 cm^3 and 0.154 cm^3, transecting only the bCC and the ILF respectively. The FA and MD of in-tract lesions were compared to those of the remaining NAWM tract. Our in-tract lesions had higher FA and lower MD values compared to values reported by Hu et al. (2011). This observation is a result of the higher FA threshold during fiber tracking.

Our observations show that WM tracts can be delineated using deterministic tractography without having to use an FA threshold as low as 0.1 in order to prevent early termination of WM tracts. Results from our study also show variable degrees of FA and MD alteration of in-tract lesions, but generally lower FA and higher MD compared to the NAWM tracts. The altered diffusivities in the in-tract lesions reflect disrupted and damaged tissue microstructure, while edema and inflammatory processes increases intracellular space (Filippi et al. 2000).

Our results also indicate that NAWM alteration can be detected in low disability RRMS patients by using deterministic tractography. In-tract lesions are present in all of the tracts

investigated. Careful lesion removal must follow successful fiber tracking in order to avoid the diluting effect of the tractography-derived parameters.

7.5 Future Directions

Diffusion tensor imaging studies often report the averaged diffusion parameters of selected WM tracts or regions-of-interest. Investigation of the NAWM tracts in our group of patients revealed only slight changes to the measured diffusion parameters. An assessment of the FA and MD trend along each tract in smaller sub-sections, starting from within lesions and moving outwards, may provide additional details that are more sensitive to the diffusion changes in NAWM, especially in regions closest to the lesions.

A longitudinal study may also monitor along-tract diffusion changes as an effect of Wallerian degeneration in the NAWM tracts. In addition, parallel testing of WM tracts tracked at lower FA threshold (0.1 – 0.2) in comparison to the 0.25 threshold in MS patients and controls, may allow for verification of the findings from this preliminary study.

CHAPTER 8 LIMITATIONS AND FUTURE DIRECTIONS

While both methods (MRS and DTI) used in the studies above have provided many insights into the metabolic and structural differences between MS patients and controls, both methodologies have their inherent drawbacks and limitations too

One inherent drawback pertains to both studies, which included only nineteen MS patients and eighteen age-matched healthy individuals as a control group. The patient group was further sub-grouped into two roughly equal sets of individuals. Given the small number of subjects in each sub-group, we may have missed true positives that were too statistically weak to be deemed significant. In future studies, we recommend increasing the number of patients in each subgroup of patients to match the number of control subjects.

The following section will address some of the technical and methodological limitations pertaining specifically to MRS and DTI.

8.1 Limitations of the MRS study

Firstly, MRS of the brainstem is particularly difficult due to its location. The magnetic susceptibility at air/tissue interface, particularly around the sinus (Figure 8.1), which is included in our region-of-interest, may have caused ineffective shimming and

inadequate water suppression of some voxels in the pontine that were especially close to this area. Defining a smaller shimming area that was concentrated in the pontine might have improved the quality of the spectra acquired.

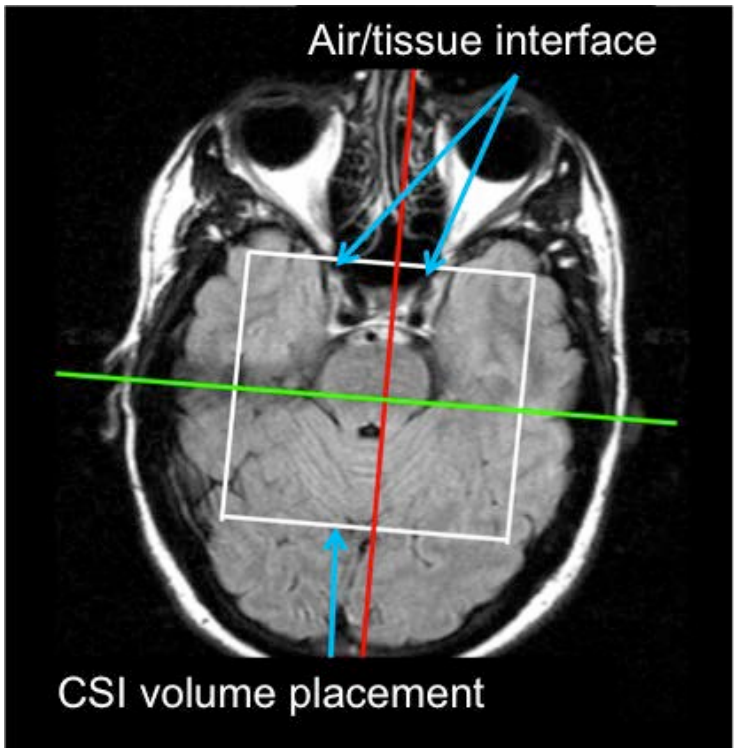

Figure 8.1: Region of magnetic susceptibility at air/tissue interface near the sinus. The white square box represents the region-of-interest that bounds the area of the CSI volume on an axial slice.

We chose to use the PRESS sequence in the MRS study due to its high SNR and because our objective was mainly to quantify the NAA concentration. Instead, we found a higher tCr ratio, which suggests either gliosis or an imbalanced Cr/PCr ratio. At TE = 135 ms, the PRESS sequence is not able to measure the low intensity signal from myoinositol (mI), a metabolite that is specific to glial

cells and is not observable in neurons (Narayana 2005; Sajja et al. 2009). Future work may include the use of stimulated echo acquisition mode (STEAM), a sequence that allows a shorter TE. Another possibility is to measure PCr using ^{31}P MRS in the same location, i.e the pontine brainstem, however, due to inherent drawbacks of ^{31}P MRS (e.g. poor spatial resolution and long scan time), to obtain a spectrum from the pontine is not promising.

Another methodological issue with this study was that the registration between the CSI slab and the high resolution MPRAGE image was done manually. This process was highly user-dependent, and the confidence level of the CSI placement was subject to the ability and reliability of the user to correctly identify the volume placement in all subjects. Identification was done based on the visual landmarks of the brain anatomy using images saved from the Siemens MRI computer. It is also noteworthy that the individual who carried out the post-processing CSI volume registration of all 37 participants was the same person who operated the MRI scan of 28 participants. The volume placement allowed us to extract the proportion of gray and white matter mix in each voxel of the CSI slab and to use it as a covariate in the statistical analysis. Incorrect registration would have led to incorrect GM% calculation and statistical comparisons. Acquisition of the spectroscopy data and MPRAGE image was performed on

two different coils. To reduce scan time, an 8-channel array coil was used for the high resolution images, while the head coil was used for the MRS. Unavoidably, the centre and orientation of the subject's head was different in both images. It is worth noting for future work, that the MPRAGE data should be imaged from the same head coil that acquired the MRS data. This minimizes head movement and simplifies the registration method.

8.2 Limitations of the Network study

The network analysis reported in Chapter 6 did not exclude white matter lesions in patients during tractography and network construction. This study inadvertently included other indirect effects, such as low FA values from lesions during edge construction in patients. One other possibility is that it missed the edges of fiber tracts containing lesions with FA values that are below the tracking threshold, which is 0.25.

Deterministic tractography has its own limitations. We chose this tractography method over probabilistic tractography because it was readily available to us. However, one might also use probabilistic tractography to perform whole brain tracking and edges constructed in the network matrix. For every voxel, this method estimates the highest probability of the fiber direction,

increasing confidence of the constructed network matrix and the fiber connections of two brain regions, or nodes.

Partial volume is another limitation of the DTI data that needs to be accounted for. Inclusion of GM, CSF or lesions in WM voxels has a diluting effect on the FA calculations and increases the diffusivity parameters. This may be a source of false positives during group comparisons of the diffusion parameters.

Arguably, another drawback is the level of FA threshold chosen during tractography. On one hand, a low FA threshold may introduce other sources of false tracking, for example, tracking into GM voxels, while some studies have used low FA values to avoid early termination of lesion containing WM voxels. And on the other hand, increasing the threshold to high of 0.3 will definitely exclude more WM lesions. As demonstrated in the results of the preliminary analysis in Chapter 7, we found that the average FA value of in-tract lesions are ~ 0.3. Currently, a guideline for performing tractography in MS patients does not exist. A study that compares performance of fiber tracking at different FA and angle threshold must be carried out. Ideally, this study will compare effects of removing lesion voxels before and after fiber tracking. This may resolve some of the ambiguities of tractography performance in MS patients.

CHAPTER 9 CONCLUSIONS

Magnetic resonance imaging (MRI) is a necessary and useful tool for imaging the human brain. Its sensitivity to pathological changes in clinical populations such as multiple sclerosis (MS) has provided better understanding of the underlying alterations in the brain due to the disease. Applications of magnetic resonance spectroscopy (MRS) and diffusion tensor imaging (DTI) have revealed some notable differences between our groups of low disability relapsing-remitting MS patients and healthy controls.

As discussed in Chapter 5, the application of MRS in MS patients with fatigue has revealed metabolic dysfunction of the total creatine in the pontine brainstem. This finding suggests two possible alterations of the brain mechanism in MS patients suffering from fatigue. One possible explanation is the proliferation of glia cells affecting its regular function, while another possibility is energy metabolic dysfunction of the creatine and phosphocreatine in the pontine region in patients with fatigue.

The whole brain involvement in MS disease is related to the focal injuries seen in MS lesions. Using DTI tractography and graph theoretical analysis as described in Chapter 6, the efficacy of the cerebral connectivity in low disability RRMS patients was found to be lower in patients with a high lesion load. It is also worth

noting that the brain connectivity in patients with low lesion load remained intact and comparable to that of controls.

A preliminary investigation in Chapter 7 in the same group of patients above using deterministic tractography has revealed that the integrity of several functional white matter tracts is disrupted in MS patients. We also showed that white matter tracts are traceable even when brain lesions intersect portions of the tracts.

It is imperative to understand the pathological changes that affect the white matter in MS patients, and MRI has the advantage of providing high contrasting images of soft tissue in the brain. New research findings from the application of conventional and non-conventional MRI techniques have provided extensive indications of these changes and offered added information that physician and patients can use in better understanding this disease.

BIBLIOGRAPHY

Achard S, Salvador R, Whitcher B, Suckling J, Bullmore E. 2006. A resilient, low-frequency, small-world human brain functional network with highly connected association cortical hubs. J Neurosci 26:63–72.

Anderson VM, Wheeler-kingshott CAM, Abdel-Aziz K, Miller DH, Toosy A, Thompson AJ, Ciccarelli O. 2011. A comprehensive assessment of cerebellar damage in multiple sclerosis using diffusion tractography and volumetric analysis. Mult Scler 17:1079–87.

Ashburner J, Friston KJ. 2000. Voxel-Based Morphometry — The Methods. Neuroimage 821:805– 821.

Aston-jones G, Rajkowski J, Cohen J. 1999. Role of Locus Coeruleus in Attention and Behavioral Flexibility. Biol Psychiatry 3223:1309–1320.

Van Au Duong M, Audoin B, Le Fur Y, Confort-Gouny S, Malikova I, Soulier E, Viout P, Ali-Cherif A, Pelletier J, Cozzone PJ, et al. 2007. Relationships between gray matter metabolic abnormalities and white matter inflammation in patients at the very early stage of MS: a MRSI study. J Neurol 254:914–23.

Audoin B, Guye M, Reuter F, Au Duong M-V, Confort-Gouny S, Malikova I, Soulier E, Viout P, Chérif AA, Cozzone PJ, et al. 2007. Structure of WM bundles constituting the working memory system in early multiple sclerosis: a quantitative DTI tractography study. Neuroimage 36:1324–30.

Bakshi R, Miletich RS, Henschel K, Shaikh Z a, Janardhan V, Wasay M, Stengel LM, Ekes R, Kinkel PR, Bakshi R, Miletich RS, Henschel K, Shaikh ZA, Janardhan V, Wasay M SL, et al. 1999. Fatigue in multiple sclerosis: cross-sectional correlation with brain MRI findings in 71 patients. Neurology 53:1151–1153.

Basser P, Pajevic S, Pierpaoli C, Duda J, Aldroubi A. 2000. In vivo fiber tractography using DT-MRI data. Magnetic Resonance in Medicine / Society of Magnetic Resonance in Medicine 44:625–32.

Basser PJ, Mattiello J, LeBihan D. 1994. Estimation of the Effective Self-Diffusion Tensor from the NMR Spin Echo. J Magn Reson Imaging 103:247–254.

Beck C a, Metz LM, Svenson LW, Patten SB. 2005. Regional variation of multiple sclerosis prevalence in Canada. Mult Scler 11:516–9.

Behrens T, Woolrich M, Jenkinson M, Johansen-Berg H, Nunes R, Clare S, Matthews P, Brady J, Smith S. 2003. Characterization and propagation of uncertainty in diffusion-weighted MR imaging. Magnetic Resonance in Medicine / Society of Magnetic Resonance in Medicine 50:1077–88.

Benjamini Y, Hochberg Y. 2000. On the Adaptive Control of the False Discovery Rate in Multiple Testing With Independent Statistics. J Educ Behav Stat 25:60–83.

Bhagat YA, Beaulieu C. 2004. Diffusion anisotropy in subcortical white matter and cortical gray matter: changes with aging and the role of CSF-suppression. J Magn Reson Imaging 20:216–27.

Blomstrand E, Perrett D, Parry-Billings M, Newsholme EA. 1989. Effect of sustained exercise on plasma amino acid concentrations and on 5-hydroxytryptamine metabolism in six different brain regions in the rat. Acta Physiol Scand 136:473–481.

Bodini B, Battaglini M, De Stefano N, Khaleeli Z, Barkhof F, Chard D, Filippi M, Montalban X, Polman C, Rovaris M, et al. 2011. T2 lesion location really matters: a 10 year follow-up study in primary progressive multiple sclerosis. J Neurol Neurosurg Psychiatry 82:72–7.

Bottomley P. 1984. Selective volume method for performing localized NMR spectroscopy.

Bullmore E, Sporns O. 2009. Complex brain networks: graph theoretical analysis of structural and functional systems. Nat Rev Neurosci 10:186–98.

Calabrese M, Rinaldi F, Grossi P, Mattisi I, Bernardi V, Favaretto A, Perini P, Gallo P. 2010. Basal ganglia and frontal/parietal cortical atrophy is associated with fatigue in relapsing-remitting multiple sclerosis. Mult Scler 16:1220–1228.

Calabrese M, Rocca MA, Atzori M, Mattisi I, Favaretto A, Perini P, Gallo P, Filippi M. 2010. A 3-year magnetic resonance imaging study of cortical lesions in relapse-onset multiple sclerosis. Ann Neurol 67:376–83.

Capello E, Uccelli A, Pizzorno M, Mancardi G. 2007. Neuropathological Advances in Multiple Sclerosis. In: Filippi M, Rovaris M, Comi G, editors. Neurodegeneration in Multiple Sclerosis. Milan. p. 3–9.

Caramanos Z, Narayanan S, Arnold DL. 2005. 1H-MRS quantification of tNA and tCr in patients with multiple sclerosis: a meta-analytic review. Brain 128:2483–506.

Catani M, Howard RJ, Pajevic S, Jones DK. 2002. Virtual in Vivo Interactive Dissection of White Matter Fasciculi in the Human Brain. Neuroimage 17:77–94.

Ceccarelli A, Rocca MA, Valsasina P, Rodegher M, Falini A, Comi G, Filippi M. 2010. Structural and functional magnetic resonance imaging correlates of motor network dysfunction in primary progressive multiple sclerosis. Eur J Neurosci 31:1273–1280.

Cercignani M, Horsfield M a. 1999. An optimized pulse sequence for isotropically weighted diffusion imaging. J Magn Reson 140:58–68.

Cercignani M, Inglese M, Pagani E, Comi G, Filippi M. 2001. Mean Diffusivity and Fractional Anisotropy Histograms of Patients with Multiple Sclerosis. American Journal of Neuroradiology 22:952–958.

Chang L, Ernst T, Poland RE, Jenden DJ. 1996. In vivo proton magnetic resonance spectroscopy of the normal aging human brain. Life Sci 58:2049–2056.

Chan-Palay V, Asan E. 1989. Alterations in catecholamine neurons of the locus coeruleus in senile dementia of the Alzheimer type and in Parkinson's disease with and without dementia and depression. J Comp Neurol 287:373–392.

Chard DT, Griffin CM, Mclean MA, Kapeller P, Kapoor R, Thompson AJ, Miller DH. 2002. Brain metabolite changes in cortical grey and normal-appearing white matter in clinically early relapsing- remitting multiple sclerosis. Brain 125:2342–2352.

Chard DT, Griffin CM, Parker GJM, Kapoor R, Thompson AJ, Miller DH. 2002. Brain atrophy in clinically early relapsing - remitting multiple sclerosis. Brain 125:327–337.

Charil A, Dagher A, Lerch JP, Zijdenbos AP, Worsley KJ, Evans AC. 2007. Focal cortical atrophy in multiple sclerosis: relation to lesion load and disability. Neuroimage 34:509–17.

Chaudhuri A, Behan PO. 2004. Fatigue in neurological disorders. Lancet 363:978–88.

Chen JT, Narayanan S, Collins DL, Smith SM, Matthews PM, Arnold DL. 2004. Relating neocortical pathology to disability progression in multiple sclerosis using MRI. Neuroimage 23:1168–75.

Chwastiak LA, Gibbons LE, Ehde DM, Sullivan M, Bowen JD, Bombardier CH, Kraft GH. 2005. Fatigue and psychiatric illness in a

large community sample of persons with multiple sclerosis. J Psychosom Res 59:291–8.

Ciccarelli O, Toosy AT, Hickman SJ, Parker GJM, Wheeler-Kingshott CAM, Miller DH, Thompson AJ. 2005. Optic radiation changes after optic neuritis detected by tractography-based group mapping. Hum Brain Mapp 25:308–16.

Ciccarelli O, Werring DJ, Barker GJ, Thompson AJ, Miller DH. 2001. Investigation of MS normal-appearing brain using diffusion tensor MRI with clinical correlations. Neurology 56:926–933.

Commowick O, Fillard P, Clatz O, Warfield SK. 2008. Detection of DTI white matter abnormalities in multiple sclerosis patients. Medical image computing and computer-assisted intervention□: MICCAI ... International Conference on Medical Image Computing and Computer-Assisted Intervention age (Rochester, N.Y.) 11:975–982.

Compston A, Coles A. 2008. Multiple sclerosis. Lancet 372:1502–1517.

Conturo TE, Lori NF, Cull TS, Akbudak E, Snyder a Z, Shimony JS, McKinstry RC, Burton H, Raichle ME. 1999. Tracking neuronal fiber pathways in the living human brain. Proc Natl Acad Sci U S A 96:10422–7.

Dasenbrock HH, Smith SA, Ph D, Ozturk A, Sheena K, Calabresi PA, Reich DS, Farrell SK. 2011. Diffusion Tensor Imaging of the Optic Tracts in Multiple Sclerosis: Association with Retinal Thinning and Visual Disability. J Neuroimaging 21:1–17.

Davie CA, Barker GJ, Thompson AJ, Tofts PS, McDonald WI, Miller DH. 1997. 1H magnetic resonance spectroscopy of chronic cerebral white matter lesions and normal appearing white matter in multiple sclerosis. J Neurol Neurosurg Psychiatry 63:736–42.

Davie CA, Hawkins CP, Barker GJ, Brennan A, Tofts PS, Miller DH, Mcdonald WI. 1994. Serial proton magnetic resonance spectroscopy in acute multiple sclerosis lesions. Brain 117:49–58.

DeBoy CA, Zhang J, Dike S, Shats I, Jones M, Reich DS, Mori S, Nguyen T, Rothstein B, Miller RH, et al. 2007. High resolution diffusion tensor imaging of axonal damage in focal inflammatory and demyelinating lesions in rat spinal cord. Brain 130:2199–210.

Droogan AG, Clark CA, Werring DJ, Barker GJ, McDonald WI, Miller DH. 1999. Comparison of multiple sclerosis clinical subgroups using navigated spin echo diffusion-weighted imaging. Magn Reson Imaging 17:653–661.

Evangelou N, Esiri MM, Smith S, Palace J, Matthews PM. 2000. Quantitative pathological evidence for axonal loss in normal appearing white matter in multiple sclerosis. Ann Neurol 47:391–5.

Faivre A, Rico A, Zaaraoui W, Crespy L, Reuter F, Wybrecht D, Soulier E, Malikova I, Confort-Gouny S, Cozzone PJ, et al. 2012. Assessing brain connectivity at rest is clinically relevant in early multiple sclerosis. Mult Scler 0:1–8.

Fernando KTM, McLean M a, Chard DT, MacManus DG, Dalton CM, Miszkiel K a, Gordon RM, Plant GT, Thompson AJ, Miller DH. 2004. Elevated white matter myo-inositol in clinically isolated syndromes suggestive of multiple sclerosis. Brain 127:1361–9.

Filippi M, Agosta F. 2010. Imaging biomarkers in multiple sclerosis. J Magn Reson Imaging 31:770–88.

Filippi M, Cercignani M, Inglese M, Horsfield M, Comi G. 2001. Diffusion tensor magnetic resonance imaging in multiple sclerosis. Neurology 56:304–11.

Filippi M, Iannucci G, Cercignani M, Assunta Rocca M, Pratesi a, Comi G. 2000. A quantitative study of water diffusion in multiple sclerosis lesions and normal-appearing white matter using echo-planar imaging. Arch Neurol 57:1017–21.

Filippi M, Rocca M., Colombo B, Falini A, Codella M, Scotti G, Comi G. 2002. Functional Magnetic Resonance Imaging Correlates of Fatigue in Multiple Sclerosis. Neuroimage 15:559 –567.

Filippi M, Rocca MA. 2007. Conventional MRI in multiple sclerosis. J Neuroimaging 17 Suppl 1:3S–9S.

Filippi M, Rocca MA. 2011. MR Imaging of Multiple Sclerosis. Radiology 259:659–681.

Fink F, Klein J, Lanz M, Mitrovics T, Lentschig M, Hahn HK, Hildebrandt H. 2010. Comparison of diffusion tensor-based tractography and quantified brain atrophy for analyzing demyelination and axonal loss in MS. J Neuroimaging 20:334–44.

Fisk J, Pontefract A, Ritvo P, Archibald C, Murray T. 1994. The impact of fatigue on patients with multiple sclerosis. J Neurol Sci 21:9–14.

Forn C, Rocca M a, Valsasina P, Boscá I, Casanova B, Sanjuan A, Ávila C, Filippi M. 2012. Functional magnetic resonance imaging correlates of cognitive performance in patients with a clinically isolated syndrome suggestive of multiple sclerosis at presentation: an activation and connectivity study. Mult Scler 18:153–63.

Gadea M, Martínez-Bisbal MC, Marti-Bonmatí L, Espert R, Casanova B, Coret F, Celda B. 2004. Spectroscopic axonal damage of the right locus coeruleus relates to selective attention impairment in early stage relapsing-remitting multiple sclerosis. Brain 127:89–98.

Gallo A, Esposito F, Sacco R, Docimo R, Bisecco A, Della Corte M, D'Ambrosio A, Corbo D, Rosa N, Lanza M, et al. 2012. Visual resting-state network in relapsing-remitting MS with and without previous optic neuritis. Neurology 79:1458–65.

Ge Y, Law M, Grossman RI. 2005. Applications of diffusion tensor MR imaging in multiple sclerosis. Ann N Y Acad Sci 1064:202–19.

Ge Y. 2006. Multiple Sclerosis: The Role of MR Imaging. AJNR Am J Neuroradiol 27:1165–1176.

Gonen O, Catalaa I, Babb J, Ge Y, Mannon L, Kolson D, Grossman R. 2000. Total brain N-acetylaspartate: a new measure of disease load in MS. Neurology 54:15–9.

Gong G, He Y, Concha L, Lebel C, Gross DW, Evans AC, Beaulieu C. 2009. Mapping Anatomical Connectivity Patterns of Human Cerebral Cortex Using In Vivo Diffusion Tensor Imaging Tractography. Cereb Cortex 19:524–536.

Gorgoraptis N, Wheeler-Kingshott CAM, Jenkins TM, Altmann DR, Miller DH, Thompson AJ, Ciccarelli O. 2010. Combining tractography and cortical measures to test system-specific hypotheses in multiple sclerosis. Mult Scler 16:555–565.

Guo AC, MacFall JR, Provenzale JM. 2002. Multiple sclerosis: diffusion tensor MR imaging for evaluation of normal-appearing white matter. Radiology 222:729–36.

Guye M, Bettus G, Bartolomei F, Cozzone PJ. 2010. Graph theoretical analysis of structural and functional connectivity MRI in normal and pathological brain networks. MAGMA 23:409–21.

Hagmann P, Kurant M, Gigandet X, Thiran P, Wedeen VJ, Meuli R, Thiran J-P. 2007. Mapping human whole-brain structural networks with diffusion MRI. PLoS One 2:e597.

Harrison DM, Shiee N, Bazin P-L, Newsome SD, Ratchford JN, Pham D, Calabresi PA, Reich DS. 2013. Tract-specific quantitative MRI better correlates with disability than conventional MRI in multiple sclerosis. J Neurol 260:397–406.

Hattingen E, Magerkurth JJ, Pilatus U, Hübers A, Wahl M, Ziemann U, Hubers A. 2011. Combined 1 H and 31 P spectroscopy provides new insights into the pathobiochemistry of brain damage in multiple sclerosis. NMR Biomed 24:536–546.

He J, Inglese M, Li BSY, Babb JS, Grossman RI, Gonen O. 2005. Relapsing-Remitting Multiple Sclerosis: Metabolic Abnormality in Nonenhancing Lesions and Normal-appearing White Matter at MR Imaging: Initial Experience. Neuroradiology 234:211–217.

He Y, Chen ZJ, Evans AC. 2007. Small-world anatomical networks in the human brain revealed by cortical thickness from MRI. Cereb Cortex 17:2407–19.

He Y, Dagher A, Chen Z, Charil A, Zijdenbos A, Worsley K, Evans A. 2009. Impaired small-world efficiency in structural cortical networks in multiple sclerosis associated with white matter lesion load. Brain 132:3366–79.

Heide AC, Richards TL, Alvord EC, Peterson J, Rose LM. 1993. Diffusion imaging of experimental allergic encephalomyelitis. Magnetic resonance in medicine: official journal of the Society of Magnetic Resonance in Medicine / Society of Magnetic Resonance in Medicine 29:478–84.

Hochberg Y, Benjamini Y. 1990. More powerful procedures for multiple significance testing. Stat Med 9:811–8.

Horsfield MA, Lai M, Webb SL, Barker GJ, Tofts PS, Turner R, Rudge P, Miller DH. 1996. Apparent diffusion coefficients in benign and secondary progressive multiple sclerosis by nuclear magnetic resonance. Magn Reson Med 36:393–400.

Hu B, Ye B, Yang Y, Zhu K, Kang Z, Kuang S, Luo L, Shan H. 2011. Quantitative diffusion tensor deterministic and probabilistic fiber tractography in relapsing-remitting multiple sclerosis. Eur J Radiol 79:101–7.

Husted CA, Goodin DS, Hugg JW, Maudsley AA, Tsuruda JS, De Bie SH, Fein G, Matson GB, Weiner MW. 1994. Biochemical alterations in multiple sclerosis lesions and normal-appearing white matter detected by in vivo 31P and 1H spectroscopic imaging. Ann Neurol 36:157–65.

Induruwa I, Constantinescu CS, Gran B. 2012. Fatigue in multiple sclerosis - A brief review. J Neurol Sci 323:9–15.

Iturria-Medina Y, Canales-Rodríguez E, Melie-García L, Valdés-Hernández P, Martínez-Montes E, Alemán-Gómez Y, Sánchez-Bornot J. 2007. Characterizing brain anatomical connections using diffusion weighted MRI and graph theory. Neuroimage 36:645–60.

Jones D, Pierpaoli C. 2005. Confidence mapping in diffusion tensor magnetic resonance imaging tractography using a bootstrap approach. Magnetic Resonance in Medicine / Society of Magnetic Resonance in Medicine 53:1143–9.

Jones D, Simmons A, Williams S, Horsfield M. 1999. Non-invasive assessment of axonal fiber connectivity in the human brain via diffusion tensor MRI. Magn Reson Med 42:37–41.

Kapeller P, Mclean MA, Griffin CM, Chard D, Parker GJM, Barker GJ, Thompson AJ, Miller DH. 2001. Preliminary evidence for neuronal damage in cortical grey matter and normal appearing white matter in

short duration relapsing-remitting multiple sclerosis: a quantitative MR spectroscopic imaging study. J Neurol 248:131–138.

Ke Y, Cohen BM, Lowen S, Hirashima F, Nassar L, Renshaw PF. 2002. Biexponential Transverse Relaxation (T2) of the Proton MRS Creatine Resonance in Human Brain. Magn Reson Med 47:232–238.

Kern KC, Sarcona J, Montag M, Giesser BS, Sicotte NL. 2011. Corpus callosal diffusivity predicts motor impairment in relapsing-remitting multiple sclerosis: a TBSS and tractography study. Neuroimage 55:1169–77.

Kezele IB, Arnold DL, Collins DL. 2008. Atrophy in white matter fiber tracts in multiple sclerosis is not dependent on tract length or local white matter lesions. Mult Scler 14:779–85.

Kirov II, Patil V, Babb JS, Rusinek H, Herbert J, Gonen O. 2009. MR Spectroscopy Indicates Diffuse Multiple Sclerosis Activity During Remission. J Neurol Neurosurg Psychiatry 80:1330–1336.

Korf J, Aghajanian GK, Roth RH. 1973. Increased turnover of norepnephrine in the rat cerebral cortex during stress: Role of the locus coeruleus. Neuropharmacology 12:933–938.

Krupp LB, LaRocca NG, Muir-Nash J, Steinberg AD. 1989. The fatigue severity scale: Application to patients with multiple sclerosis and systemic lupus erythematosus. Archives of Neurology 46:1121–1123.

Kurtzke JF. 1983. Rating neurologic impairment in multiple sclerosis: an expanded disability status scale (EDSS). Neurology 33:1444–52.

Laganà MM, Ceccarelli A, Giulia Preti M, Venturelli C, Pia Sormani M, Cavarretta R, Baselli G, Cecconi P, Caputo D, Rovaris M. 2011. Atlas-Based Versus Individual-Based Fiber Tracking of the Corpus Callosum in

Patients with Multiple Sclerosis: Reliability and Clinical Correlations. J Neuroimaging:1–10.

LaRocca NG. 2011. Cognitive Impairment and Mood Disturbances. In: Giesser BS, editor. Primer on Multiple Sclerosis. Los Angeles: Oxford University Press. p. 241–262.

Larsson H, Thomsen C, Frederiksen J, Stubgaard M, Henriksen O. 1992. In vivo magnetic resonance diffusion measurement in the brain of patients with multiple sclerosis. Magn Reson Imaging 10:7–12.

Latora V, Marchiori M. 2001. Efficient Behavior of Small-World Networks. Phys Rev Lett 87:3–6.

Lebel C, Caverhill-Godkewitsch S, Beaulieu C. 2010. Age-related regional variations of the corpus callosum identified by diffusion tensor tractography. Neuroimage 52:20–31.

Lebel C, Walker L, Leemans A, Phillips L, Beaulieu C. 2008. Microstructural maturation of the human brain from childhood to adulthood. Neuroimage 40:1044–55.

Lebel CA. 2010. Diffusion Tensor Imaging of Human Brain Development.

Li Y, Jewells V, Kim M, Chen Y, Moon A, Armao D, Troiani L, Markovic-Plese S, Lin W, Shen D. 2012. Diffusion tensor imaging based network analysis detects alterations of neuroconnectivity in patients with clinically early relapsing-remitting multiple sclerosis. Hum Brain Mapp 00:1–16.

Liu M, Beaulieu C, Gross W, Concha L, Gross DW. 2011. Distinct white matter abnormalities in different idiopathic generalized epilepsy syndromes. Epilepsia 52:2267–2275.

Liu Y, Duan Y, He Y, Yu C, Wang J, Huang J, Ye J, Parizel PM, Li K, Shu N. 2011. Whole brain white matter changes revealed by multiple diffusion metrics in multiple sclerosis: A TBSS study. Eur J Radiol:1–7.

Liu Y, Mitchell PJ, Kilpatrick TJ, Stein MS, Harrison LC, Baker J, Ditchfield M, Li K, Egan GF, Butzkueven H, et al. 2012. Diffusion tensor imaging of acute inflammatory lesion evolution in multiple sclerosis. J Clin Neurosci 19:1689–1694.

Loder C, Allawi J, Horrobin DF. 2002. Treatment of multiple sclerosis with lofepramine , L -phenylalanine and vitamin B 12: mechanism of action and clinical importance: roles of the locus coeruleus and central noradrenergic systems. Med Hypotheses 59:594–602.

Mainero C, Benner T, Radding a, Van der Kouwe a, Jensen R, Rosen BR, Kinkel RP. 2009. In vivo imaging of cortical pathology in multiple sclerosis using ultra-high field MRI. Neurology 73:941–8.

Mesaros S, Rocca M a, Riccitelli G, Pagani E, Rovaris M, Caputo D, Ghezzi A, Capra R, Bertolotto A, Comi G, et al. 2009. Corpus callosum damage and cognitive dysfunction in benign MS. Hum Brain Mapp 30:2656–66.

Mills R. 1973. Self-Diffusion in Normal and Heavy-Water in Range 1-45 Degrees. Journal of Physical Chemistry 77:685–688.

Minden SL, Frankel D, Hadden L, Perloffp J, Srinath KP, Hoaglin DC. 2006. The Sonya Slifka Longitudinal Multiple Sclerosis Study: methods and sample characteristics. Mult Scler 12:24–38.

Molina AG, Rajo PR, Gomez PV, Junque C, Rovira TR. 2008. Orbitofrontal dysfunction in multiple sclerosis: Iowa Gambling Task. Psicothema 20:445–9.

Moll NM, Rietsch AM, Thomas S, Ransohoff AJ, Lee J-C, Fox R, Chang A, Ransohoff RM. 2011. Multiple Sclerosis Normal-Appearing White Matter: Pathology-Imaging Correlations. Ann Neurol 70:764–773.

Morgante F, Dattola V, Crupi D, Russo M, Rizzo V, Ghilardi MF, Terranova C, Girlanda P, Quartarone A. 2011. Is central fatigue in multiple sclerosis a disorder of movement preparation? J Neurol 258:263–72.

Mori S, Crain BJ, Chacko VP, Van Zijl PC. 1999. Three-dimensional tracking of axonal projections in the brain by magnetic resonance imaging. Ann Neurol 45:265–9.

Mottershead JP, Schmierer K, Clemence M, Thornton JS, Scaravilli F, Barker GJ, Tofts PS, Newcombe J, Cuzner ML, Ordidge RJ, et al. 2003. High field MRI correlates of myelin content and axonal density in multiple sclerosis--a post-mortem study of the spinal cord. J Neurol 250:1293–301.

Multiple Sclerosis Council for Clinical Practice G. 1998. Fatigue and Multiple Sclerosis: Evidence-Based Management Strategies for Fatigue in Multiple Sclerosis. In: Washington, DC: Paralyzed Veterans Association of America.

Narayana P, Doyle T, Lai D, Wolinsky J. 1998. Serial proton magnetic resonance spectroscopic imaging, contrast-enhanced magnetic resonance imaging, and quantitative lesion volumetry in multiple sclerosis. Ann Neurol 43:56–71.

Narayana PA. 2005. Magnetic Resonance Spectroscopy in the Monitoring of Multiple Sclerosis. J Neuroimaging 15:46S–57S.

National Multiple Sclerosis Society M. Who gets MS? Available from: http://www.nationalmssociety.org/about-multiple-sclerosis/what-we-know-about-ms/who-gets-ms/index.aspx

Newcombe J, Cuzner ML, Röyttä M, Frey H. 1980. White matter proteins in multiple sclerosis. J Neurochem 34:700–8.

Newcombe J, Woodroofe M, Cuzner M. 1986. Distribution of glial fibrillary acidic protein in gliosed human white matter. J Neurochem 47:1713–9.

Nordmann J, Saraux H, Roullet E. 1987. Contrast sensitivity in multiple sclerosis: a study in 35 patients with and without optic neuritis. Opthalmologica 195:199–204.

Ordidge R, Gordon R. 1983. Methods and apparatus of obtaining NMR spectra.

Ormerod IEC, Bronstein A, Rudge P, Johnson G, Macmanus D, Halliday AM, Barratt H, Du Boulay EP, Kendal BE, Moseley IF, et al. 1986. Magnetic resonance imaging in clinically isolated lesions of the brain stem. J Neurol Neurosurg Psychiatry 49:737–743.

Ozturk A, Smith SA, Gordon-Lipkin EM, Harrison DM, Shiee N, Pham DL, Caffo BS, Calabresi PA, Reich DS. 2010. MRI of the Corpus Callosum in Multiple Sclerosis: Association with Disability. Mult Scler 16:1–19.

Pardini M, Bonzano L, Mancardi GL, Roccatagliata L. 2010. Frontal networks play a role in fatigue perception in multiple sclerosis. Behav Neurosci 124:329–336.

Pellicano C, Gallo A, Li X, Ikonomidou VN, Evangelou IE, Ohayon JM, Stern SK, Ehrmantraut M, Cantor F, McFarland HF, et al. 2010. Relationship of Cortical Atrophy to Fatigue in Patients With Multiple Sclerosis. Neurology 67:447–453.

Polak PE, Kalinin S, Feinstein DL. 2011. Locus coeruleus damage and noradrenaline reductions in multiple sclerosis and experimental autoimmune encephalomyelitis. Brain 134:665–77.

Polman CH, Reingold SC, Banwell B, Clanet M, Cohen JA, Filippi M, Fujihara K, Havrdova E, Hutchinson M, Kappos L, et al. 2011. Diagnostic criteria for multiple sclerosis: 2010 Revisions to the McDonald criteria. Ann Neurol 69:292–302.

Polman CH, Reingold SC, Edan G, Filippi M, Hartung H, Kappos L, Lublin FD, Metz LM, Mcfarland HF, Connor PWO, et al. 2005. Diagnostic Criteria for Multiple Sclerosis□: 2005 Revisions to the " McDonald Criteria ". 11:840–846.

Posner MI, Petersen SE. 1990. The attention system of the human brain. Annu Rev Neurosci 13:25–42.

Preziosa P, Rocca MA, Caputo D. 2011. Intrinsic Damage to the Major White Matter Tracts in Patients with Different Clinical Phenotypes of Multiple Sclerosis□: A Voxelwise Purpose□: Methods□: Results□: Radiology 260:541–550.

Provencher SW. 2001. Automatic quantitation of localized in vivo 1H spectra with LCModel. NMR Biomed 14:260–264.

Reich DS, Ozturk A, Calabresi P a, Mori S. 2010. Automated vs. conventional tractography in multiple sclerosis: variability and correlation with disability. Neuroimage 49:3047–56.

Reich DS, Smith S a, Zackowski KM, Gordon-Lipkin EM, Jones CK, Farrell JAD, Mori S, Van Zijl PCM, Calabresi PA. 2007. Multiparametric magnetic resonance imaging analysis of the corticospinal tract in multiple sclerosis. Neuroimage 38:271–279.

Riccitelli G, Rocca MA, Forn C, Colombo B, Comi G, Filippi M. 2011. Voxelwise Assessment of the Regional Distribution of Damage in the Brains of Patients with Multiple Sclerosis and Fatigue. AJNR Am J Neuroradiol 32:874–9.

Richiardi J, Gschwind M, Simioni S, Annoni J-M, Greco B, Hagmann P, Schluep M, Vuilleumier P, Van De Ville D. 2012. Classifying minimally disabled multiple sclerosis patients from resting state functional connectivity. Neuroimage 62:2021–2033.

Rigotti D, Inglese M, Kirov I, Perry N, Herbert J, Grossman RI, Gonen O. 2012. Two-year Serial Whole-Brain N-Acetylaspartate in Relapsing Remitting Multiple Sclerosis Patients. In: Vol. 20. p. 3122.

Rigotti DJ, Gonen O, Grossman RI, Babb JS, Falini A, Benedetti B, Filippi M. 2011. Global N-Acetyl-aspartate Declines Even In Benign Multiple Sclerosis. AJNR Am J Neuroradiol 32:204–209.

Rimkus CDM, Junqueira TDF, Lyra KP, Jackowski MP, Machado MAR, Miotto EC, Callegaro D, Otaduy MCG, Leite CC Da. 2011. Corpus Callosum Microstructural Changes Correlate with Cognitive Dysfunction in Early Stages of Relapsing-Remitting Multiple Sclerosis : Axial and Radial Diffusivities Approach. Mult Scler 2011:1–7.

Rocca MA, Agosta F, Colombo B, Mezzapesa DM, Falini A, Comi G, Filippi M. 2007. fMRI Changes in Relapsing-Remitting Multiple Sclerosis Patients Complaining of Fatigue after IFN Beta -1A Injection. Hum Brain Mapp 382:373–382.

Roelcke U, KAppos L, Lechner-Scott J, Brunnschweiler H, Huber S, Ammann W, Plohmann A, Dellas S, Maguire R, Missimer J, et al. 1997. Reduced glucose metabolism in the frontal cortex and basal ganglia of multiple sclerosis patients with fatigue: A 18 F-fluorodeoxyglucose positron emission tomography study. Neurology 48:1566–71.

Rolak LA. 2011. Diagnosis of Multiple Sclerosis. In: Giesser BS, editor. Primer on Multiple Sclerosis. Oxford University Press. p. 81–89.

Rooney W, Goodkin D, Schuff N, Meyerhoff D, Norman D, Weiner M. 1997. 1H MRSI of normal appearing white matter in multiple sclerosis. Mult Scler 3:231–237.

Roosendaal SD, Geurts JJG, Vrenken H, Hulst HE, Cover KS, Castelijns J a, Pouwels PJW, Barkhof F. 2009. Regional DTI differences in multiple sclerosis patients. Neuroimage 44:1397–403.

Roosendaal SD, Schoonheim MM, Hulst HE, Sanz-Arigita EJ, Smith SM, Geurts JJG, Barkhof F. 2010. Resting state networks change in clinically isolated syndrome. Brain 133:1612–1621.

Rovaris M, Gallo A, Falini A, Benedetti B, Rossi P, Comola M, Scotti G, Comi G, Filippi M. 2005. Axonal injury and overall tissue loss are not related in primary progressive multiple sclerosis. Arch Neurol 62:898–902.

Sailer M, Fischl B, Salat D, Tempelmann C, Schönfeld MA, Busa E, Bodammer N, Heinze H-J, Dale A. 2003. Focal thinning of the cerebral cortex in multiple sclerosis. Brain 126:1734–44.

Sajja BR, Wolinsky JS, Narayana PA. 2009. Proton Magnetic Resonance Spectroscopy in Multiple Sclerosis. Neuroimaging Clin N Am 19:45–58.

Salamon N, Sicotte N, Drain a, Frew A, Alger JR, Jen J, Perlman S, Salamon G. 2007. White matter fiber tractography and color mapping of the normal human cerebellum with diffusion tensor imaging Imagerie par tenseur de diffusion et tractographie sélective des voies cérébelleuses du cerveau normal. J Neuroradiol 34:115–128.

Sepulcre J, Masdeu JC, Goñi J, Arrondo G, Vélez de Mendizábal N, Bejarano B, Villoslada P. 2009. Fatigue in multiple sclerosis is associated with the disruption of frontal and parietal pathways. Mult Scler 15:337–344.

Shah A. 2009. Fatigue in multiple sclerosis. Phys Med Rehabil Clin N Am 20:363–72.

Shu N, Liu Y, Li J, Li Y, Yu C, Jiang T. 2009. Altered anatomical network in early blindness revealed by diffusion tensor tractography. PLoS One 4:e7228.

Shu N, Liu Y, Li K, Duan Y, Wang J, Yu C, Dong H, Ye J, He Y. 2011. Diffusion Tensor Tractography Reveals Disrupted Topological Efficiency in White Matter Structural Networks in Multiple Sclerosis. Cereb Cortex 21:2565–77.

Simon JH, Zhang S, Laidlaw DH, Miller DE, Brown M, Corboy J, Bennett J. 2006. Identification of fibers at risk for degeneration by diffusion tractography in patients at high risk for MS after a clinically isolated syndrome. J Magn Reson Imaging 24:983–8.

Smith S, Jenkinson M, Johansen-Berg H, Rueckert D, Nichols T, Mackay C, Watkins K, Ciccarelli O, Cader M, Matthews P, et al. 2006. Tract-based spatial statistics: voxelwise analysis of multisubject diffusion data. Neuroimage 31:1487–505.

Song S-K, Yoshino J, Le TQ, Lin S-J, Sun S-W, Cross AH, Armstrong RC. 2005. Demyelination increases radial diffusivity in corpus callosum of mouse brain. Neuroimage 26:132–40.

Spanò B, Cercignani M, Basile B, Romano S, Mannu R, Centonze D, Caltagirone C, Bramanti P, Nocentini U, Bozzali M. 2010. Multiparametric MR investigation of the motor pyramidal system in patients with “truly benign” multiple sclerosis. Mult Scler 16:178–88.

Sperling R a, Guttmann CR, Hohol MJ, Warfield SK, Jakab M, Parente M, Diamond EL, Daffner KR, Olek MJ, Orav EJ, et al. 2001. Regional magnetic resonance imaging lesion burden and cognitive function in multiple sclerosis: a longitudinal study. Arch Neurol 58:115–21.

Staub F, Bogousslavsky J. 2001. Fatigue after stroke: A major but neglected issue. Cerebrovasc Dis 12:75–81.

Steen C, Wilczak N, Hoogduin JM, Koch M, De Keyser J. 2010. Reduced creatine kinase B activity in multiple sclerosis normal appearing white matter. PLoS One 5:e10811.

De Stefano N, Matthews PM, Arnold DL. 1995. Reversible Decreases in N-Acetylaspartate After Acute Brain Injury. Magn Reson Med 34:721–727.

Suhy J, Rooney WD, Goodkin DE, Capizzano AA, Soher BJ, Maudsley A, Waubant E, Andersson P, Weiner M. 2000. 1H MRSI comparison of white matter and lesions in primary progressive and relapsing-remitting MS. Mult Scler 6:148–155.

Tartaglia MC, Narayanan S, Francis SJ, Santos AC, Stefano N De, Lapierre Y, Arnold DL, De Stefano N. 2004. The Relationship Between Diffuse Axonal Damage and Fatigue in Multiple Sclerosis. Arch Neurol 61:201–207.

Tartaglia MC, Narayanan S, De Stefano N, Arnaoutelis R, Antel SB, Francis SJ, Santos AC, Lapierre Y, Arnold DL. 2002. Choline is increased in pre-lesional normal appearing white matter in multiple sclerosis. J Neurol 249:1382–90.

Tedeschi G, Dinacci D, Lavorgna L, Prinster A, Savettieri G, Quattrone A, Livrea P, Messina C, Reggio A, Servillo G, et al. 2007. Correlation between fatigue and brain atrophy and lesion load in multiple sclerosis patients independent of disability. J Neurol Sci 263:15 – 19.

Téllez N, Alonso J, Río J, Tintoré M, Nos C, Montalban X, Rovira a. 2008. The basal ganglia: a substrate for fatigue in multiple sclerosis. Neuroradiology 50:17–23.

Trapp BD, Peterson J, Ransohoff RM, Rudick R, Mörk S, Bö L. 1998. Axonal transection in the lesions of multiple sclerosis. N Engl J Med 338:278–85.

Tzourio-Mazoyer N, Landeau B, Papathanassiou D, Crivello F, Etard O, Delcroix N, Mazoyer B, Joliot M. 2002. Automated anatomical labeling of activations in SPM using a macroscopic anatomical parcellation of the MNI MRI single-subject brain. Neuroimage 15:273–289.

Urenjak J, Williams SR, Gadian DG, Noble M. 1993. Proton nuclear magnetic resonance spectroscopy unambiguously identifies different neural cell types. J Neurosci 13:981–9.

Vrenken H, Barkhof F, Uitdehaag BMJ, Castelijns JA, Polman CH, Pouwels PJ. JW. 2005. MR spectroscopic evidence for glial increase but not for neuro-axonal damage in MS normal-appearing white matter. Magn Reson Med 53:256 –266.

Wakana S, Jiang H, Zijl PCM Van. 2004. Fiber Tract–based Atlas of Human White Matter Anatomy. Radiology 230:77–87.

Watts DJ, Strogatz SH. 1998. Collective dynamics of “small-world” networks. Nature 393:440–2.

Weber-Fahr W, Ende G, Braus DF, Bachert P, Soher BJ, Henn FA, Büchel C. 2002. A Fully Automated Method for Tissue Segmentation and CSF-Correction of Proton MRSI Metabolites Corroborates Abnormal Hippocampal NAA in Schizophrenia. Neuroimage 16:49 – 60.

Werring DJ, Brassat D, Droogan AG, Clark CA, Symms MR, Barker GJ, MacManus DG, Thompson AJ, Miller DH. 2000. The pathogenesis of lesions and normal-appearing white matter changes in multiple sclerosis: a serial diffusion MRI study. Brain 123 (Pt 8:1667–76.

Wiltshire K, Concha L, Gee M, Bouchard T, Beaulieu C, Camicioli R. 2010. Corpus Callosum and Cingulum Tractography in Parkinson's Disease. Can J Neurol Sci 37:595–600.

Winterfeld M, Debuch H. 1977. The glycerophospholipid content of the white matter of normal and MS brains. J Neurol 215:261–72.

Zhang J, Jones M, DeBoy CA, Reich DS, Farrell JAD, Hoffman PN, Griffin JW, Sheikh KA, Miller MI, Mori S, et al. 2009. Diffusion tensor magnetic resonance imaging of Wallerian degeneration in rat spinal cord after dorsal root axotomy. J Neurosci 29:3160–71.

APPENDIX A

Demographics shown in Table A.1 below is of nineteen women with relapsing-remitting MS that participated in our study. They fit the selection criteria, which are low disability measured by the expanded disability status scale (EDSS) and do not suffer from depression. From the fatigue severity scale (FSS), these women suffer from various levels of fatigue. Also shown below is the T_2-hyperintense lesion load (cm^3) in each patient.

Table A.1: Demographic of the relapsing-remitting multiple sclerosis (RRMS) patients that includes the age, date of study, expanded disability status scale (EDSS), fatigue severity scale (FSS) and the lesion load (LL) of each patient that participated in our study. Patients were identified using random code assignment to ensure patients' privacy and identity remained anonymous.

No.	ID	Age	Study Date	EDSS	FSS	LL (cm^3)
1	Subj01	37	3-Nov-09	0.0	46	1.63
2	Subj02	50	12-Nov-09	2.0	53	20.63
3	Subj03	40	18-Nov-09	1.0	31	1.18
4	Subj04	41	18-Nov-09	1.0	50	0.50
5	Subj05	43	26-Nov-09	1.5	59	1.18
6	Subj06	33	3-Dec-09	1.5	57	6.11
7	Subj07	42	9-Dec-09	1.0	28	1.98
8	Subj08	42	9-Dec-09	2.0	52	0.44
9	Subj09	40	27-Jan-10	2.5	53	3.98
10	Subj10	29	4-May-12	1.5	18	9.12

No.	ID	Age	Study Date	EDSS	FSS	LL (cm^3)
11	Subj11	47	18-May-12	1.5	9	3.68
12	Subj12	30	10-Jul-12	1.5	59	7.93
13	Subj13	43	22-Aug-12	1.5	11	1.88
14	Subj14	46	28-Aug-12	2.0	42	37.17
15	Subj15	42	29-Aug-12	1.5	34	0.15
16	Subj16	33	29-Aug-12	1.5	17	16.25
17	Subj17	38	29-Aug-12	1.5	14	15.18
18	Subj18	56	5-Sep-12	2.0	49	36.87
19	Subj19	27	5-Sep-12	1.5	32	0.06

APPENDIX B

Figure B.1 below is a plot of lesion load versus fatigue scores in the patient group. No correlation between lesion load and fatigue in either group, or when all patients analyzed as one group.

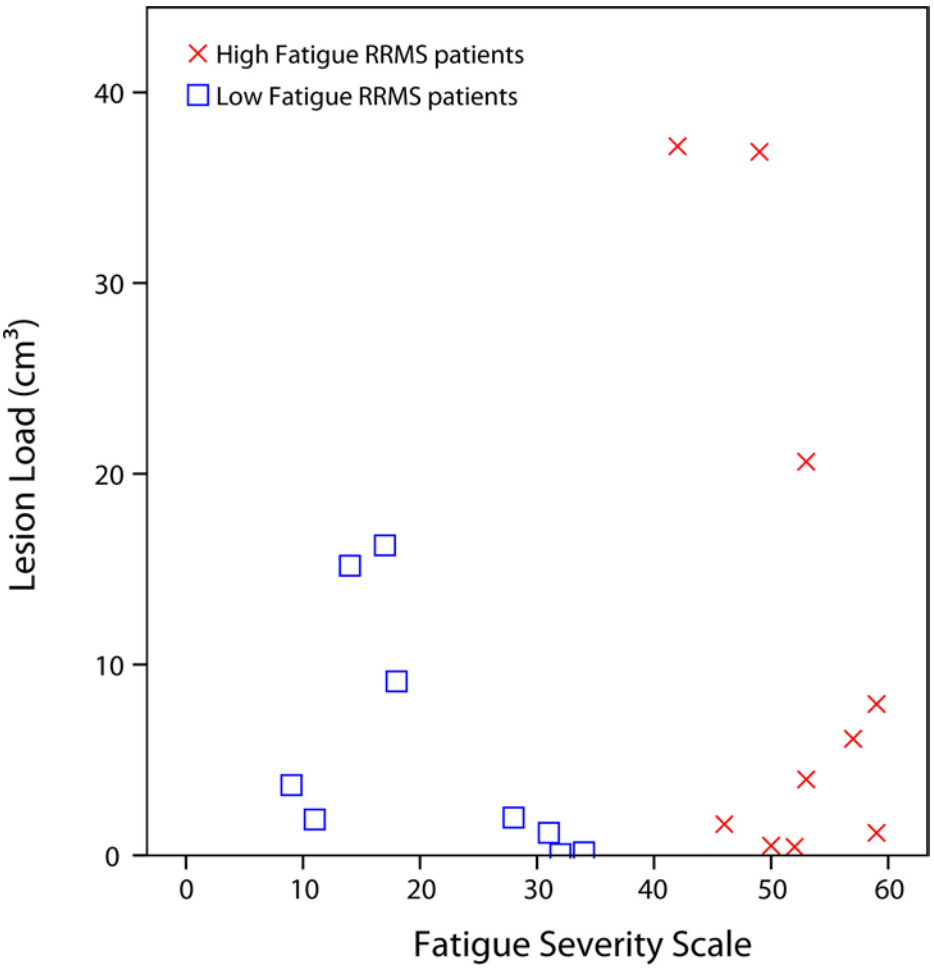

Figure B.1: Scatterplot of the lesion load versus fatigue score measured by the fatigue severity scale (FSS) in nineteen (19) relapsing-remitting multiple sclerosis patients (RRMS) with low and high fatigue scores.

APPENDIX C

This section includes the seed and target mask used to identify and delineate the superior cerebellar peduncle (SCP) and middle cerebellar peduncle (MCP). Take note that the region-of-interest drawn on the masks are bigger than those drawn in manual white matter delineation. Images shown here are from data with voxel size 2x2x2.5 cm^3 that covered whole brain including the cerebellum in 50 axial slices. Tracts shown in Figure C.1 and Figure C.2 were drawn on coloured FA (a,b) and b_0 (c) images of a 40 year old healthy female volunteer. Other white matter tracts delineated in Chapter 7 made use of priori knowledge as demonstrated in previous studies (Catani et al. 2002; Wakana et al. 2004; Salamon et al. 2007; Anderson et al. 2011). A detailed guide can also be found in previous dissertation by Catherine Lebel (2010).

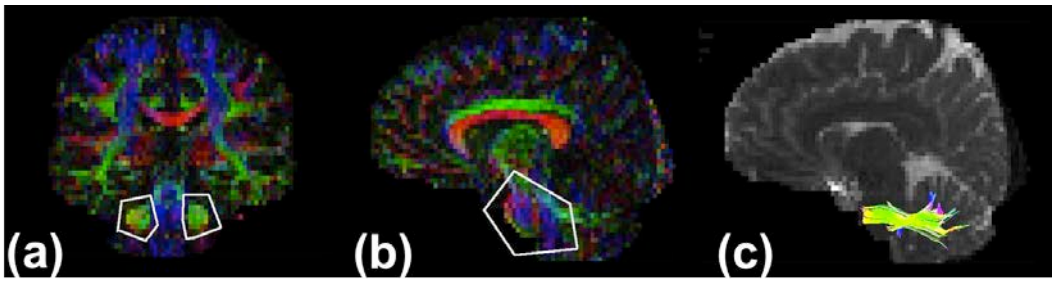

Figure C.1: The (a) seed mask and (b) target mask used in fiber tracking to delineate the (c) middle cerebellar peduncle (MCP) tract.

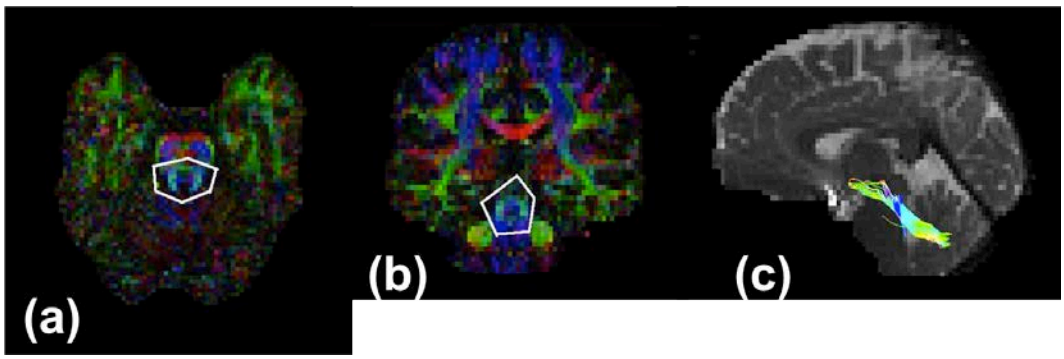

Figure C.2: The (a) seed mask and (b) target mask used in fiber tracking to delineate the (c) superior cerebellar peduncle (SCP) tract.

APPENDIX D

Identified lesions in specific tracts of MS patients included in the study.

Table D.1: In-tract lesions identified in eleven white matter tracts in nineteen multiple sclerosis patients with low disability.

No.	ID	MCP	SCP	UNF	Cing	SLF	CST	IFO	gCC	bCC	sCC	ILF
1	Subj01					√	√	√	√	√	√	√
2	Subj02			√		√	√	√	√	√	√	√
3	Subj03						√	√	√	√	√	√
4	Subj04							√			√	√
5	Subj05					√	√	√	√		√	√
6	Subj06	√				√	√	√	√	√	√	√
7	Subj07						√			√		√
8	Subj08								√		√	√
9	Subj09		√			√	√			√	√	√
10	Subj10				√	√	√	√	√	√	√	√
11	Subj11			√	√	√	√	√	√	√	√	
12	Subj12				√	√	√	√	√	√	√	√
13	Subj13				√	√		√	√		√	√
14	Subj14			√	√	√	√	√	√	√	√	√
15	Subj15											√
16	Subj16			√	√	√	√	√	√	√	√	√
17	Subj17			√	√	√	√	√	√	√	√	√
18	Subj18		√	√	√		√	√	√	√	√	√
19	Subj19									√		

Appendix E

Images following this section depict whole brain view of the lesion load distribution in relapsing remitting multiple sclerosis patients. Each figure has different number of patients contributing to the intensity of each voxel. The colourbar in every figure shows the percentage of patients contributing to each coloured voxel. Normalized lesion location for every subject were added and normalized to the number of patients contributing to the group.

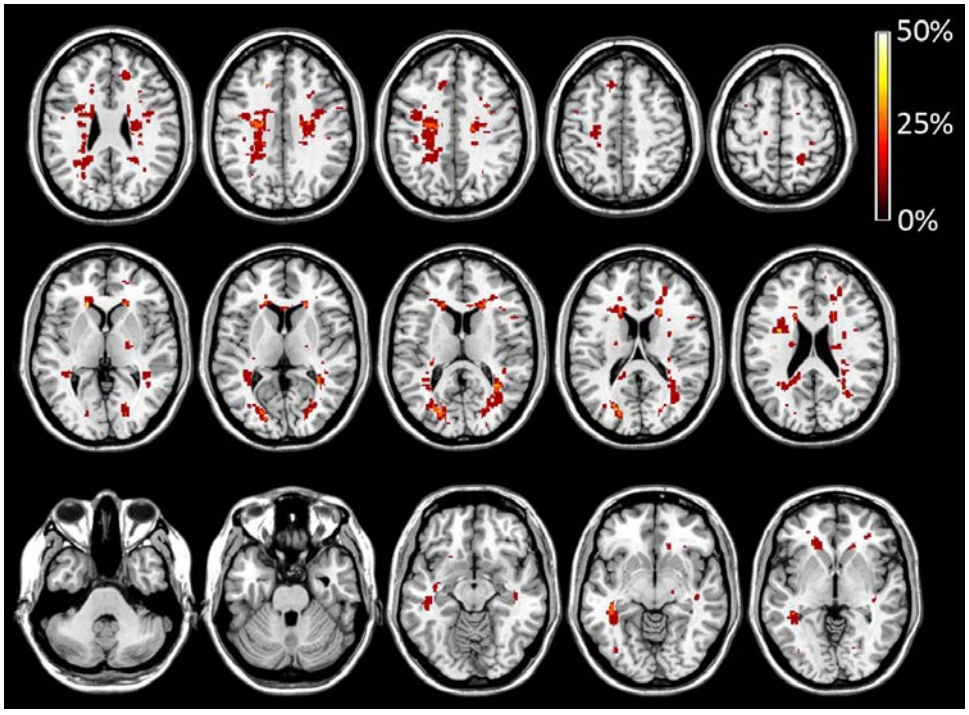

Figure E.1: Whole brain lesion distribution map of RRMS patients in the low fatigue group (n=7).

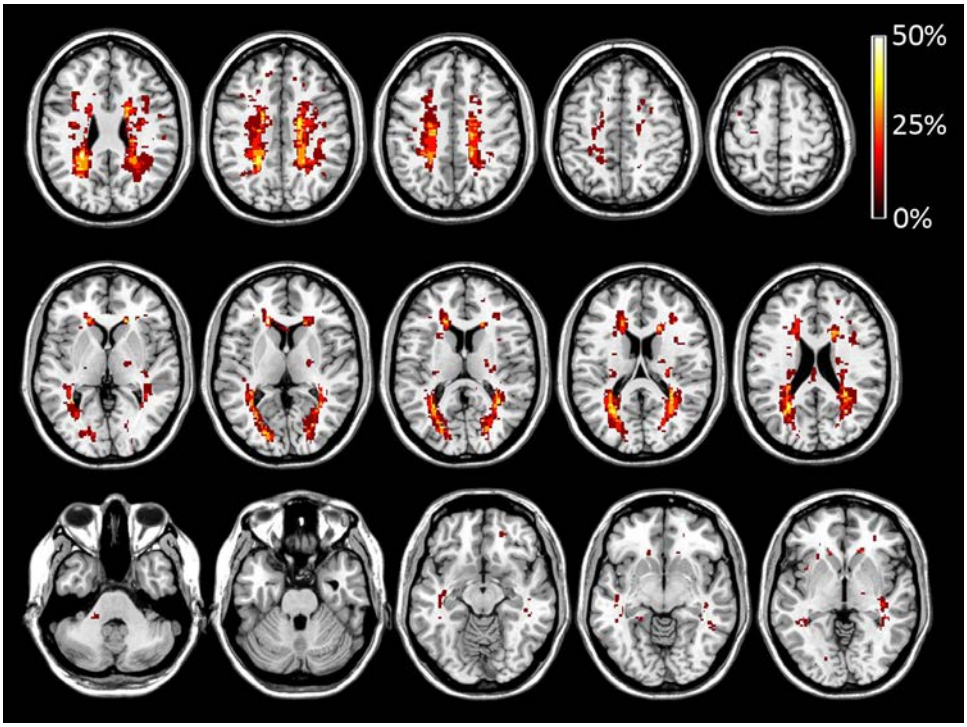

Figure E.2: Whole brain lesion distribution map of RRMS patients in the high fatigue group (n=10).

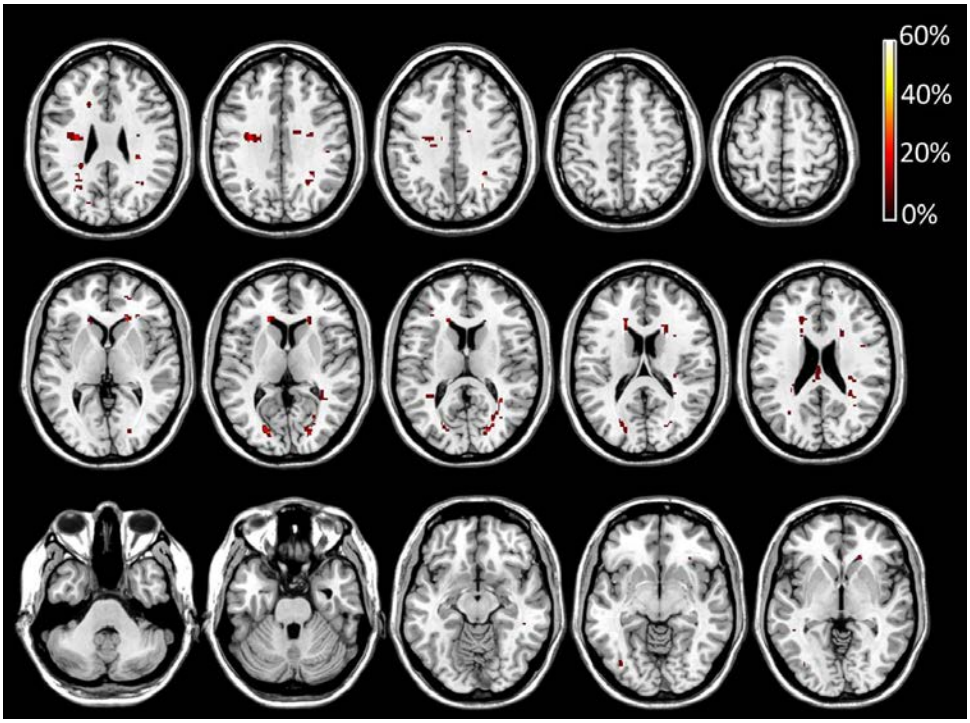

Figure E.3: Whole brain lesion distribution map of RRMS patients in the low lesion load group (n=9).

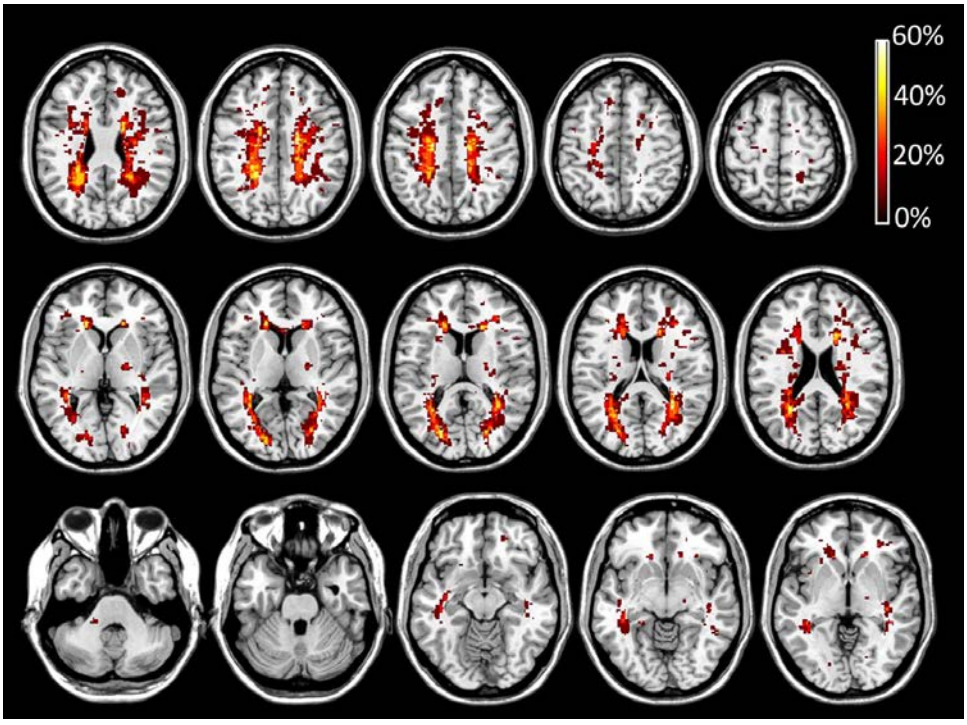

Figure E.4: Whole brain lesion distribution map of RRMS patients in the high lesion load group (n=10).